Fall 1-31-2005

The testing of semiconductor-based adsorption modified photosensitive sensors for their response to a volatile organic compound, oxygen, humidity, and heating

Roberta Rosty
New Jersey Institute of Technology

ABSTRACT

THE TESTING OF SEMICONDUCTOR-BASED ADSORPTION MODIFIED PHOTOSENSITIVE SENSORS FOR THEIR RESPONSE TO A VOLATILE ORGANIC COMPOUND, OXYGEN, HUMIDITY AND HEATING

by
Roberta Rosty

Two thin-film sensors, composed of different thicknesses (approximately 0.5 microns and 4.5 microns) of a cadmium sulfide layer coated with Rhodamine B fluorescent dye on a glass substrate, were tested for change in photoconductivity due to exposure to different concentrations of gaseous organic molecules in the parts-per-million (ppm) range.

It was theorized that the gaseous organic molecules would adsorb to the dyed semiconductor surface and that some energy would be transferred to the adsorbed analyte rather than to the cadmium sulfide semiconductor layer through the dye, thereby decreasing the photoconductivity of the surface in an amount proportional to the analyte concentration to which the sensor was exposed. Toluene was chosen as a typical organic vapor to test for the purpose of this study. [1]

The effect of oxygen, nitrogen, helium, humidity and temperature on these sensors was also studied and the results obtained are outlined in this report. Both sensors were able to detect toluene concentrations in the parts-per-million range in the absence of oxygen. The thicker sensor had a photoelectric response that was about ten times as large as the thinner sensor, presumably due to a greater porosity and surface area.

The sensor with the thicker cadmium sulfide layer was able to detect toluene in the 0 to 30 ppm concentration range in air at room temperature. At a concentration higher than 30 ppm of toluene, it is believed that the concentration of toluene was enough

to provide an alternate pathway for the surface current, which led to a sudden increase in the surface photoconductivity.

The thicker sensor was also tested at a higher temperature and it was shown that a higher temperature led to lower resistances, presumably due to the desorbing of gases from the sensor surface plus an increased ability of electrons to partially overcome some of the intergrain resistance at the polycrystalline grain boundaries in the cadmium sulfide layer. [2]

Results from experimental studies showed that this sensor could detect both the presence and concentration of oxygen in the sensor chamber with the 0.5 and 4.5 micron cadmium sulfide thin-film sensor, whether the surface had a Rhodamine B dye layer or not. The dye was shown, however, to increase the photosensitivity of the sensor.

Exposure of the sensor to a large enough quantity of a vaporous polar substance like water, caused a decrease of the resistance due to the provision of an alternate pathway for the surface current, and in certain instances, concentrations could be predicted.

THE TESTING OF SEMICONDUCTOR-BASED ADSORPTION MODIFIED PHOTOSENSITIVE SENSORS FOR THEIR RESPONSE TO A VOLATILE ORGANIC COMPOUND, OXYGEN, HUMIDITY AND HEATING

by
Roberta Rosty

A Dissertation
Submitted to the Faculty of
New Jersey Institute of Technology
and Rutgers, The State University of New Jersey - Newark
In Partial Fulfillment of the Requirements for the Degree of
Doctor of Philosophy in Environmental Science

Department of Chemistry and Environmental Science

January 2005

APPROVAL PAGE

THE TESTING OF SEMICONDUCTOR-BASED ADSORPTION MODIFIED PHOTOSENSITIVE SENSORS FOR THEIR RESPONSE TO A VOLATILE ORGANIC COMPOUND, OXYGEN, HUMIDITY AND HEATING

Roberta Rosty

Dr. Barbara B. Kebbekus — Date
Professor of Chemistry and Environmental Science, NJIT, Graduate Advisor

Dr. Joseph W. Bozzelli — Date
Chairman and Distinguished Professor of Chemistry and Environmental Science, NJIT

Dr. Durgamadhab Misra — Date
Professor of Electrical and Computer Engineering, NJIT

Dr. Somenath Mitra — Date
Professor of Chemistry and Environmental Science, NJIT

Dr. Vladimir Zaitsev — Date
Associate Professor of Physics, Moscow State University

BIOGRAPHICAL SKETCH

Author: Roberta Rosty

Degree: Doctor of Philosophy

Date: January 2005

Undergraduate and Graduate Education:

- Doctor of Philosophy in Environmental Science,
  New Jersey Institute of Technology, Newark, NJ, 2005
- Master of Science in Environmental Science,
  New Jersey Institute of Technology, Newark, NJ, 2000
- Degree of Engineer in Chemical Engineering,
  New Jersey Institute of Technology, Newark, NJ, 1997
- Master of Science in Chemical Engineering,
  New Jersey Institute of Technology, Newark, NJ, 1981
- Bachelor of Science in Chemical Engineering,
  New Jersey Institute of Technology, Newark, NJ, 1977

Major: Environmental Science

Presentations and Publications:

R. Rosty, B. Kebbekus, V. Zaitsev, "The Testing of a Semiconductor-based Adsorption Modified Photosensitive Sensor for Its Response to a Volatile Organic Compound, Oxygen, Humidity and Temperature", Sensors and Actuators B: Chemical, 2004 (in press).

R. Rosty, D. Martinelli, A. Devine, M. J. Bodnar, J. Beetle, " Surface Preparation of Polyolefins Prior to Adhesive Bonding", The 32nd International SAMPE Symposium and Exhibition, California, April 6-9, 1987. The SAMPE Journal pp. 34-37, July/August Issue, 1987.

M. J. Bodnar, J. Osterndorf, and R. Rosty, "Adhesive Bond Strength and Durability Studies Using Three Different Engineering Plastics and Various Surface Preparations", The SAMPE Journal, pp. 15-19, July/August Issue, 1989.

This dissertation and research project is dedicated to my family

and in memory of

Dr. H. T. Chen, Dr. J. E. McCormick and Mrs. Annette Damiano.

ACKNOWLEDGEMENT

The author would like to thank Dr. Barbara B. Kebbekus for her technical guidance and patience during the experimentation and preparation of this research project, and for her hard work in editing this dissertation and the resultant journal article. The author would also like to thank Dr. Kebbekus for allowing her to take part in such an interesting and challenging research topic.

The author would also like to thank Dr. Joseph Bozzelli, Dr. Somenath Mitra, Dr. Vladimir Zaitsev, and Dr. Durgamadhab Misra for their many helpful technical comments and for taking time from their busy schedules to be a part of my dissertation committee.

The author would also like to thank Dr. Yogesh Gandhi and Dr. Mark Ladolcetta for helping her with the lab equipment (GC, integrators, gauges, etc.) needed for this experimentation and for their helpful comments and suggestions.

The author would like to thank Ms. Clarisa Gonzalez-Lenahan of the Graduate Studies Office for all the time and effort she spent in reviewing this dissertation.

Finally, the author would like to thank New Jersey Institute of Technology and the many excellent professors and staff who have encouraged, guided and trained her during her collegiate endeavors with their technical knowledge and expertise.

TABLE OF CONTENTS

TABLE OF CONTENTS
(Continued)

Chapter **Page**

TABLE OF CONTENTS
(Continued)

Chapter **Page**

TABLE OF CONTENTS
(Continued)

Chapter **Page**

TABLE OF CONTENTS
(Continued)

TABLE OF CONTENTS
(Continued)

Chapter **Page**

TABLE OF CONTENTS
(Continued)

Chapter **Page**

TABLE OF CONTENTS
(Continued)

Chapter **Page**

TABLE OF CONTENTS
(Continued)

Chapter **Page**

TABLE OF CONTENTS
(Continued)

Chapter **Page**

LIST OF TABLES

LIST OF TABLES
(Continued)

LIST OF TABLES
(Continued)

Table **Page**

LIST OF FIGURES

LIST OF FIGURES
(Continued)

Figure **Page**

LIST OF FIGURES
(Continued)

Figure **Page**

LIST OF FIGURES
(Continued)

Figure **Page**

LIST OF FIGURES
(Continued)

Figure **Page**

LIST OF FIGURES
(Continued)

Figure **Page**

CHAPTER 1

INTRODUCTION

Numerous experimental research studies [1-10] have focused on using thin films of various semiconductor materials as gas sensors. The change in the electrical properties of these thin films when exposed to various gases is the basis of detection. [3-6, 8-13]

Many gas sensors have also been developed using fluorescent dyes to indicate gas exposure. With these sensors, the change in fluorescence is used to indicate exposure of the sensor to a particular gas. [14-26] In this study, a gas sensor was made combining by these two technologies: a thin film semiconductor material made of cadmium sulfide plus the addition of a fluorescent dye layer (Rhodamine B dye) to increase the photoconductivity of the semiconductor. [1]

It was theorized that the gaseous organic molecules would adsorb to the dyed ionic cadmium sulfide surface, due to their polarity. Some light energy would be transferred within the dye molecule from the excited electronic state into vibrational modes. If the vibrational states of the dye and the analyte adsorbed on the sensor surface were in resonance, it was believed that some of the energy being transferred through the dye, would be absorbed by the analyte on the surface rather than by the semiconductor layer. This reduction in energy available to electrons to overcome the semiconductor bandgap energy, would correlate with a reduction in surface current and a corresponding increase in resistance proportional to the concentration of analyte to which the sensor was exposed. [1] Previous studies in vacuum with low pressures of organic vapors confirmed this theory. [1, 27]

The initial results of this study are detailed in References 1 and 27. The work cited in Reference 1 explains the background and theory of the sensor work accomplished at NJIT. Reference 1 also contains experimental results at atmospheric pressures but in the absence of oxygen. The initial sensor was composed of a glass surface substrate that had been thinly covered with a 0.5 micron layer of a cadmium sulfide semiconductor material and then coated with a fluorescent dye. It was supplied by Dr. Vladimir Zaitsev of Moscow State University, Moscow, Russia. [28]

The sensor was tested for its response to different gas mixtures of toluene and nitrogen. Toluene is a pollutant because it is an ozone precursor, and it is important to be able to detect small amounts of these types of gaseous materials in the environment. Toluene was selected as a typical organic vapor for this study, as a model for test purposes.

The sensor was able to detect small amounts of toluene in nitrogen gas mixtures. The response of the sensor to different toluene/nitrogen mixtures was shown in this study to follow the Elovich Adsoption Equation.

Further research, as outlined in this report, characterized the photoconductivity (by measuring the change in resistance) of a thin cadmium sulfide semiconductor sensor dyed with a fluorescent Rhodamine B dye to several different types of gases: toluene, oxygen, nitrogen and water vapor at atmospheric pressure.

Other objectives included testing: the effect of the cadmium sulfide layer thickness through the use of two different thicknesses (approximately 0.5 and 4.5 microns), the effect of the fluorescent Rhodamine B dye, and the effect of the sensor temperature on the photo- electric response.

The experimentation in this portion of the study was aimed at testing not only different gas mixtures of toluene and nitrogen, but also different gas mixtures of toluene and air, to determine the practicality of using the sensor to detect concentrations in the parts-per-million (ppm) range of volatile organic compounds (VOC's) like toluene in an ambient environment.

The objective of testing the sensor under ambient conditions was to determine if it would be a practical, usable sensor of volatile organic compounds at various test sites and facilities. In order to be a practical environmental sensor, it would need to be able to function with air as the major component of the sample.

The sensor containing an 0.5 micron thick layer of cadmium sulfide and Rhodamine B dye layer was able to detect toluene when it was in a nitrogen gas mixture but not in an ambient air environment, due to the sensor's huge response (change in resistance) to oxygen versus its much smaller response to toluene.

This study was then expanded, beyond the initial scope, to determine the response of the sensor to oxygen as well as to volatile organic compounds. The sensor was tested with both synthetic air and room air. The synthetic air contained approximately 20% oxygen and 80% nitrogen, while the atmospheric air contained oxygen and nitrogen plus compounds such as water and carbon dioxide and other impurities. Different pressures of sample gas were used to provide different partial pressures of oxygen.

Oxygen sensors are important in fields such as medicine, industry and scientific research and so this research work had very practical applications. [14]

The results from the testing of the sensor with different mixtures of moisture and nitrogen show that the sensor can detect various concentrations of moisture when oxygen

is not present. When oxygen is present the polar water molecules and the oxygen ions vie for the same cationic sites on the sensor surface, and analysis of results has to take this factor into account.

The resistance of the sensor increases when only a small amount of moisture in nitrogen is present in the sensor chamber (9% moisture was tested). When a larger amount of moisture in nitrogen was tested (45% and up), the resistance decreased versus time, showing that the conductivity of the surface increases, probably due to the provision of a more energetically favorable, alternative pathway for the electrons to transverse the surface.

Another sensor chip with a 4.5 micron thick cadmium sulfide layer was fabricated in the NJIT laboratory and dyed with Rhodamine B fluorescent dye in the same way as the first sensor chip. The new sensor chip had a larger response to oxygen presumably due to a larger surface area and porosity. It was therefore able to detect toluene in the 0 to 30 ppm range.

A mechanism change occurred at a 30 ppm toluene concentration resulting in a reduction in resistance versus toluene concentration.

At a higher temperature (47 °C), the increase of resistance with toluene concentration due to absorption of energy by the adsorbed toluene on the sensor surface was no longer seen at small toluene concentrations because of the magnitude and predominance of other phenomena such as the reduction of intergrain resistances and the desorption of toluene at higher temperatures. [2]

CHAPTER 2

LITERATURE SURVEY

According to reference 29, " a sensor is a device that receives and responds to a signal or stimulus." Sensor materials listed in reference include: organics, inorganics, conducting, insulating or semiconducting materials or a biological substance or a liquid or gas plasma.

Detection occurs through the following means: biological, chemical, electric, magnetic or electromagnetic wave, heat temperature, mechanical displacement or wave, radioactivity, radiation, etc. The stimulus may be: acoustical, biological, chemical, electrical, optical, mechanical, thermal or by magnetic or radiation means. [29]

There are many different classes of sensors such as:

2.1 Occupancy and Motion Detectors

These types of detectors are used to sense objects and people by their motion. The applications for these types of detectors include: security, surveillance and energy management (electric lights control). [29]

2.2 Velocity and Acceleration Sensors

2.2.1 Electromagnetic Velocity Sensor

Uses the principle that voltage is proportional to the magnet's velocity when a magnet is moved through a coil of wire to induce a voltage.

2.2.2 Capacitive Accelerometer

Contains a stationary plate and one attached to the inertial mass, forming a capacitor, whose value is modulated by the acceleration.

2.2.3 Piezoresistive Accelerometers

Contains strain gauges and the strain can be directly related to the mass displacement.

2.2.4 Piezoelectric Accelerometers

Sensing elements are usually ceramic piezoelectric materials. The force seismic mass exerted on a crystal is proportional to the acceleration.

2.2.5 Thermal Accelerometers

A seismic mass is suspended by a thin cantilever and positioned in close proximity with a heat sink or between two heat sinks.

2.2.6 Piezoelectric Cables

A vibration sensor built with a mineral insulated cable that generates an electric signal when the cable is compressed. Applications include: vibration detectors in compressor blades in turboshaft aircraft engines, detection of insects in silos and automobile detection when the cables are buried in highway pavement. [29]

2.3 Force and Strain Sensors

Force sensors can be qualitative or quantitative.

2.3.1 Strain Gauges

A resistive elastic sensor, and its resistance to an applied force is a function of unit deformation (strain). Strain gauges are usually used with Wheatstone bridges.

2.3.2 Tactile Sensors

A sensor used to measure force; applications include robotics and "touch screen" displays.

2.3.3 Piezoelectric Force Sensor

A medical application for this type of sensor is when it was placed in the mattress of a baby's crib to monitor if a baby had stopped breathing. Normally when a baby breathes its body will slightly shift and if this doesn't occur the sensor will detect it. [29]

2.4 Pressure Sensors

2.4.1 Pressure Sensor

A simple but efficient mercury filled U-shaped sensor is used for measuring gas pressure. This sensor has drawbacks because it is susceptible to contamination of the gas by mercury vapors.

2.4.2 Piezoresistive Sensors

In piezoresistive sensors, a change in resistivity is proportional to applied pressure.

2.4.3 Capacitive Sensors

A pressure-to-electric output conversion sensor.

2.4.4 Variable Reluctance Pressure (VRP) Sensors

Uses a magnetically conductive diaphragm to modulate the magnetic resistance of a differential transformer.

2.4.5 Optoelectronic Sensors

Operates with light interference phenomena and consists of an optical pressure chip, a light emitting diode (LED) and a detector chip. [29]

2.5 Flow Sensors

Measures the flow of mass in a system.

2.5.1 Thermal Transport Sensors

The sensor measures flow by sensing changes in temperature due to heating.

2.5.2 Ultrasonic Sensors

Measures the amount of flow due to the detection of frequency caused by flowing medium.

2.5.3 Electromagnetic Sensors

Measures the flow of conductive liquids.

2.5.4 Microflow Sensors

Miniaturized gas flow sensors, operated on the method of thermal transport.

2.5.5 Breeze Sensors

Detects changes in gas movement. [29]

2.6 Acoustic Sensors (Microphones)

2.6.1 Resistive Microphones

Comprised of a moving diaphragm with stress sensitive resistors and a displacement sensor, which converts the diaphragm's deflections into an electrical signal.

2.6.2 Condenser (Capacitive) Microphones

Converts a distance between a parallel plate capacitor into electrical voltage.

2.6.3 Fiber-Optic Microphones

Utilized for hostile environments such as in turbojets or rocket engines.

2.6.4 Piezoelectric Microphones

Applications are voice activated and blood pressure measurement devices.

2.6.5 Electret Microphones

An electret is a close relative to piezoelectric materials. " An electret microphone is an electrostatic transducer consisting of a metallized electret diaphragm and backplate separated from the diaphragm by an air gap."

2.6.6 Solid-State Acoustic Detectors

Acoustic waves propagating in solids are used extensively in electronic devices such as electric filters, delay lines, microactuators, etc. [29]

2.7 Humidity (Hygrometers) and Moisture Sensors

2.7.1 Capacitive Sensors

An air filled capacitor can be used as a relative humidity sensor because moisture in the atmosphere changes air electrical permitivity.

2.7.2 Electrical Conductivity Sensors

The sensor contains a material of relatively low resistivity, which changes significantly under varying humidity conditions.

2.7.3 Thermal Conductivity Sensors

A thermistor based sensor is used to measure the thermal conductivity of a gas, which can be used to determine humidity.

2.7.4 Optical Hygrometer

The surface of a mirror is controlled at the threshold of dew formation. Sampled air is pumped over the mirror surface and if it crosses the deposit, moisture is released and then the reflective properties of the mirror change, which can be detected by a photodetector.

2.7.5 Oscillating Hygrometer

This hygrometer is the same as the optical chilled mirror sensor, except that the changing mass of the chilled plate is detected instead of the optical reflectivity. [29]

2.8 Light Detectors

The sensor being used in this experimentation was a light detector because it detected light in the spectral range. Light detectors are one of two different types: quantum or thermal. Quantum detectors are used in the ultraviolet to mid-infrared spectral ranges and thermal detectors are used in the mid and far infrared spectral ranges.

The theory behind a light detector is that the energy of a photon (energy concentrated into localized bundles) is given by:

$$E = h\nu \tag{2.1}$$

Where:

$h = 6.63 \times 10^{-34}$ J·s (Planck's constant)

If a semiconductor material is exposed to radiant energy: the photon transfers its energy to an electron. If the energy is sufficient for the electron to jump the energy gap, an electric current is produced.

If the energy of the photon striking the semiconductor crystal is high enough, to separate the electron from its site and push it into the conduction band, the electron will serve as a current carrier. The hole left in the valence band is also a current carrier. [29]

2.8.1 Photodiodes

Semiconductor optical sensors. [29]

2.8.2 Phototransistors

A photodiode converts photons into charge carriers – one electron and one hole per photon. [29]

2.8.3 Photoresistors

A photoconductive device like the one used in this experiment. The most common materials for fabrication are cadmium sulfide (CdS) and cadmium selenide (CdSe). Cadmium sulfide is most sensitive at shorter wavelengths. (The material used in this study was cadmium sulfide.) Cadmium sulfide is a semiconductor materials whose resistance changes with light.

A photoresistor requires a power source. [29]

In darkness, the cadmium sulfide photoresistor has a high resistance and when voltage is applied, there will be a very small current due to a temperature effect. When light is directed towards the cadmium sulfide surface, current will flow.

In the dark, electrons and holes are locked in place, but when light illuminates the cadmium sulfide semiconductor material, the electrons in the valence band absorb photons of energy and are moved up to the conduction band. This movement of electrons leaves behind free holes in the valence band, increasing the conductivity.

There is an acceptor level between the conduction band and the valence band and this acceptor level cannot accept electrons as readily as the holes can, the electrons remain in the conduction band and the current is high. Cadmium sulfide has a band gap energy of 2.41 eV and wavelength is approximately 515 nanometers. This wavelength is in the visible spectral range. [29]

2.9 Thermal Detectors (Radiation Thermometry)

Primary use of thermal detectors is for noncontact temperature measurements.

Typical infrared noncontact temperature sensors consist of:

- *Sensing Element* – responsive to infrared electromagnetic radiation.
- *Supporting Structure* – holds the sensing element.
- *Housing* – for protection from the environment.
- *Contacts* – wires or conductive epoxy.
- *Protective Window* – transparent to the wavelength of detection. [29]

2.9.1 Thermopile Sensors

Thermopiles are passive infrared sensors. (Passive infrared sensors depend on both the ambient and the object temperatures). [29]

2.9.2 Pyroelectric Sensors

A passive infrared sensor, which usually has two sensing elements in series or in parallel. [29]

2.9.3 Active Far Infrared Sensors (AFIR)

The sensor's surface is controlled to be constant, and the thermal radiation lost is measured. [29]

2.9.4 Gas Flame Detectors

These detectors use the UV spectral range. [29]

2.10 Radiation Detectors

Based on the fact that certain naturally occurring elements are not stable and are radio-active since they emit a portion of their nucleus.

2.10.1 Scintillating Detectors

A radiation detector composed of a scintillating material (a material able to convert radiation into light and an optical photon detects the light).

2.10.2 Ionization Detectors

Detectors that measure the separation of ions in an electrostatic field.

2.10.3 Semiconductor Detectors

These types of radiation detectors have the best energy resolution and are based on the fact that radiation results in a large number of carriers, which form an electric current, when an electric field is applied to the semiconductor. [29]

2.11 Electromagnetic Field Detectors

2.11.1 Magnetic Field Sensors (Magnetometers)

Sensors used to measure magnetic fields, such as a magnetic compass for navigation.

2.11.2 Flux Gate Sensor

Based on the Flux-gate principle.

2.11.3 Hall Effect Sensors

Can detect direction and intensity of magnetic fields.

2.11.4 Magnetoresistive Sensors

These sensors are based on the detection of the ability of a current-carrying magnetic material to change resistance in a magnetic field. [29]

2.11.5 Bolometers

Used for measuring r.m.s. values of electromagnetic signals over a very broad spectral range. [29]

2.12 Temperature Sensors

2.12.1 Thermoresistive Sensors

Temperature sensors based on the fact that the electrical resistances of various metals depend on temperature.

2.12.2 Resistance Temperature Detectors (RTD)

Metal sensors, usually in a wire or thin film form which use the temperature resistivities of metals for sensing temperature.

2.12.3 Silicon Resistive Sensors

Temperature sensors that use the conductive properties of bulk silicon for sensing temperatures.

2.12.4 Thermistors

A thermal resistor usually made of a metal oxide, composed of two groups: NTC (negative temperature coefficient) and PTC (positive temperature coefficient).

2.12.5 Thermoelectric Contact Sensors (Thermocouples)

The sensor is made-up of two different conducting materials. [29]

2.12.6 Semiconductor PN Junction Sensors

Temperature sensing takes place through a semiconductor pn-junction in a diode and a bipolar transistor. [29]

2.13 Optical Temperature Sensors

Temperature sensing by one of the following optical devices:

2.13.1 Fluoroptic Sensors

The response signal given by a special phosphor compound is used to sense temperature due to the fact that light is function of temperature.

2.13.2 Interferometric Sensors

A sensor consisting of two interfering light beams (where one beam travels through a temperature sensitve medium. The delay of the beam is dependent on temperature.

2.13.3 Thermochromic Solution Sensors

A sensor based on the theory that the spectral absorption of a thermochromic solution such as cobalt chloride is temperature dependent. [29]

2.14 Acoustic Temperature Sensors

A temperature sensor based on the relationship between the temperature of a material and the speed of sound. These types of sensors are used for measuring temperatures in extreme conditions such as for cryogenic temperature ranges or in nuclear reactors. [29]

2.15 Piezoelectric Temperature Sensors

A temperature sensor based on the fact that the angle of cut in a crystal shows a slight temperature dependence. [29]

2.16 Chemical Sensors

Sensors able to detect various chemicals.

2.16.1 Enzyme Sensors

Sensors that use enzymes selective ability to react with a specific chemical to detect that chemical. [29]

2.16.2 Catalytic Sensors

The heat liberated in a catalytic reaction of a chemical such as a combustible gas is measured. [29]

2.17 Thermal Sensors

Thermal sensors detect the heat change resulting from a chemical reaction. [29]

2.18 Electrochemical Sensors

The electrochemical sensors measure voltage, electric current or conductivity/resistivity due to a chemical reaction.

2.18.1 Potentiometric Sensors

Sensors that measure the electrical potential change due to a redox reaction.

2.18.2 Chemical Sensors that use Field Effect Transistors (CHEMFET)

Sensors - Solid state sensors that are either: ion selective, gas selective, enzyme-selective or immuno-selective. Applications for CHEMFET sensors include medical monitoring.

2.18.3 Conductometric Sensors

The change in conductivity of the electrolyte in an electrochemical cell is detected.

2.18.4 Amperometric Sensors

An application is oxygen sensors. An electrolytic solution is used to transport oxygen to the metal cathode and current is dependent on the partial pressure of the oxygen. [29]

2.19 Concentration Sensors

Physical sensors that respond to the concentration of a particular chemical.

2.19.1 Resistive Sensors

A sensor consisting of a matrix material whose resistance changes in the presence of a particular material.

2.19.2 Gravimetric Sensors

Sensors that detect mass by a shift in the resonant frequency of a piezoelectric crystal. [29]

2.19.3 Microbalance Odor Sensors

Based on the shift in the natural frequency of a quartz crystal coated with a odor sensitive membrane. Odor sensors can be classed into four groups: instrumental analysis, semiconductor gas sensors, membrane potential type and quartz microbalance sensors.

2.19.4 Fluid Density Sensors

There are five types of fluid density sensors: inertial mass, gravitational mass, buoyant force, hydrostatic pressure measurements or attenuation of γ-rays, which are then relate to the fluid density. [29]

2.20 Optical Chemical Sensors

These sensors monitor some change in the properties of radiation, such as intensity or polarization, on interaction with matter. [29]

2.21 Oxygen Sensors

Oxygen sensors are needed in many areas such as: environment, industry, transportation, medicine and agriculture. [30]

Many oxygen sensors are used as exhaust gas sensors in automobiles and may soon be used in motorcycles and diesel powered vehicles. Demand for new oxygen sensors are high due to strict European regulations for exhaust gas from cars produced

after 2000 and there is generally a demand for oxygen sensors to detect oxygen in exhaust gases from all combustion processes. [31, 32, 33]

Currently the oxygen sensors used as exhaust gas sensors use concentration cells consisting of an oxygen-ion conductor, which detects the difference of oxygen concentration between a reference electrode and a sensing electrode. The structure of these sensors is complicated and they are large in size. Resistive type oxygen sensors would be smaller in size but need a fast response time to replace current oxygen sensors. [34]

Much research has been focused on zirconia-based galvanic sensors and cobalt oxide or titania based conduction type devices and most commercial oxygen sensors are lambda sensors with a solid electrolyte of ZrO_2. [32, 33]

Potentiometric or amperometric solid state electrolyte oxygen sensors are used in many instances. Potentiometric sensors need reference gases and give logarithmic responses, which does not have adequate sensitivity in certain instances. An amperometric sensor's performance is related to its method of preparation. [30]

Conductometric sensors containing semiconducting metal oxides (TiO_2, Nb_2O_5, $SrTiO_3$, and CeO_2) are being studied because they operate at low temperatures. The surface conduction of the sensors changes in relation to adsorption of a gas. The adsorbed gas atoms either inject or extract electrons from n-type semiconducting material and studies are being made into combining different metal oxides to make sensors with larger responses. [35]

Thin-film gas sensor technology is developing to make a more compact, simpler sensor but it is still difficult to make a sensor which contains all desirable features such as: stability, reproductivity, lifetime, etc. [33]

2.21.1 Resistive Cerium Oxide Sensors [31]

Resistive oxygen sensors are compact and cerium oxide sensors have a fast-response because of a high diffusion coefficient for oxygen.

Cerium oxide porous thick films with an average particle size of 100 nm were screen printed on an alumina substrate. It was found that if 100 nm particles of cerium oxide were use, response timers were less than 1 second at 1100 K. [34]

2.21.2 SrF_2 – Based Sensors [32]

This oxygen sensor consists of a reference electrode: Air(O2)/Pt, a solid electrolyte SrF_2 and a sensing Platinum (Pt) electrode. In this sensor, there is a relationship between the electromotive force (EMF) and the oxygen partial pressure, which follow the Nernst equation. [32]

2.21.3 Gallium Oxide Thin Film Sensors

Gallium oxide thin films of about 1 micron were deposited on Si substrates. Gallium oxide is an n-type semiconductor and is able to detect oxygen at temperature over 900°C. Results show a resistance change of 4.5×10^4 ohms, with a response time of 70 seconds. [33, 36]

2.21.4 Undoped Ceria (Cerium Oxide) Sensors

Promising results have been obtained for a thin film of cerium oxide on sapphire.

The electrical conductivity (σ) Ceria is directly proportional to the partial pressure of oxygen (P_{O2}) to the −1/4 power as follows:

$$\sigma = A(T)\, P_{O2}^{-1/4}$$

where A(T) is the temperature dependent constant. [30]

Resistance changes at 700-750°C were shown to be in the 10^6ohm range from oxygen partial pressures of 0.03 to 1.5 psi. [30]

Reference 34 contains the kinetic behavior of these types of oxygen sensors. [34]

2.21.5 Ga Oxide-Zn Oxide Thin Film Sensors

A gallium oxide/ zinc oxide thin film was deposited on a single silicon crystal and prepared by the sol-gel process. The sensor could detect 100 ppm oxygen concentrations and show resistances of 10^8 ohms. [35]

2.21.6 Quenched-Luminescence Based Sensors

Molecular oxygen's ability to quench photoluminescent dyes allows its quantity to be determined. Luminescent probes can be placed in test samples for the monitoring of tissue oxygenation, oxygen uptake rates by biological samples, cellular respiration and enzyme activity. [37]

2.21.7 Electrochemical Sensors

These electrolytic type sensors are based on the use of a capillary or solid membrane, which controls gas diffusion into a cell where the following reactions with oxygen occur.

$$O_2 + 2H_2O + 4e^- \rightarrow 4OH^-$$
$$2Pb + 4OH^- \rightarrow 2PbO + 2H_2O + 4e^-$$

The current generated is proportional to the oxygen concentration. [38]

2.21.8 Strontium Titanate Based Materials Sensors

These sensors are resistive type oxygen sensors. The titanate has poor stability with the sulfur compounds present in exhaust gases, so a newly developed porous sulfur adsorber film made from earth alkaline carbonates as sulfur adsorbing components, helps to avoid this problem. [39]

This sensor measured % oxygen from 0.05 to 100% with resistances in the 10^5 ohm range. [39]

2.21.9 Cadmium Sulfide Sensors

Interactions between chemisorbed oxygen and cadmium sulfide surfaces is explored in reference 40. [40]

A cadmium sulfide thin film (20-30 microns thick) oxygen sensor was made by electrohydrodynamic spray pyrolysis of 0.01-0.06 molar solutions of $CdCl_2$ and $(NH_2)_2CS$ (670 – 750 K) on a glass substrate according to the following reaction:

$$CdCl_2 + (NH_2)_2CS + 2H_2O \rightarrow CO_2 + 2NH_4Cl + CdS \quad [40]$$

The average grain size of the films was 100 to 200 nanometers, and there was a ratio of Cd to S atoms of 2.4 at the film surface. [40]

The change in current of the CdS thin film sample to a fast change from nitrogen to dry synthetic air at 390 K was approximately 0.15 amps, showing that the CdS could detect oxygen presence. [40]

Cadmium sulfide was also shown to be able to detect the presence of oxygen in reference 41. It was determined that negative ions can be reversibly adsorbed on an insulating photoconductor at room temperature under the action of bandgap light. In

order to show a large response the photoconductive channel must be confined near the illuminated surface. [41]

The voltage used in reference 41 was 10 Volts and the light source was a microscope illuminator (0.068 Watts/square meter) with a Corning 5-58 and 1-69 filter pair. A Keithley 610-A electrometer was used. It was found that more reproducible results were obtained when the sample was first heated above 373 K. It was determined that after this treatment atmospheric sensitive photoconductivity parameters were completely reversible over the 243 K to 441 K temperature range. [41]

The change in current over time was about 8 X 10^{-6} amps over a 5-minute period due to oxygen uptake. According to reference 41: "The effect of exposing the charge covered surface to oxygen would be the initial formation of oxygen ions at the sites of the trapped electrons followed by the neutralization of the neighboring trapped holes. This mechanism not only accounts for the removal of the trapped charge on exposure to oxygen, but also explains the removal of the traps themselves. The oxygen-free surface is covered with traps for carriers of both signs. On exposure to oxygen, the adsorbed oxygen on the surface converts the surface traps into recombination centers via the chemisorption mechanism, thus reducing both the free electron lifetime and the response time, the latter much more than the former." [41]

"The mechanism causing the change in the photoconductive behavior on adsorption is evidently very complicated." [41]

The surface in CdS is excited to about 1 micron in depth. When oxygen is exposed to the CdS surface, the photocurrent drops such that the initial current follows the Elovich kinetics (after several seconds). The build-up of a steady-state surface

coverage of adsorbed ions proceeds according to the Elovich equation, while diffusion of electrons to the surface is the rate-determining step. A dynamic equilibrium is established involving the flow of charge to the surface from the bulk and the flow of gas to and from the surface. [41]

It was shown that the CdS surface was freed of adsorbed gas by passing dry nitrogen over the surface while it was illuminated with bandgap light, and the effect was found to be completely reversible at room temperature. [41]

According to reference 42, CdS crystals are all highly photosensitive in the absence of adsorbed oxygen regardless of the kind of impurity incorporated. If the pure crystal is made thin (less than a few hundred microns) enough, though oxygen adsorption obscures this property. [42]

If CdS crystals are made incorporating halogens, the halogen appears to supply electrons to reduce the effects of adsorbed oxygen and the CdS becomes more photosensitive. [42]

According to reference 6, oxygen is adsorbed on CdS surfaces in the form of radicals. [6] Experimental evidence has shown that the metal cadmium atoms are the basic centers of oxygen chemisorption on the CdS surface. [5, 8]

Table 2.1 lists the different types of oxygen sensors and their corresponding signal magnitudes in ohms.

Table 2.1 Change in Resistance and Current Data for Various Oxygen Sensors

	Oxygen Concentration		Change in Resistance	Change in Current
	Psi	%	(Ohms)	(Amps)
1) Our Sensor (CdS/Rhodamine B dye)	0→17.3	0→20	10^{10}	10^{-9}
2) CdS [41]		100		10^{-6}
3) CdS [13]		20		10^{-7}
4) Ga_2O_3 [36]		100	10^5	
5) $SrTiO_3$ [10]	14.7		10^5	
6) SnO_2 [13]		100		10^{-5}
7) Ga-Zn Oxide [35] (100 to 10,000 ppm)			10^9	
8) Cerium Oxide [30]	1.5		10^5	
9) Silicon based yttria-stabilized zirconia [43]		20		10^{-7}

2.22 Toluene Sensors

Gas detecting devices include: metal oxides, electrochemical sensors, conducting polymers, field effect transistor devices, surface acoustic wave devices and hybrid sensor arrays. [45]

Acoustic wave devices can be used for chemical sensing. Changes in wave velocity, frequency and/or amplitude can be used to determine surface charges.

Volatile Organic Compound (VOC) detection is now required in sub-part per million concentrations at ambient conditions. Other requirements for a toluene sensor include: small size, portability and low cost. [46]

2.22.1 ZnO-TiO_2 Thick Film

A resistance type gas sensor, which is a semiconductor. On contact with oxygen adsorbed oxygen transforms slowly into O^- and O^{2-} ions by extracting free electrons and conductance decreases. [47]

TiO_2 doped ZnO adsorbs more oxygen than pure ZnO. [47]

These sensors are fairly good at detecting VOC's like toluene by the following oxidation reactions:

$$VOCs + O^- \rightarrow VOCs\text{-}O + e\text{-}$$
$$VOCs + O^{2-} \rightarrow VOCs\text{-}O + 2e\text{-}$$

The sensitivity of the sensor to toluene increases with the weight percent of TiO_2 in the ZnO film. [47]

2.22.2 Piezoelectric Quartz Sensor Coated With Polydimethylsiloxane, Polycyanopropylmethylsiloxane, Polyethycellulose and Polyetherurethane

These sensors were able to predict toluene when mixed with octane or chloroform. [46]

2.22.3 An Array of Ten SnO_2/Ca, Pt Based Metal Oxide Sensors

An array of ten SnO2/Ca, Pt based metal oxide sensors were prepared with the following dopants:

Table 2.2 Dopants Used for the SnO2/Ca, Pt Based Metal Oxide Sensors

None
Pt (1 weight %)
La_2O_3 (5 weight %)
CuO (5 weight %)
Pd (3 weight %)
Sc_2O_3 (3 weight %)
TiO_2 (1 weight %)
WO_3 (10 weight %)
ZnO (1 weight %)
Pd (3 weight %) + V_2O_5 (0.5 weight %)

Sensors 4 and 8 had the largest sensitivity to toluene. [45]

Another metal-oxide gas-sensor array was made. The sensor array chip contained four pairs of sensing elements of SnO2, ZnO and WO3 with and without dopants such as Pd,

Al, Cr, Zn, Ag, and Ni. The sensor array was able to detect 100 ppm toluene concentration. [48]

A tin oxide based gas sensor array capable of measurements and analysis of toluene in a hydrocarbon mixture with butanol is explored. [49]

2.22.4 Conducting Polymers (Polyaniline and Polypyrrole) Thin Films

Exposure to vapors of aliphatic and aromatic hydrocarbons, such as toluene leads to a change in resistance of the polymer. Exposure to laboratory air saturated with toluene vapor saw a change in resistance of 10^6 ohms due to the toluene exposure of the sensor, and the sensor showed a negligible response to water vapor in air. [50, 52]

These conducting polymers have versatility in terms of composition, physical form and the nature of the analyte to be detected. A conducting polymer sensor array was tested for its ability to detect benzene, toluene, ethylbenzene and xylene. The polymer sensors containing a 4,5-dihydroxy-1,3-benzenedisulfonic acid (Na salt), tiron dopant had the highest sensitivity to toluene. [51]

Conductive polymers have been constructed into composites using carbon black, carbon fibers or conductive polymers. Conductive polymer composites have been shown to be able to detect toluene. [53]

2.22.5 Chemiresistor Coatings Prepared From Organically Encapsulated Gold Nanoparticles Sensors

Toluene molecules are adsorbed within the organic matrix with these gas-sensing films. The change in resistance over initial resistance for toluene varied from 0 to 1.8% over a 0 to 3000 ppm concentration of toluene in the vapor phase. [54]

2.22.6 Polymer-film-coated Quartz Resonator

A propylene-butyl-film-coated quartz resonator gas sensor was found to have excellent selectivity and sensitivity for toluene gas. [55]

2.22.7 Porous Silicon Based Sensors

Porous silicon has a strong room temperature visible photoluminescence and porous silicon has a porosity of 60%. These electrical devices can be used for gas sensing of toluene vapor. [56]

2.22.8 Copper (II) tetra-(tert-butyl)-5,10,15,20-tetraazaporphyrin Langmuir-Blodgett Film Sensors

There has been shown to be an interaction between the above mentioned films and toluene vapor. These films show good gas sensing of toluene vapors at room temperature. [57, 58]

Langmuir-Blodgett (LB) films of the coordination polymer poly(CuMBSH) have also been used for the detection of toluene. [58]

2.22.9 Polymer Gate FET Sensor Array

Catalytic metals, used as gate material, have a high sensitivity to hydrogen-containing gases like toluene. A poly(styrene-co-butadiene) FET was able to detect 1316 ppm of toluene at 37 °C. [59]

2.22.10 Surface Plasmon Resonance Optical Fiber Sensor Coated with Fluoropolymer

These sensors involve the use of a surface plasmon resonance (SPR) fibre optic which has a 50 nm thick silver film on a silica core of the optical fibre. A chemical sensing thin

film of fluoralkysiloxane was then deposited onto the surface. These systems are used for optical sensing. Interaction between toluene and the polymer are related by the partition coefficient, K, and the best sorption of toluene in the film leads to the lowest limit detection. [60]

2.22.11 SiO_2 and Al_2O_3 Selectively Permeable Coatings Sensors

A conductivity detector composed of SiO_2 and Al_2O_3 selectively permeable coatings prepared by chemical deposition on SnO_2 was shown to have a preference for toluene adsorption on the membrane surface. [61]

Tin oxide doped with platinum on an alumina substrate is semiconducting and can be used for the sensing of volatile organic compounds (VOC's). [62]

2.22.12 Iron Oxide Gas Sensors

Iron oxide was reported to have a high sensitivity to toluene. It was shown that compact films have a higher sensitivity to toluene than granular films. [63]

Table 2.3 Change in Resistance and Current Data for Various Toluene Sensors

	Change in Resistance (Ohms)	Change in Current (Amps)
1) Our Sensor (CdS/Rhodamine B dye) (100 ppm Toluene)	10^{10}	10^{-10}
2) Conductive Polymer Composite [53] (Saturated Atmosphere with Toluene)		10^{7}
3) Pd/WO3/SnO2 [48] (100 ppm Toluene)		10^{-6}
4) Porous Silicon Based Sensor [56] (3000 ppm Toluene)		10^{-10}

CHAPTER 3

THE ELECTRICAL AND CHEMICAL SYSTEMS USED FOR THE SENSOR EXPERIMENT

3.1 The Electrical, Chemical and Gas Chromatograph Systems Used for the Sensor Experiment

The gas sensor had three different systems included in the experimental apparatus. One system was electrical; one was chemical and the other was the system used with the gas chromatograph. The following three sections describe and provide diagrams of these three systems, which worked in tandem when performing the experiments described in this report.

3.1.1 The Electrical System for the Sensor Experiment

The following sections contain a list of the electrical equipment used in the electrical system of the sensor, as shown in Figure 3.1.

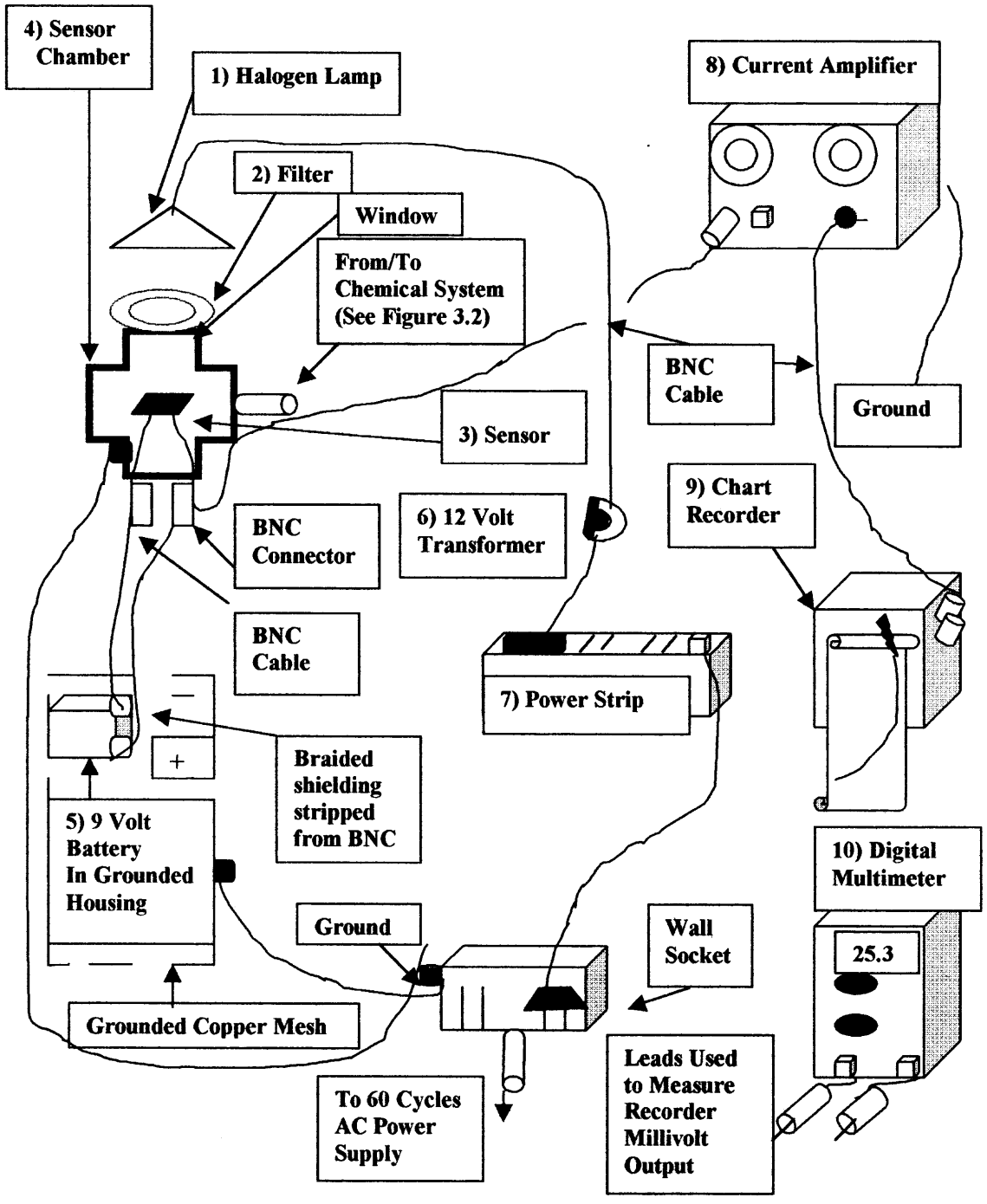

Figure 3.1 The electrical system for the sensor experiment.

The following is a list of the electrical equipment used in the electrical system for the sensor equipment:

1. Halogen Lamp – The halogen lamp was a 12-volt, 50-watt halogen flood light bulb, listed as giving crisp white light. It was bulb number MR16, manufactured by the General Electric Company.

2. Filter – The 500 nanometer central wavelength broadband interference filter was catalog number J46-157, ordered from:

   Edmund Industrial Optics
   Order dept. N997
   101 East Gloucester Pike
   Barrington, NJ 08007-1380

   The specifications of the filter are as follows:

   Tolerance = +/- 15 nanometers (400-700 nanometers)
   Full Width – Half Maximum: 80 nanometers +/- 25 nanometers
   Peak Transmittance (minimum): 60% (400 – 700 nanometers)
   Thickness: 0.18 inch, Broadband: 9.65 mm maximum
   Operating Temperature: -50°C to 75 °C
   Surface Quality: 80-50
   Angle Sensitivity: Intended for collimated input
   Blocking: ≤ 0.1%, X-ray to 1.2 microns
   Diameter: 24.15 millimeters; +/- 0.15 millimeters; 21.4 diameter minimum clear aperture.

3. Thin Film Sensor – Received from Dr. Vladimir Zaitsev of Moscow State University, Moscow, Russia. The sensor consists of a glass substrate on which a 0.5 micron thick cadmium sulfide (CdS) film had been deposited from a water solution. [64] A thicker filmed sensor (4.5 micron CdS film) was manufactured in house.

4. Sensor Chamber – The grounded sensor chamber was made of stainless steel and has an inside diameter of 6 centimeters. The chamber has four arms and is shaped as shown in Figure 3.1. It has a Pyrex glass window on the top vertical arm, which is facing the halogen lamp. The bottom vertical arm, opposite the top one with the window, has two BNC connectors, which connect the sensor with the electrical system. One of the horizontal arms was connected to the chemical system, shown in Figure 3.2, and was where gases were introduced and evacuated from the chamber.
   The chamber was obtained from Kurt J. Lesker Co.

5. 9 Volt Battery In Grounded Housing – The 9 volt battery used to supply the power to the sensor experiment was a common, household battery. The battery was placed in a metallic housing, which was grounded to the wall socket shown in Figure 3.1. This grounded housing was then surrounded with a copper wire mesh, which was also grounded, as shown in Figure 3.1. The voltage on the battery was checked frequently, using the digital multimeter, shown in Figure 3.1.

6. 12 Volt Transformer – The 12 volt transformer used was model number TW60A, and manufactured by Westek Co. The specifications on the transformer were:
   Primary volt: 120 volts; 60 hertz; 0.5 amps
   Secondary volt: 11.5 VAC; 5 amps, 60 watts

7. Power Strip – The power strip used was an Electricord XP, (Model A-1195004-AS), three line surge protector. The specifications on the power strip were as follows:
   Maximum load: 15 amps – 120 AC; 60 hertz
   Maximum suppression: 500 volts

8. Current Amplifier – (Picoammeter) model number 427, serial number 25017, Manufactured by: Keithley Instruments, Cleveland, Ohio.
   Range: 10^4 to 10^{11} volt/amp
   Output: +/- 10 volts at up to 3 milliamperes
   Output Accuracy: +/-2% of reading to the 10^9 volt/ampere range; +/- 4% of reading on the 10^{10} and 10^{11} volt/ampere range, exclusive of noise, drift and current offset.
   Current Suppression: 10^{-10} ampere to 10^{-3} ampere in eight-decade ranges with 0.1% resolution (10 turn potentiometer). Stability is +/- 0.2% of suppressed value per °C +/- 0.2% per day. [65]

9. Chart Recorder – The chart recorder was number 68B5, manufactured by Kipp and Zonen, Holland. The recorder was type BD41, number EV41, 875038. The specifications of the recorder were as follows:
   Approximately 110 volts, 300 milliamps, and 50/60 hertz.

10. Digital Multimeter – The LCD digital multimeter (catalog number 22-185A) was manufactured by Micronta, Radio Shack, (A Division of Tandy Corporation), Fort Worth, Texas 76102.

    The specifications of the multimeter were as follows:
    The digital multimeter was used to measure the potential output of the current amplifier in millivolts.
    The ranges and accuracy for these readings was: +/- 0.8% of the reading and +/-0.2% of the full scale and +/- 1 in the last digit.
    Operating Temperature: 0°C to 50°C

11. Megohmmeter – model 1000, serial #8705, catalog #185.100, manufactured by the AEMC Corp., 99 Chauncy St., Boston, Mass. 02111. (Used to double check the magnitude of the resistance readings).

Additional Equipment for Miscellaneous Experiments

12. 12 Volt Lead-Acid Battery- A 12 volt DC, 5 A rechargeable lead-acid battery was purchased from Radio Shack. The battery was catalog number 23-289 and is suitable for alarm system battery backup, hobbies and other 12-volt applications.

3.1.2 The Chemical System for the Sensor Experiment

The chemicals and equipment used in the chemical system of the sensor, shown in Figure 3.2, are listed in the following two sections.

3.1.2.1 Chemicals. A list of the chemicals used is as follows:

1. Conductive Paint – The silver paint used to make contact between the copper clips and the sensor was a high purity paint used for scanning electron microscope (SEM) sample preparation. The paint was air drying and conductive. It was catalog number 1050313 and obtained from:

   Division of Structure Probe, Inc.
   P.O. Box 342
   West Chester, PA 19380
   (800) – 242-4SPI

2. Zero Air - The specifications of zero air are: total hydrocarbons < 2.0 ppm, water < 3.0 ppm, O2 < 19.5 – 21.5%. The air was obtained from: Matheson Gas Products, 30 Seaview Drive, Secaucus, NJ 07096.

3. Zero Nitrogen – The specifications on the cylinder were: 99.998% N2, CH4 < 0.5 ppm. It was obtained from: Matheson Gas Products, East Rutherford, NJ.

4. Toluene – The toluene used was 99% pure, by gas chromatographic analysis, and was manufactured by J.T. Baker Chemical Company. (CAS# 108-38-3)

5. Rhodamine B Dye – Xanthene derivative, fluorescent dye. [66]

6. Ethanol – The ethanol used was 95% denatured and was CAS# 64-17-5.

7. Potassium Carbonate – Anhydrous, Ventron Alfa Products, Beverly, Mass.

8. Potassium Acetate Crystals – 1-2919, Baker Chemical Co., Phillipsburg, NJ 08865.

9. Sodium Bromide – S-255, Fisher Scientific, Fair Lawn, NJ.

10. Potassium Hydroxide – Food grade, pellets, USP-FCC, 1-3146, J.T. Baker Chemical Co., Phillipsburg, NJ.

11. Sodium Chloride – 3616, granular, USP, Brothers Chemical Co., Orange, NJ.

12. Potassium Chloride – Crystalline, reagent, ACS, Brothers Chemical Co., Orange, NJ.

3.1.2.2 Equipment. Figure 3.2 is a schematic of the equipment used in the chemical system of the sensor experiment.

The following is a list of the equipment used for the chemical system of the gas sensor:

1. Vacuum Pump - manufactured by E. H. Sargent and Co., Chicago, Illinois. The vacuum pump was a Duo Seal vacuum pump, serial # 40626-0, manufactured by the W.M. Welch Manufacturing Co. The motor was an AC, 1/3 horsepower, 1725-RPM motor by General Electric. (MCD #5KH35KG113E)

2. Pressure Gauge - (used to monitor the pressure of the sensor chamber) was serial #AK00796, model# 61D-1A-0030 manufactured by Pennwalt, Wallace & Tiernan, Belleville, NJ. The pressure gauge measures a maximum of 30 psia (pounds per square inch absolute) and the case can take a maximum pressure of 150 psig (pounds per square inch gauge). The instrument was calibrated at 25°C for gaseous service and vertical mounting.

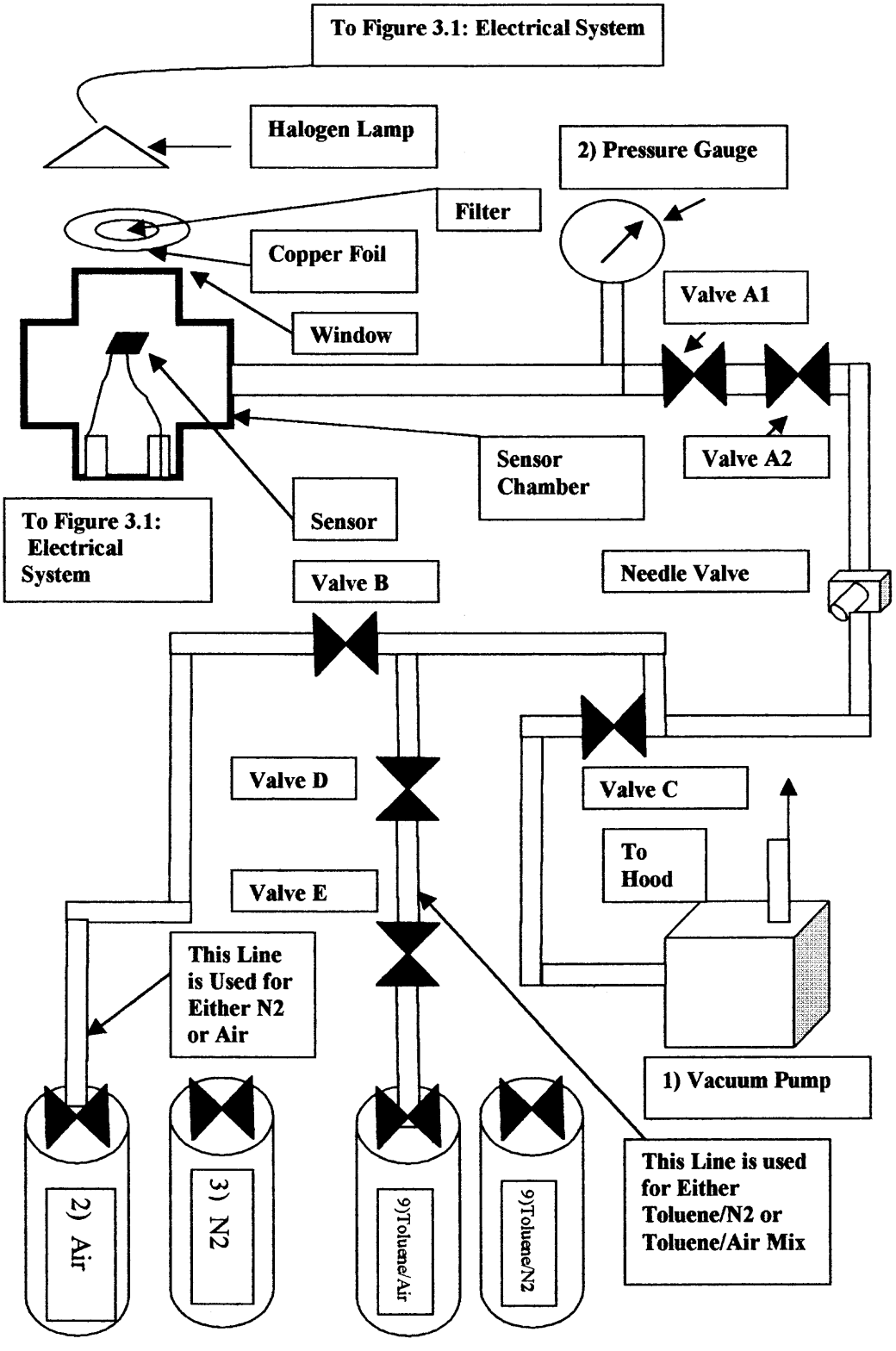

Figure 3.2 The chemical system for the sensor experiment.

3. Pressure Gauge and Regulator on Air Tank – Model 19-590 manufactured by Matheson Gas Products, East Rutherford, NJ. (The regulator was set at 40 psi throughout this experiment).

4. Pressure Gauge and Regulator on Nitrogen Tank- Model 11A; manufacturer: Scott Specialty Gases, Plumsteadville, PA. (The regulator was set at 40 psi throughout this experiment).

5. Pressure Gauge Used for Making Up Toluene/Air or Toluene/Nitrogen Gas Mixtures for Testing with the Sensor - Manufactured by SPAN Instruments, Plano, TX 10109. The maximum pressure on the face dial was 30 psig and the maximum vacuum on the face dial was 30"Hg (inches of mercury).

6. Syringe - 10-microliter glass chamber, GasTight #1701 and Microliter #701 manufactured by the Hamilton Co., Reno, Nevada.

7. Heat Gun – Master-Mite Heat Gun, model 10008, 120 volts AC, 60 hertz, 4.5 amps, serial #69991, manufactured by Master Appliance Corp.

8. Soldering Gun – 30 watt, 110/120 volt.

9. Gas Make-Up Tanks - Small, stainless steel interior passivated grab sampling containers, maximum pressure = 40 psig, serial numbers 02065 and 02067. Manufactured by: Scientific Instrumentation Specialists, Moscow, ID, USA.Large, cylindrical tank – 2000 psig, 28" high and 6" in diameter.

10. Bubbler – 29/42, Lab Glass Inc., Vineland, NJ.

11. Tubing – for the bubbler, Fisherbrand, ¼" ID X 1/16" wall.

12. Powerstat – Type 116, 120-volt, The Superior Electric Co., Bristol, Conn.

13. Thermocouple Thermometer – Model 115-KC-A-DSS, 115-volt, serial # 000474, Omega.

14. Compressor/Blower – This piece of equipment had no markings, NJIT Equipment # 00313.

3.1.3 The Gas Chromatograph System for the Sensor Experiment

This section contains a list of the equipment used in the gas chromatograph system of the sensor as shown in Figure 3.3.

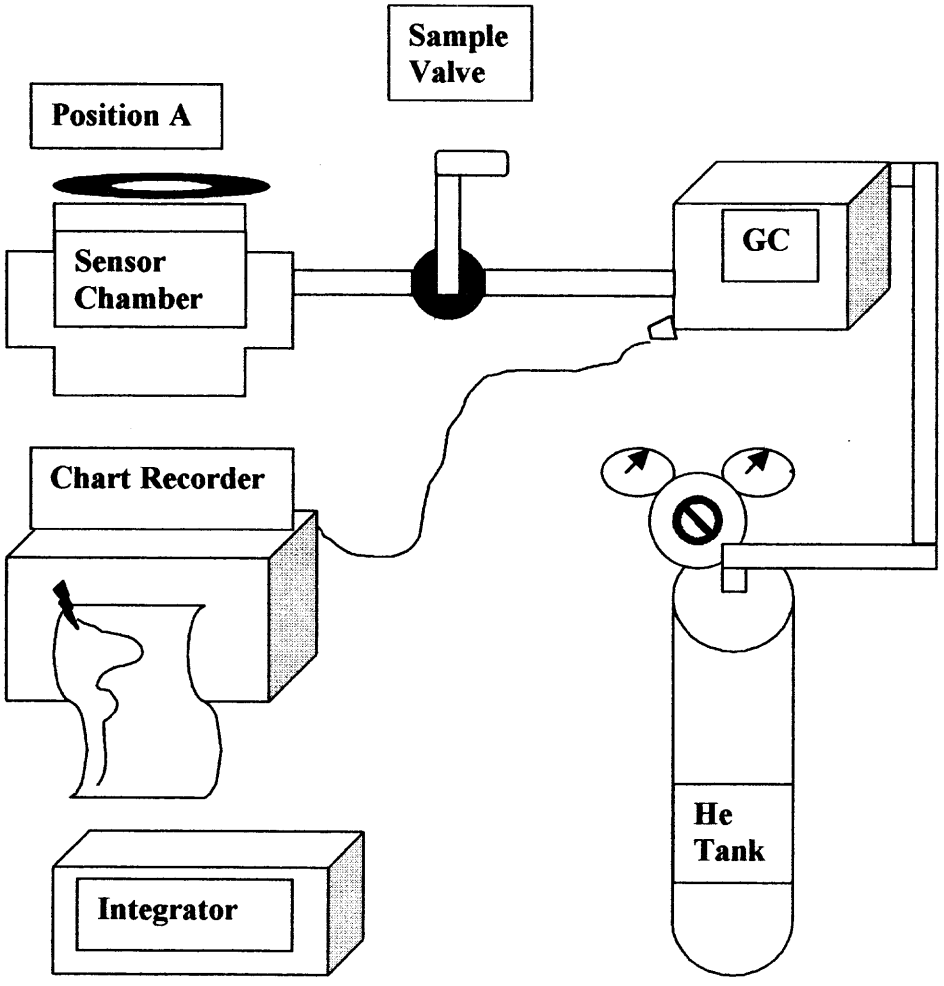

Figure 3.3 Flow diagram of the sensor/ GC set-up.

The equipment and supplies used in the gas chromatograph experiment are as follows:

1. Molecular Sieve - Binderless molecular sieve 5A, 60/80 mesh, #05432. Supplier: Applied Science Laboratories, Inc., P.O. Box 440, State College, PA, 16801.

2. Gas Chromatograph - Model GC-8A, serial # G5103 YS; 15-volt AC, 1500 VA, Shimadzu Corp; Kyoto, Japan.

3. Helium Gas Cylinder– Cylinder #841091Y; 291 cubic foot/2500 psig; received 2/3/94; zero grade, Manufacturer: Spectra Gases, Inc., 320 Mt. Pleasant Ave., Newark, NJ 07104.

4. Pressure Regulator for the Helium Gas Cylinder – Matheson tag # A-29050; reconditioned date 6-2-83; The Matheson Co., East Rutherford, NJ.

5. Timer - #1405, 120 V, 60 hertz, Kwik-set, LabChron timer; Manufacturer: Lab-Line Instruments, Inc., Designers and Manufacturers.

6. Integrator – Model #3390A; serial #2149A12788; 104-127 volts; 48-66 hertz, 40 VA maximum; 1 amp fuse; Manufacturer: Hewlett Packard.

7. Chart Recorder – Model # 1243, serial #1010; Manufacturer: Soltec.

8. Oven – Stabil-Therm oven; model #OV-8A; serial # XA-1550; temperature range = 38 to 260 °C; maximum watts = 500; 115 volts/1 phase; 50-60 cycles AC; Manufacturer: Blue M Electric Co., 138th and Chatham Sts, Blue Island, Illinois, USA.

9. Soap Film Flowmeter – 1-10-100 milliliter; #0101-0113; Manufacturer: Hewlett Packard.

10. Sampling Valve for the Gas Chromatograph - Manufacturer: Valco Instruments, P.O. Box 19032, Houston, Texas 77024. A diagram of the sampling valve is shown in Figure 3.4.

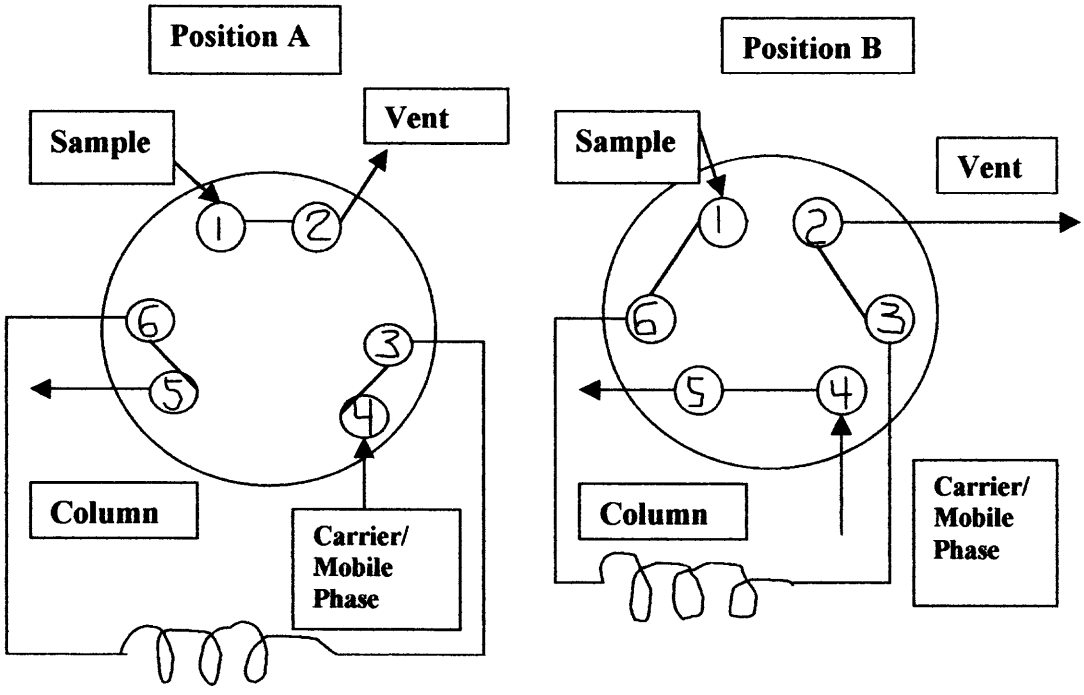

Figure 3.4 Sampling valve for the gas chromatograph. [70]

11. Porapak Q – 80/100, 6' X 1/8" stainless steel, 250° temperature limit, column # R09339, catalog # 1-2441, Alltech, Deerfield, IL.

CHAPTER 4

EXPERIMENTAL PROCEDURES

The experimental work for this portion of the report involved numerous runs. These experimental procedures and the corresponding results given in Chapter 6 and the Appendix are meant to be representative of the results, and do not include all of the data which were obtained. (The procedures shown in Sections 4.1 through 4.28 were performed with the halogen lamp on at all times while the procedure was being carried out unless specifically noted).

The data obtained from these experiments are listed in the Appendix. (Synthetic air is commercially available, zero grade air composed of approximately 20% oxygen and 80% nitrogen.)

4.1 Preparation of the Sensor Chip

The sensor chip, received from Dr. Zaitsev, was coated with a Rhodamine B dye made from a (0.1 milliliter)/ethanol (5.3 milliliter) mixture for 15 minutes and allowed to dry.

4.2 Preparation of the Thick Film (4.5 micron) Cadmium Sulfide Sensor/the Chemical Deposition of Cadmium Sulfide on a Glass Substrate [65]

The following chemical reaction was used to deposit cadmium sulfide on a thin glass substrate (1" X 3" and 1 millimeter thick). (The substrate used was Gold Seal microscope slides.) [65]

$$Cd(NH_3)_4^{2+} + SC(NH_2)_2 + 2OH^- \rightarrow CdS_{(s)} + CH_2N_2 + 4NH_3 + 2H_2O$$

The reactants and concentrations used to achieve this reaction are:

0.033M Cadmium Acetate ($Cd(OOCCH_3)_2 \bullet 2H_2O$)
1M Ammomium Acetate ($CH_3CO_2NH_4$)
0.067M Thiourea (H_2NCSNH_2)
28-30% Ammonium Hydroxide (NH_4OH)

The procedure used for deposition was as follows:

1. The proper amount of distilled water was placed into a 100 milliliter beaker containing a magnetic stirrer and the water was heated to 90°C on a hot plate/stirrer.

2. The chemicals were then added in the following order:

    a) Cadmium Acetate
    b) Ammonium Acetate
    c) Ammonium Hydroxide Solution (28-30%)

    Note: It was experimentally determined that the addition of the ammonium hydroxide solution to the 90°C water followed by the addition of the cadmium acetate resulted in the immediate precipitation of a white solid from the bath. The white solid was not soluble to any great extent in the water. When additional water was added, the solid still did not dissolve in the solution. It is believed that the precipitate was cadmium hydroxide, which is a white solid that isn't very soluble in water. [65]

3. After the above three chemicals (a-c) were added, the glass slide was added to the beaker and the solution was heated back to 90°C.

4. After the solution reached a temperature in the 85-90°C range, the thiourea additions were started. Reference 65 states that the thiourea must be added at 5 minute intervals, and cannot be added too fast or precipitation of the cadmium sulfide will occur at too fast of a rate for proper deposition on the glass slide to occur. It was also determined by experimentation that addition of thiourea at too fast a rate resulted in a rapid precipitation of cadmium sulfide, and was not good for deposition onto the glass slide. The thiourea was added at 5 to 10 minute intervals over an approximate 4 and ½ hour deposition period. The time differed for deposition numbers 18 and 20 due to other activities that required a shorter deposition time. [65]

5. The depositions were continued until after the 20^{th} deposition, when the cadmium sulfide film started to delaminate from the sides of the microscope slide. It was determined that this was the limit to the thickness of the cadmium sulfide thin film on the slide, and the depositions were discontinued at this point.

6. A portion of the slide containing the cadmium sulfide thin film was broken off from the rest of the slide using a diamond tipped pen. The size of the piece broken off was approximately equal in length and width to the original sensor chip.

7. The chip that had been sectioned off was then put into a muffle furnace at 500 °C for 30 minutes and allowed to cool.

8. The chip was then attached to the electrical setup in the same way as the original chip had been, using silver conductive paint to make sure that there was good electrical contact.

A chronological history of the cadmium sulfide deposition is listed in Table 4.1.

Table 4.1 The Deposition of Cadmium Sulfide on the Test Sensor Chip

Deposition #	Area of Square Covered $(Inch)^2$	Amount of Thiourea Added (grams)	Time of Deposition (Hours)	Amount of Ammonium Acetate Added (grams)
1	4.50	0.52	4.40	7.71
2	4.50	0.52	4.40	7.71
3	2.24	0.26	4.40	3.90
4	2.24	0.26	4.40	3.90
5	2.24	0.26	4.40	3.90
6	2.24	0.26	4.40	3.90
7	2.24	0.39	4.40	5.85
8	2.24	0.39	4.40	5.85
9	2.24	0.39	4.40	5.85
10	2.24	0.39	4.40	5.85
11	2.24	0.39	4.40	5.85
12	2.24	0.39	4.40	5.85
13	2.24	0.39	4.40	5.85
14	2.24	0.39	4.40	5.85
15	2.24	0.39	4.40	5.85
16	2.24	0.39	4.40	5.85
17	2.24	0.39	4.40	5.85
18	2.24	0.39	1.00	5.85
19	2.24	0.39	4.40	5.85
20	2.24	0.39	3.70	5.85

Deposition #	Amount of Cadmium Acetate Added (grams)	Amount of Ammonium Hydroxide Added (grams)	Amount of Distilled Water Added (mls)
1	0.88	29	51
2	0.88	29	51
3	0.44	14	26
4	0.44	14	20
5	0.44	14	20
6	0.44	14	20
7	0.66	20	20
8	0.66	20	20
9	0.66	20	20
10	0.66	20	20
11	0.66	20	20
12	0.66	20	20
13	0.66	20	20
14	0.66	6	30
15	0.66	6	30
16	0.66	6	30
17	0.66	6	30
18	0.66	6	30
19	0.66	6	30
20	0.66	6	30

4.3 Test of the Response of the Sensor to Nitrogen
(Results discussed in Section 6.1)

1. The halogen lamp, power strip, recorder and current amplifier were turned on.

2. The vacuum pump was turned on and the sensor chamber was evacuated for 10 minutes. A final absolute pressure of approximately 4.2 psia registered on the pressure gauge.

3. Nitrogen was then added into the sensor chamber until a pressure of 22 psia was reached, and the sensor was left exposed to the nitrogen for 10 minutes.

4. Steps 2 and 3 were repeated two more times.

5. Then the sensor chamber was evacuated for another 10 minutes until a pressure of 4.7 psia was obtained in the sensor chamber.

6. The chamber was then filled with nitrogen gas until a pressure of 22 psia was reached on the pressure gauge.

7. The sensor was exposed to the nitrogen gas for 1 hour.

The following settings were used for this experiment:

Battery = 8.83 volts
Current Amplifier Settings:
Gain = 10^9 volt/amp
10^{-9} amp suppression

(During the run the difference between the mV readings obtained with the suppression on was approximately 20 mV less than those obtained when the zero suppression was used on the current amplifier). For this reason, 20 mV was added to each of the readings obtained with the suppression on.

4.4 Test of the Response of the Sensor to Synthetic Air
(Results shown in Section 6.2)

The following procedure was used for the synthetic air run on:

1. The halogen lamp, power strip, recorder and current amplifier were turned on.

2. The vacuum pump was turned on and the sensor chamber was evacuated for ten minutes. A final absolute pressure of approximately 4.5 psia registered on the pressure gauge.

3. Synthetic air was then added into the sensor chamber until a pressure of 22 psia was reached.

4. Steps 2 and 3 were repeated two more times.

5. Then the sensor chamber was evacuated for another 11 minutes until a pressure of 4.3 psia was obtained in the sensor chamber.

6. The chamber was then filled with synthetic air until a pressure of 22 psia was reached on the pressure gauge.

7. The air was exposed to the sensor for one hour.

The following settings were used for this experiment:

Battery = 8.84 volts
Current Amplifier Settings:
Gain = 10^9 volt/amp
10^{-9} amp suppression

(On 8/23/01, it was determined that a 10^{-8} amp suppression caused a decrease of 21.4 mV, whereas on 11/30/01 it was determined that a 10^{-10} amp suppression caused a decrease of 12.6 mV in the reading. These two values were averaged at 17.0 mV, and this was the value that was added to each of the readings to correct for the fact that the suppression was on while readings were being taken).

4.5 Test of the Response of the Sensor to Different Partial Pressures of Oxygen in Synthetic Air

(Results shown in Subsection 6.2.1)

1. The vacuum pump was used to evacuate the sensor chamber for 10 minutes.

2. A final absolute pressure of approximately 4.2 to 4.4 psia registered on the pressure gauge.

3. Nitrogen was then admitted into the sensor chamber and exposed to the sensor for 10 minutes.

4. Steps 2 and 3 were repeated alternatively, with vacuum (Step 2) being the last step until a baseline potential of 30.5 millivolts registered on the chart recorder.

5. Synthetic air was admitted into the sensor chamber. The amount varied for the various runs, and the pressures which registered on the absolute pressure gauge were as listed in Table 4.2.

Table 4.2 The Partial Pressure of Synthetic Air Admitted into the Sensor Chamber

4.7 to 22 psia (17.3 psia)
4.4 to 13 psia (8.6 psia)
4.4 to 9 psia (4.6 psia)
4.3 to 17 psia (12.7 psia)
4.3 to 20 psia (15.7 psia)
4.3 to 5.0 psia (0.7 psia)
4.6 to 7.0 psia (2.4 psia)

6. The air was allowed to stay exposed to the sensor for 30 minutes for each run. At the end of each run, steps 1 through 4 were repeated before starting the next run for the day. At the end of the day, the sensor chamber was cleaned out by evacuating and filling it with nitrogen, 10 minutes each, 3 times.

The following settings were used for this experiment:

Battery = 9.00 volts

Current Amplifier Settings:
10^{-10} amp suppression

(12.8 millivolts was added to the readings on 1/17, 12.6 millivolts was added to the readings on 1/18, 13.2 milivolts was added to the readings on 1/22 and 12.7 was added to the readings on 1/23)
Gain = 10^8 volts/amp

4.6 Resistance Versus Sensor Exposure Time to Synthetic Air and Nitrogen Mixtures Made-Up in the Sensor Chamber and Analyzed by a Gas Chromatograph/Chart Recorder

(Results shown in Subsection 6.2.2.1)

The procedure for these experiments was as follows:

1. Vacuum was applied to the sensor chamber for ten minutes followed by nitrogen (at 15 psig) for ten minutes. This procedure was repeated until a baseline of 26.3 millivolts was reached.

2. The amounts of air and nitrogen, as listed in Table 4.3, were added into the sensor chamber, for the different runs. (The air went in to the sensor chamber first so that the first exposure of the sensor to a higher oxygen content was not affecting the results).

Table 4.3 The Partial Pressures of Synthetic Air and Nitrogen Added to the Sensor Chamber

Run #	% O2	Amount of Synthetic Air	Amount of N2
1)	18.0	23.5"Hg to 15 psig	None
2)	8.9	24 "Hg to 1 psig	1 to 15 psig
3)	14.9	22.5"Hg to 10 psig	10 to 15 psig
4)	9.0	24.5"Hg to 1 psig	1 to 15 psig
5)	4.9	23.8"Hg to 12"Hg	12"Hg to 15 psig
6)	0	None	24.2"Hg to 15 psig
7)	3.2	22.5"Hg to 16.5"Hg	16.5"Hg to 15 psig
8)	1.3	20.5"Hg to 17.5"Hg	17.5"Hg to 15 psig
9)	3.2	24.5"Hg to 15.5"Hg	15.5"Hg to 15 psig
10)	5.0	22"Hg to 12"Hg	12"Hg to 15 psig
11)	12.5	24.5"Hg to 5.5 psig	5.5 to 15.0 psig
12)	15.5	24.5"Hg to 10 psig	10.0 to 15.0 psig
13)	19.5	24"Hg to 15 psig	None
14)	4.5	23.5"Hg to 11.5"Hg	11.5"Hg to 15 psig
15)	6.8	24.5"Hg to 3.5"Hg	3.5"Hg to 15 psig
16)	10.8	24.5"Hg to 2.5 psig	2.5 to 15 psig

3. The mixture was allowed to sit in the sensor chamber for 60 minutes.

4. The concentration of oxygen in the mixture in the sensor chamber was determined by sending a small amount of the gas mixture in the chamber to a gas chromatograph.

4.7 Resistance Versus Sensor Exposure Time to Synthetic Air and Nitrogen Mixtures Made-Up in a Mixing Tank and Analyzed by a Gas Chromatograph/Chart Recorder

(Results shown in Subsection 6.2.2.2)

This experiment was different from the experimental procedure outlined in Section 4.6, because a smaller sampling loop was put into the GC sampling valve setup. Also the

synthetic air/nitrogen mixes were being made up in a tank, and the samples going into the GC were flowing at the time of measurement. For the duration of the sensor run, the air mixtures were just allowed to flow into a closed sensor chamber from a vacuum pressure of about 23 inches of closed until the run was over when the sample was then mercury to a pressure of 15 psig. The exit valve to the sensor chamber was then left sent to the GC for measurement. (The gas mixture was flowing into the GC at the time of sampling.)

The data obtained from these runs can be found in the Table A.7 and were measured using a chart recorder and weighing of the different portions of the curves as in Section 4.6.

4.8 Resistance Versus Sensor Exposure Time to Synthetic Air and Nitrogen Mixtures Made-Up in a Mixing Tank and Analyzed by a Gas Chromatograph/Integrator and Having an Initial Purge (10 Seconds) of the Sensor Chamber

(Results shown in Subsection 6.2.2.3)

This experimental procedure was different from the experimental procedure outlined in Section 4.7. GC data was taken using an electronic integrator and the sensor chamber was purged for the initial 10 seconds of the sensor run, and then the purge valve was closed and the synthetic air/nitrogen mixture allowed to fill the gas chamber to 15 psig. This was done to make sure that the gas mixture going into the GC was the same mixture that the sensor was exposed to for the 70 minutes duration time of the sensor run. (The gas mixture was flowing into the GC at the time of sampling).

4.9 Analysis of Resistance Versus Sensor Exposure Time to Different Synthetic Air/Nitrogen Mixtures Made-Up in a Mixing Tank and Allowed to Flow Through the Sensor Chamber for One Minute

(Results shown in Subsection 6.2.2.4)

The sensor chamber was prepared as outlined in experimental procedures Sections 4.6 through 4.8, by vacuum pumping and then nitrogen exposure for ten minutes each until the proper baseline reading was reached. The nitrogen/synthetic air mixtures were made up in a tank, and were allowed to flow through the gas sensor chamber for the first minute.

After the first minute the gas mixture was allowed to flow into the gas chromatograph for analysis.

4.10 Resistance Versus Sensor Exposure Time to Synthetic Air During Adsorption and Desorption

(Results shown in Subsection 6.2.2.5)

In this experiment, the sensor chamber was prepared as outlined in experimental procedure Sections 4.6 through 4.9. Starting at the same baseline resistance, synthetic air was then allowed to flow through the chamber for 25 minutes, and then vacuum was applied for the next ten minutes. Helium gas was applied for the ten minutes following the vacuum application to see if it had a greater desorbing ability than nitrogen. For the rest of the run, vacuum application and nitrogen addition were alternated for ten minutes each.

This experiment was repeated with atmospheric air using a compressor, starting at the same baseline resistance. The helium gas was not applied at anytime during the desorption run, however.

4.11 Determination of the Difference in Resistance Versus Time Between Two Identical Runs of Synthetic Air Versus Atmospheric Air
(Results shown in Subsection 6.4.1)

The sensor chamber was prepared as outlined in experimental procedure Sections 4.6 through 4.8, by vacuum pumping and nitrogen exposure for ten minutes each until the proper baseline reading was reached.

The purpose of this experiment was to determine the difference between the sensor's response to atmospheric air and the synthetic air. Atmospheric air was allowed to fill the chamber to zero psig on the pressure gauge and the response of the sensor was recorded. The run was then repeated in exactly the same way only with the synthetic air instead of the atmospheric air and the results were again recorded.

4.12 Repeat of the Experiment Outlined in Section 4.10 but Using Atmospheric Air Instead of Synthetic Air
(Results shown in Subsection 6.4.2)

This experiment used the same experimental procedure as outlined in Section 4.10, except that the air being used was atmospheric air (using a compressor) instead of synthetic air.

The baseline resistance or starting point resistance value for this experiment was the same as for the experimental procedure outlined in Section 4.10.

4.13 Repeat of the Experiment Outlined in Section 4.11 Using a Different Initial Resistance Value for the Atmospheric Air Run than the One Used for the Synthetic Air Run
(Results shown in Subsection 6.4.3)

In this experiment, the atmospheric air curve of resistance versus time obtained from the experimental procedure outlined in Section 4.11 was redone using a different baseline (a

much lower resistance value), to better correspond with the equilibrium resistance value obtained with the desorption portion of the curve.

A potential of 64.5 millivolts was used as the baseline with the atmospheric air instead of 27.3 millivolts, which had been used for both the synthetic and atmospheric air in Figure 6.33.

4.14 Testing of the Effect of Humidity on the Sensor

The objective of this series of experiments was to test the effect of gaseous water in nitrogen and synthetic air gases on the sensor. The method used was as follows:

A bubbler was used to humidify the gases. Different saturated salt solutions were placed in the bubbler and the gas was bubbled through the saturated salt solution prior to sensor exposure. This procedure was used to obtain various amounts of relative humidity in both nitrogen and synthetic air. The synthetic air and nitrogen gases were bubbled through the bubbler containing a saturated salt solution.

The amount of relative humidity in the resultant gas mixtures were calculated by using the Greenspan saturated salt table values.

The different salts used included: potassium hydroxide, potassium acetate, potassium carbonate, sodium bromide, sodium chloride and potassium chloride. The details on the chemical brands used are listed in Subsection 3.1.2.1.

The resistance of the sensor was measured versus exposure time to various nitrogen/water and synthetic air/water mixtures versus dry nitrogen and synthetic air. The data and results are shown in Section 6.5.

4.15 Preparation of Toluene in Air/Nitrogen Gas Mixtures

1. A 6-Liter spherical tank, as shown in Figure 4.1, was evacuated to 10 inches Hg.

2. Then synthetic air was allowed to flow into the tank until a pressure of 27.5 psig was registering on the pressure gauge.

3. Steps 1 and 2 were then repeated another four times.

4. The tank was then evacuated down to a pressure of 10 "Hg.

5. The piping inlet to the tank contained a fitting with a Teflon diaphragm type inlet, suitable for syringe injection of a liquid, and a pressure gauge as shown in Figure 4.1, labeled as the syringe insertion point.

4.16 Test of the Response of the Sensor to Toluene in Nitrogen

(Results can be found in Subsection 6.7.1)

The following procedure was used for the toluene/nitrogen run:

1. The halogen lamp, power strip, recorder and current amplifier were turned on.

2. The vacuum pump was turned on and the sensor chamber was evacuated for ten minutes. A final absolute pressure of approximately 4.4 to 4.7 psia registered on the pressure gauge.

3. Nitrogen was then added into the sensor chamber until a pressure of 22 psia was reached.

4. Steps 2 and 3 were repeated two more times.

5. Then the sensor chamber was evacuated until the graph baseline of about 48.7 mV was obtained.

6. The chamber was then filled with nitrogen gas until the following pressure was reached on the pressure gauge. Different pressures of nitrogen gas were used for different final concentration of gas as shown below:

Table 4.4 Concentrations of Toluene/Nitrogen Mixtures in Parts Per Million Versus the Pressure Obtained with Nitrogen

Concentration (ppm)	Pressure (psia) Obtained with Nitrogen
0.0	22.0
2.4	21.0
5.0	20.0
7.3	19.0
10.0	17.9
18.2	14.6
35.4	7.5

7. The sensor chamber was shut off using valve #A1.

8. The lines were conditioned by evacuating them for five minutes.

9. Then the 50 ppm gas mixture was put into the lines for two minutes followed by an evacuation for a couple of seconds.

10. Step 9 was repeated one more time.

11. The 50 ppm gas mixture was then put into the sensor chamber to make a total pressure of 22 psia on the gauge.

12. The gas mixture was allowed to stay in contact with the sensor for an hour.

13. The sensor was then cleaned by evacuation for ten minutes followed by filling the chamber with nitrogen, up to 22 psia, for another ten minutes.

14. Step 13 was then repeated two more times.

The following settings were used for this experiment: Gain = 10^8 volt/amp

Table 4.5 The Potential Readings on the Chart Recorder at Different Suppression Settings Versus Toluene/Nitrogen Concentrations

Concentration (ppm)	Recorder Reading (mV) With 10^{-8} Amp Suppression	Recorder Reading (mV) With Zero Suppression	mV Difference
2.4	40.0	60.0	20.0
5.0	34.0	55.4	21.4
7.3	33.5	52.7	19.2
10.0	40.0	60.0	20.0
18.2	33.5	52.7	19.2
35.4	34.0	55.4	21.4

4.17 Test of the Response of the Sensor to 35.4 ppm of Toluene in Nitrogen
(Results can be found in Subsection 6.7.1)

(Nitrogen data is from Figure 6.1 data graphed in Section 6.1); The procedure is given in Section 4.16.

4.18 Synthetic Air Run
(Results can be found in Subsection 6.7.1)

The procedure for the synthetic air run was made on:

1. The halogen lamp, power strip, recorder and current amplifier were turned on.
2. The vacuum pump was turned on and the sensor chamber was evacuated for ten minutes. A final absolute pressure of approximately 4.4 psia registered on the pressure gauge.
3. Nitrogen was then added into the sensor chamber until a pressure of 22 psia was reached, and the nitrogen was left exposed to the sensor for ten minutes.
4. Steps 2 and 3 were repeated two more times.
5. Then the sensor chamber was evacuated until the graph baseline of 27.2 mV on the 10-millivolt scale on the recorder was obtained.
6. The chamber was then filled with synthetic air until a pressure of 22 psia was reached on the pressure gauge.
7. The air was then evacuated immediately from the sensor until a pressure of 7 psia was reached. Steps 6 and 7 were then repeated.

4.19 Test of the Response of the Sensor to Synthetic Air
(Results can be found in Subsection 6.7.2)

The following procedure was used for the synthetic air run:

1. The halogen lamp, power strip, recorder and current amplifier were turned on.

2. The vacuum pump was turned on and the sensor chamber was evacuated for 10 minutes. A final absolute pressure of approximately 4.2 psia registered on the pressure gauge.

3. Synthetic air was then added into the sensor chamber until a pressure of 22 psi was reached. Steps 2 and 3 were repeated two more times.

4. Then the sensor chamber was evacuated for about 10 minutes until the graph baseline of about 61.5 mV on the 50 millivolt chart recorder scale was obtained.

5. The chamber was then filled with air until a pressure of 22 psia was reached on the pressure gauge. The air was allowed to stay in contact with the sensor for an hour.

   The following settings were used for this experiment:

   Battery = 8.84 volts
   Current Amplifier Settings:
   10^{-9} amp suppression
   Gain = 10^{9} volt/amp

4.20 Test of the Response of the Sensor to 29.3 ppm Toluene in Air
(Results can be found in Subsection 6.7.2)

The procedure used for the 29.3 ppm toluene/air run is shown below:

1. The procedural steps given in Section 4.19 preceded the steps shown in this section.

2. The vacuum pump was used to evacuate the sensor chamber for 15 minutes. A final absolute pressure of approximately 4.6 psia registered on the pressure gauge.

3. The chamber was then filled with synthetic air until a pressure of ten psia was reached on the pressure gauge.

4. The sensor chamber was shut off using valve #A1.

5. The lines were conditioned by evacuating them for five minutes.

6. Then the 50 ppm gas mixture was put into the lines for two minutes followed by an evacuation for a couple of seconds.

7. Step 6 was repeated one more time.

8. The 50 ppm gas mixture was then added to the sensor chamber to make a total pressure of 22 psia on the pressure gauge.

9. The gas mixture was allowed to stay in contact with the sensor for an hour. The following settings were used for this experiment: Battery = 8.84 volts;

   Current Amplifier Settings: 10^{-9} amp suppression (17 millivolts were added to the actual readings); Gain = 10^{9} volts/amp

4.21 Test of the Response of the Sensor to Synthetic Air
(Results can be found in Subsection 6.7.2).

The procedure is the same as that given in Section 4.4.

4.22 Test of the Response of the Sensor to 10 ppm Toluene in Air
(Results can be found in Subsection 6.7.2).

1. After the initial air run described in Section 4.4, the vacuum pump was used to evacuate the sensor chamber for 42 minutes. A final absolute pressure of approximately 4.3 psia registered on the pressure gauge.

2. Synthetic air was then added into the sensor chamber until a pressure of 17.9 psia was reached.

3. The sensor chamber was shut off using valve #A1.

4. The lines were conditioned by evacuating them for 5 minutes.

6. Then the 50 ppm gas mixture was put into the lines for 2 minutes followed an evacuation for a couple of seconds.

7. Step 5 was repeated one more time

8. Valve A1 was then opened and the 50 ppm gas mixture was then put into the sensor chamber to make a total pressure of 22 psia on the pressure gauge.

9. The gas mixture was allowed to stay in contact with the sensor for an hour.

The following settings were used for this experiment:
Battery = 8.84 volts; *Current Amplifier Settings:*
10^{-9} amp suppression (17 millivolts was added to the readings)

4.23 Test of the Response of the Sensor to 35.4 ppm Toluene in Air
(Results can be found in Subsection 6.7.2)

The following procedure was used for the 35.4 ppm toluene/air run:

1. The procedure given in Section 4.4 and Section 4.22 was first performed before this procedure.

2. The vacuum pump was used to evacuate the sensor chamber for ten minutes. A final absolute pressure of approximately 4.4 psia registered on the pressure gauge.

3. Synthetic air was then added into the sensor chamber until a pressure of 22 psia was reached.

4. Steps 2 and 3 were repeated three more times.

5. Then the sensor chamber was evacuated for about 25 minutes until the graph baseline of about 76 mV on the 50 millivolt chart recorder scale was obtained.

6. The chamber was then filled with air until a pressure of 7.5 psia was reached on the pressure gauge.

7. The sensor chamber was shut off using valve #A1.

8. The lines were conditioned by evacuating them for five minutes.

9. Then the 50 ppm gas mixture was put into the lines for 2 minutes followed by an evacuation for a couple of seconds.

10. Step 9 was repeated one more time.

11. The 50 ppm gas mixture was then put into the sensor chamber to make a total pressure of 22 psia on the pressure gauge.

12. The gas mixture was allowed to stay in contact with the sensor for an hour.

The following settings were used for this experiment:

Battery = 8.84 Volts
Current Amplifier Settings:
10^{-9} amp suppression (17 millivolts were added to the actual readings);
Gain = 10^{9} volts/amp

4.24 Test of the Response of the Sensor to 20 ppm Toluene in Air

(Results can be found in Subsection 6.7.2)

The following procedure was used for the 20 ppm toluene/air run:

The procedure given in Section 4.19 was performed before those shown in this section.

1. The vacuum pump was used to evacuate the sensor chamber for ten minutes. A Final absolute pressure of approximately 4.5 psia registered on the pressure gauge.

2. Air was then added into the sensor chamber until a pressure of 22 psia was reached.

3. Steps 2 and 3 were repeated three more times.

4. Then the sensor chamber was evacuated for about seven minutes until the graphbaseline of about 61.5 mV on the 50 millivolt chart recorder scale was obtained. Air was admitted into the sensor chamber until a pressure of 13.8 psia was obtained.

5. The sensor chamber was shut off using valve #A1.

6. The lines were conditioned by evacuating them for 5 minutes.

7. Then the 50 ppm gas mixture was put into the lines for 2 minutes followed by an evacuation for a couple of seconds.

8. Step 8 was repeated one more time.

9. Valve A1 was then opened and the 50 ppm gas mixture was then put into the sensor chamber to make a total pressure of 22 psia on the pressure gauge.

10. The gas mixture was allowed to stay in contact with the sensor for an hour.

The following settings were used for this experiment:

Battery = 8.84 volts

Current Amplifier Settings:

10^{-9} amp suppression (17 millivolts was added to each reading)
Gain = 10^{9} volts/amp

4.25 Testing of the Effect of Heat on the Sensor

A heating tape was wrapped around the sensor chamber as shown in Figure 4.2.

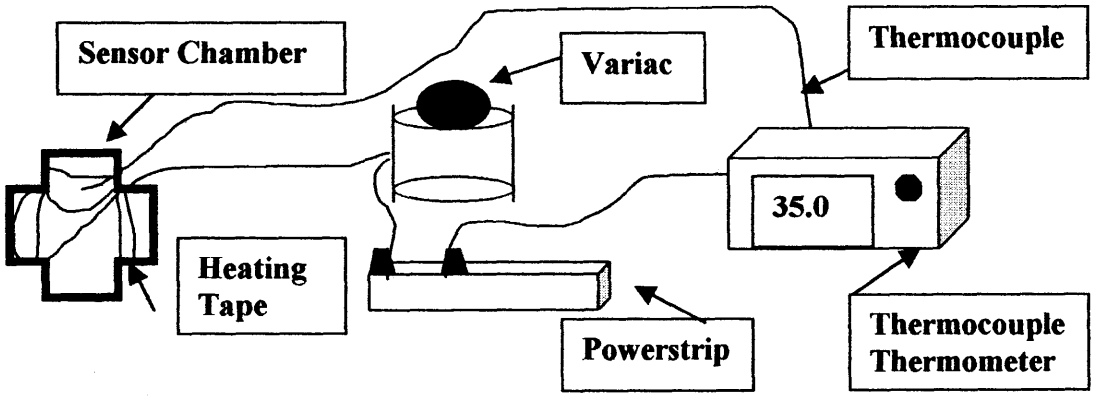

Figure 4.2 Heating tape set-up.

It was connected to a variac to regulate the temperature. A themocouple was attached to the outside wall of the stainless steel sensor chamber to measure the wall temperature of the sensor. (The thermocouple couldn't be placed inside the chamberbecause there is no provision for inserting it and it would interfere with the vacuum application.

4.25 Experiments to Minimize Electrical Noise

The initial measurements of the very high resistance of the sensors, initially had a lot of noise associated with them, which could be seen by the erratic readings on the chart recorder. In order to minimize this noise and obtain more reliable readings, experiments were undertaken to reduce the noise.

4.26.1 Experiment #1 – Using the Power Supply from a Spectrophotometer Instead of the 12-Volt Transformer

The 12-volt transformer, used to power the lamp was replaced by a power supply from a Spectronic 20 spectrometer, to determine if the transformer was the source of noise.

This experiment was undertaken to see if the 12-volt transformer was the source of the noise. The results from this experiment were that the halogen lamp was not as bright with the spectrophotometer as it had been with the 12 volt transformer. No change in response could be obtained with different concentrations of toluene, due to this decrease in the luminescence of the lamp.

4.26.2 Experiment #2 – Using a 12 Volt, DC, 5A Lead Acid Battery Instead of the 12-Volt Transformer

A Radio Shack 12 volt DC, 5A rechargeable lead acid battery was tried instead of the 12-volt transformer to check again if the 12-volt transformer was the cause of the noise.

When the12 volt DC battery was used to power the halogen lamp, it was still as noisy as it had been before with the 12-volt transformer, so it was concluded that the 12-volt transformer was not the source of the noise.

4.26.3 Experiment #3 – Checking the Effect of the Room Fluorescent Lighting on the Sensor

The fluorescent lighting in the room was shut off, but the noise continued; so the fluorescent lights were not the source of the noise.

Several references such as References 69 and 71 were consulted on noise problems. Dr. Farmer from the Microelectronics Lab at NJIT was also consulted on this topic. Since the sources of noise can be vast, the following methods were used to reduce the noise experienced in early experiments:

1. Using a single power strip, instead of multiple ones.
2. Keeping electrical wires separated and secured to benches.
3. Putting foam padding underneath the stand that holds the sensor chamber to help cushion any vibrations.
4. Grounding the sensor chamber, as well as the battery and the battery housing and the copper netting around the battery housing.
5. Keeping the electrical wire lengths as short as possible, by bringing the equipment closer together.
6. Using only BNC cable.
7. Using a sturdier stand to hold the sensor chamber. [69, 71]

The result was that the noise was reduced sufficiently so that reliable data could be obtained for the sensor experiment.

4.27 Procedure for Operating the Gas Chromatograph

The procedure for operating the gas chromatograph (to determine oxygen concentration is:

1. Open helium gas cylinder into the gas chromatograph (GC). (Figure 4.3)

2. Check flow rate of the helium coming out of the column with a soap film flowmeter. Make sure the flow rate of the helium gas is at least 30 milliliters per minute.

3. Set the injector/detector temperature at 200°C and the column temperature as low as possible. Paper towels that were soaked with very cold water were wrapped around the column. This reduced the column temperature a few degrees Celsius. [The lowest room temperatures gave the best separation results].

4. Turn the GC power on (Set the polarity at the positive setting and the attenuation at 1).

5. Set the GC current at 120 milliamps, polarity at positive, and attenuation to 1.

6. Wait until the injector/detector and the column temperature both say, "Ready" on the front panel of the GC.

7. Zero the output from the GC to the recorder using the fine and course zero knobs on the GC and the multimeter.

8. If using the chart recorder, connect the recorder to the GC and reposition the pen on the chart recorder if necessary.

   If using the integrator, connect the integrator to the GC and set the integrator at the following settings:

   Thresh = 3, peak width = 0.01 to 0.04, area reject = 0, and attenuation ($2\uparrow$) = 8,

   Chart speed = 1 to 5.

   Make sure the integrator is zeroed before the run starts.

4.28 Procedure for Testing the Flow of Helium Gas to the Gas Chromatograph

The procedure for testing the flow of helium gas to the gas chromatograph is as follows:

1. Attach the rubber tubing from the soap film flow meter to the TCD Vent #1.

2. Squeeze the rubber bulb at the bottom of the soap film flow meter (which was filled with soapy water) until a soap film reaches the 10-milliliter mark. (The glass inside the soap film flow meter needs to be wetted a bit until the soap film can reach the 10-milliliter mark.)

3. Then squeeze the bulb until a soap film reaches the zero milliliter mark, and set the timer at the instant when the soap film reaches the zero mark.

4. When the soap film reaches the 10-milliliter mark on the flow meter, the timer was stopped.

5. Steps 1-4 were repeated for TCD vent #2.

6. The flow of the helium gas, in milliliter/minute units, was then calculated. An example follows:

   If it took 17.3 seconds for the soap film to travel the 10 milliliters, then the flow of the gas in that vent line was:

(10 milliliters/17.3 seconds)(60 seconds/minute) = 34.7 milliliters/minute.

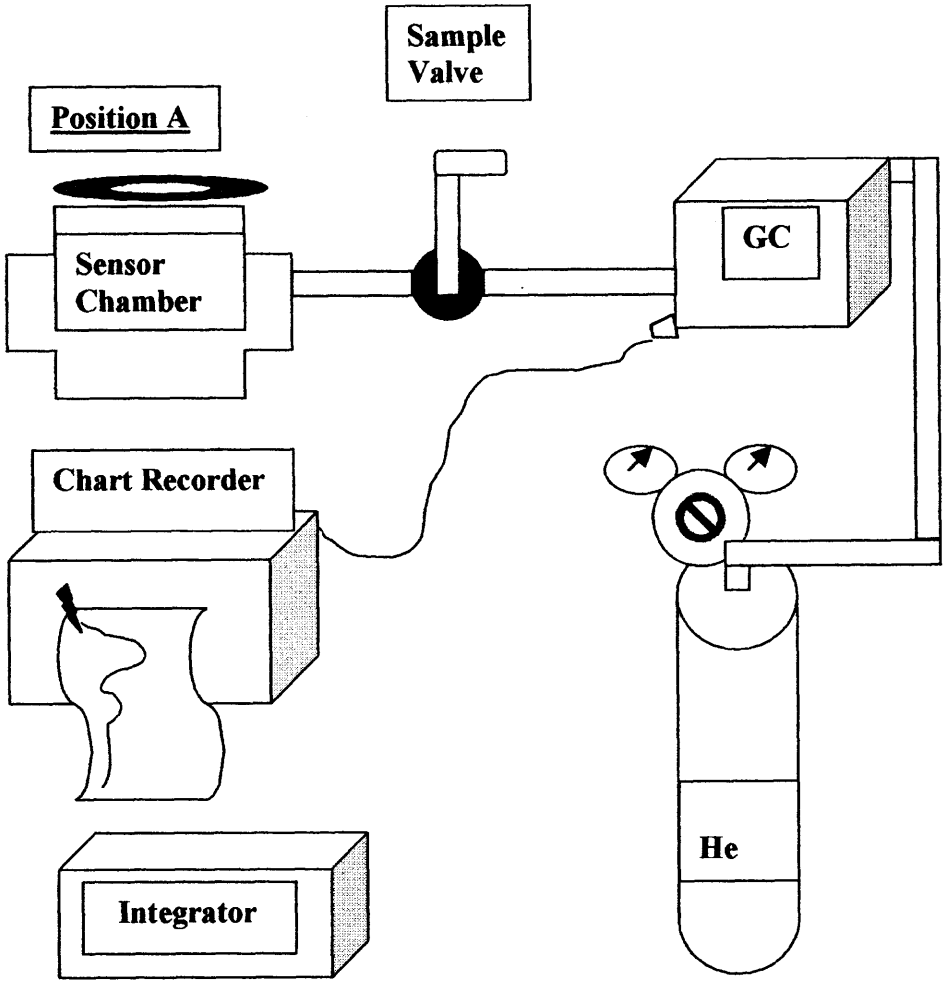

Figure 4.3 Flow diagram of the sensor/ GC set-up.

CHAPTER 5

CALCULATIONS

5.1 Calculation of the Resistance of the Sensor Exposed to Various Gas Mixtures

The constant-voltage method of making high resistance measurements was utilized in this experiment for determining the photoresistance of the sensor from its output readings which were in potential units of millivolts. This procedure requires the use of a picoammeter and a constant voltage source, and is described in Reference 66.

The picoammeter used for this experiment was the Keithley model #427 current amplifier and the constant voltage source used was a 9-volt household battery.

An electrical schematic of this constant voltage method is shown below:

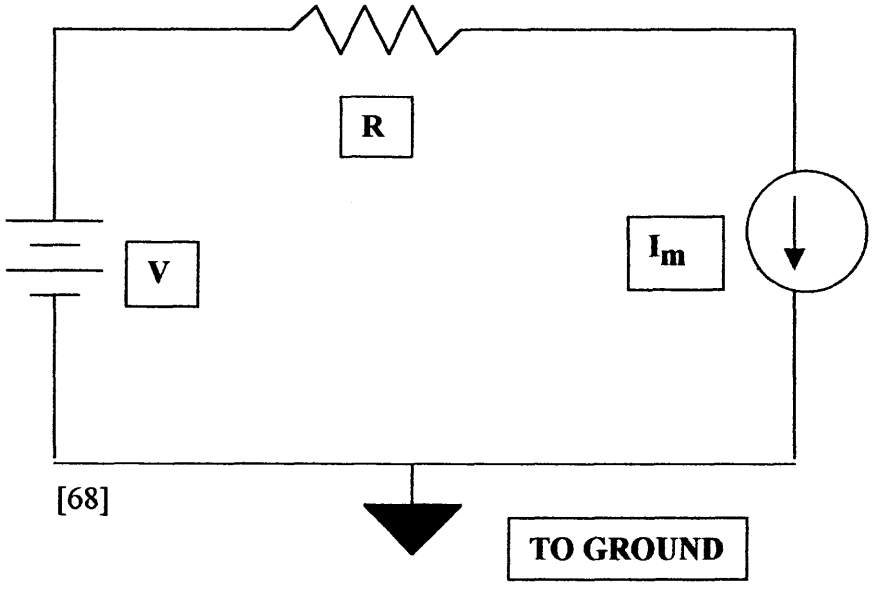

Figure 5.1 Constant voltage method for measuring high resistance. [66]

The resistance over the sensor resulting from the different concentrations of toluene/air or toluene/nitrogen gas mixtures, was calculated using the following equation:

$$V = IR \tag{5.1}$$

Where:

V = The voltage of the battery placed in series with the sensor (In this case it was approximately 9-volts, and was measured to the second decimal place using a multimeter).

I = The current which was calculated using the gain (y amp/V) set on the current amplifier, and the potential reading recorded by the chart recorder in x millivolts (mV).

The calculation to obtain the current, I, in amperes from this x and y data was as follows:

(x millivolts from chart recorder)(1 V/1000 mV)(y amps/V) = amps

R = V/I; The calculated resistance of the sensor, is obtained by dividing V by I. The resultant data is R in units of volts/amp or ohms.

The potentials across the copper clips that were attached to the sensor were the type of data that was obtained from this experimentation. The potentials resulting when the halogen lamp was on were greater than those obtained when the lamp was off. (An example of data obtained with the sensor was:

Table 5.1 An Example of the Potentials Obtained at One Point During Experimentation When the Halogen Light Was On or Off

Light on: 55 millivolts
Light off: 8.2 millivolts

This means that the photoresistance (with the light on) is less than the dark resistance (with the light off), because the resistance is inversely proportional to the potentials that were obtained from these experiments.

5.2 Calculations for the Preparation of Toluene in Air or Nitrogen Gas Mixtures with a Concentration of 100 ppm

The 6-liter spherical tank is rated for a pressure of 40 psig maximum.

Set the total pressure = 30 psig.

Using the Ideal Gas law:

$$P_T V = n_T R T \qquad (5.2)$$

Where:

P_T = 30 psig + 14.7 = 44.7 psia

V = 6 liters

R = 0.08206 liter · atmospheres/ mole · K

T = 21 + 273 = 294 K

n_T = [(44.7 psia)(6 liters)(1atm/14.7 psia)]/[(0.08206 liter·atm/mol·K)(294 K)]

n_T = 0.756 mole

100 ppm = 100 moles toluene/ 10^6 moles total = x / 0.756 moles

x = 7.56 X 10^{-5} moles toluene

The molar mass (MM) of toluene ($C_6H_5CH_3$) is:

C: 7 X 12.01 = 84.07

H: 8 X 1.01 = 8.08

92.15

MM = 92.15 grams/mole of toluene

The density of toluene is 0.866 grams/cubic centimeter (cc)

The volume of toluene needed for 100 ppm standard is:

7.56×10^{-5} moles toluene (92.15 grams/mole) (1 cc /0.866 grams) = 0.00804 cubic centimeters of toluene

Converting this to microliters (μL):

0.00804 cc toluene(1 liter/1000 cc)(10^6 μL/1liter) = 8.0 μL toluene + 30 psig nitrogen or air to make up a 100 ppm gas mixture

5.3 Calculations for Making Up a Six Liter Tank of Toluene in Air or Nitrogen with a Concentration of 50 ppm

The amount of toluene needed would be half of what is used for the 100 ppm standard or 4 μL of toluene for 30 psig of air or nitrogen.

A larger (28" height and 6" in diameter), cylindrical tank capable of holding gas up to a pressure of 2000 psig, was made-up with 50 ppm of toluene in nitrogen in part I of this lab experimentation and was used in the lab work described in this report as well as the 6 liter tank. [27]

5.4 Calculation of Concentrations of Toluene in Nitrogen or Air Gas Mixtures in Parts Per Million (ppm)

The absolute pressure gauge was checked against a manometer and it was found that its zero point was approximately 1.5 psia. So, the calculations for the concentration were done as follows:

Example: The sensor chamber was filled with nitrogen gas to a pressure of 7.5 psia and then it was filled up to 22 psia with a 50 ppm toluene/nitrogen gas mixture.

The calculation was done as follows:

[(22psia – 7.5 psia) (50 ppm)]/ (20.5 psia total) = 35.4 ppm of toluene in nitrogen

The calculations for the concentration of toluene in air mixtures were done the same way. An integrator was not working at this point in the experimental procedure, so the output from the GC was sent to a chart recorder and the percentage of oxygen in the mixture was determined by weighing the different portions of the curves.

5.5 Calculations of the Bandgap Energy and Halogen Lamp Light Intensity

$E = hc/\lambda = (6.63 \times 10^{-34}\ J{\cdot}s)(3 \times 10^{8}\ m/s)(10^{9}\ nm/m)/(500nm) = 3.98 \times 10^{-19}$ Joules

Cadmium sulfide layer : Bandgap Energy = 2.4 eV $(1.602 \times 10^{-19}\ J/eV) = 3.84 \times 10^{-19}$ J

Light Meter : 380 foot candles = Light the reaches the sensor from the halogen light with the filter in place

380 foot candles (1 Lumens/square foot/1 foot candle)$(1/4\ inch)^2$ $(1\ foot/12\ inches)^2$ = 0.165 Lumens

CHAPTER 6

DISCUSSION OF RESULTS

6.1 The Response of the Sensor to Nitrogen

The sensor was experimentally tested with gas mixtures containing very small amounts of toluene, in the parts per million (ppm) concentration ranges with the balance of the gas mixture containing nitrogen. (All of the experimental results in chapter 6, unless otherwise noted, were obtained using the sensor chip fabricated with a 0.5 micron thick cadmium sulfide layer and a Rhodamine B dye layer on a glass substrate. The results also refer to data obtained with the halogen lamp on continuously during all experimental runs.)

To determine the response of the sensor to the toluene vapor alone, the specific response of the sensor to a nitrogen environment, where no other gaseous contaminants were present, was studied. This experiment was required in order to determine the effect of the background gas in the toluene/nitrogen gaseous mixture. (The next section covers the specific response of the sensor to air alone for analysis of mixtures containing toluene in an air balance gas).

Figure 6.1 contains experimental results, which show the change in photoresistance (resistance obtained with the halogen lamp on) versus sensor exposure time when the gas exposed to the sensor was entirely nitrogen, without any toluene.

The y-axis is the change in the resistance, in 10^{10} ohms units. The x-axis is the time of exposure of the sensor to the nitrogen in minutes. The length of the experiment was 60 minutes of sensor exposure time.

The data graphed in Figure 6.1 show that exposure of the sensor to nitrogen has little effect on the resistance of the sensor. Nitrogen, which is an inert gas, does not appear to have much initial effect on the resistance of the sensor. Over a longer period of time, from 30 to 60 minutes, the change in photoresistance was slight, approximately negative 0.5 x 10^{10} ohms.

6.2 The Response of the Sensor to Synthetic Air (Oxygen)

The sensor was also tested with gas mixtures containing small amounts of toluene, in the parts per million (ppm) concentration ranges with the balance of the gas mixture containing air (either synthetic or atmospheric). To determine the response of the sensor to the toluene vapor alone, the specific response of the sensor to both types of air was tested.

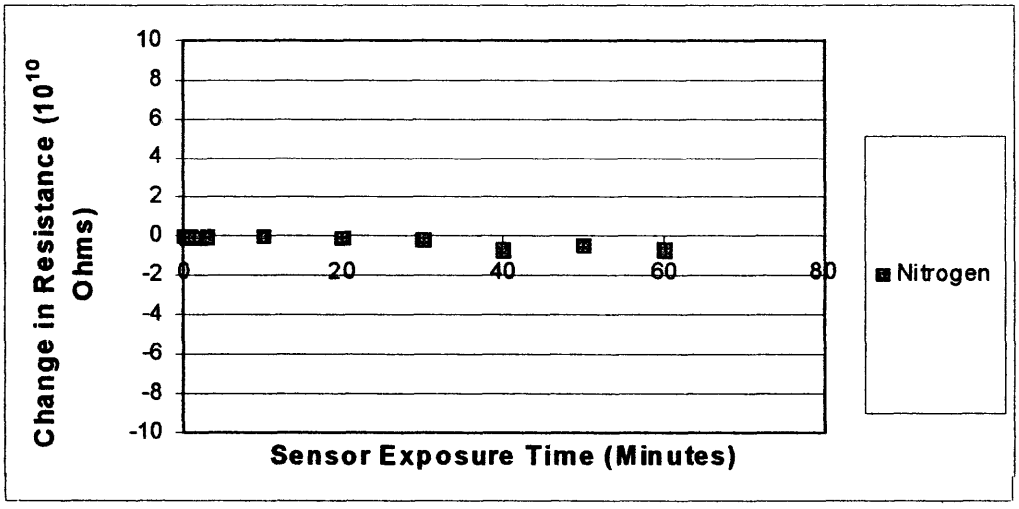

Figure 6.1 Change in resistance of nitrogen versus time of sensor exposure.

In this section, the results obtained from the testing of synthetic air are discussed. (Synthetic air or zero grade air is a commercially available mixture of 80% nitrogen and 20% oxygen).

It can be seen from Figure 6.2 that the sensor reacts very differently to synthetic air as opposed to a pure nitrogen environment, indicating that the oxygen in the air is causing a large change in the resistance of the sensor.

The effect of the air on the photoresistance of the sensor is not only large but also very fast. The photoresistance of the sensor rises at a rapid rate, for the first 10 minutes of air exposure time, resulting in a change in photoresistance of about 5.5 X 10^{10} ohms.

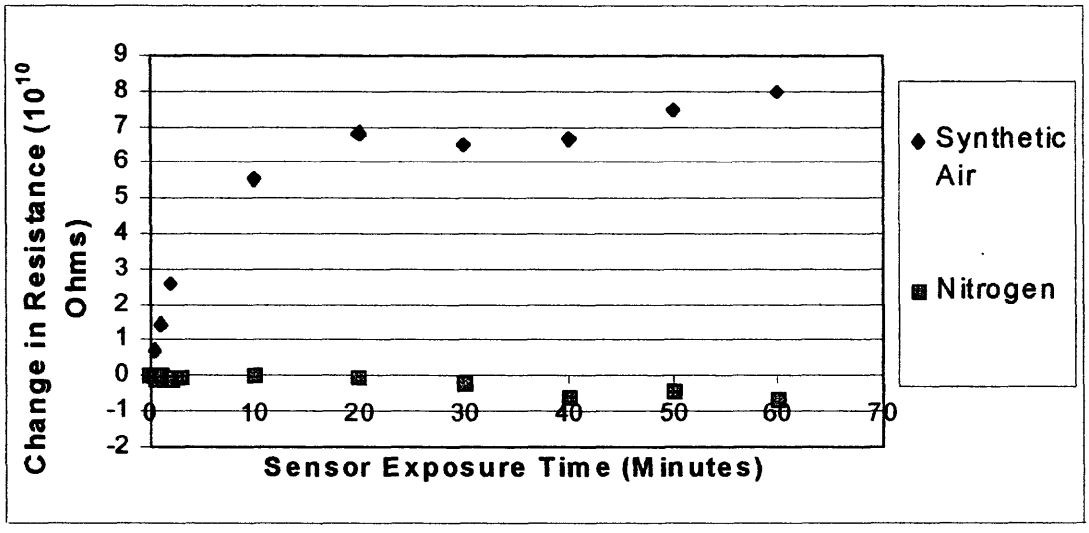

Figure 6.2 Change in resistance of synthetic air and nitrogen versus time of sensor exposure.

The change in photoresistance starts to level off at an exposure time of around 20 minutes, at a photoresistance value of 7 to 8 x 10^{10} ohms.

It is quite evident that there is a large surface effect on the sensor due to air exposure, as compared to nitrogen gas exposure, which must be attributed to the presence of oxygen.

From Figure 6.2, it can be concluded that for optimum detection of the toluene in a gaseous mixture, it would be better if it were mixed with nitrogen than with air. The

lack of a response by the sensor to nitrogen aids in studying the effects of an organic gas such as toluene on the photoresistance of the sensor.

6.2.1 The Response of the Sensor When the Amount of Oxygen in the Sensor Chamber and the Total Pressure Varied

Since the sensor being investigated was shown to be a fast acting oxygen sensor, an investigation was undertaken to determine if the sensor being studied would determine

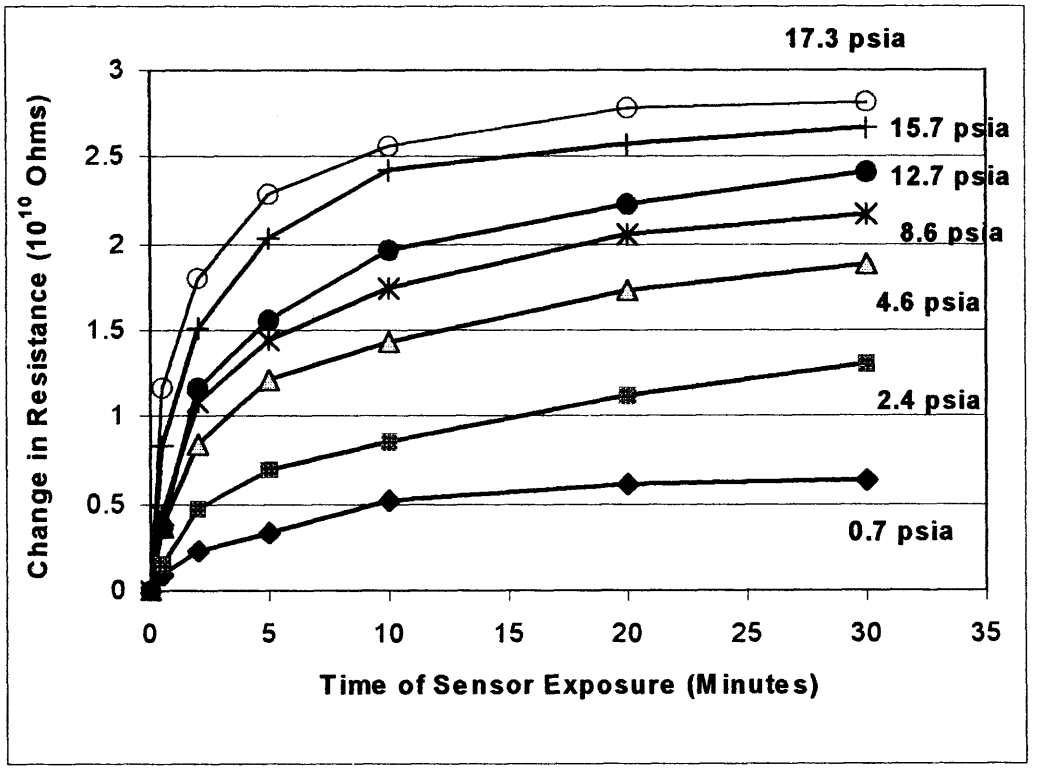

Figure 6.3 Detection of partial pressures of synthetic air.

not only the presence of oxygen but also the concentration (partial pressure) of oxygen present.

Figure 6.3 contains experimental data that show the results obtained when different partial pressures of synthetic air (commercially available zero grade air

containing only nitrogen and oxygen) were admitted into the chamber. It can be seen that the sensor being studied, in addition to being able to detect oxygen, can also detect the quantity of oxygen present. (For this experiment the total pressure of gas in the sensor chamber was equal to the partial pressure of the synthetic air for each run).

The photoresistance is shown to increase as the partial pressure of the oxygen increases.

The initial slopes of the change in photoresistance of the sensor to oxygen in synthetic air versus the partial pressures of the synthetic air admitted into the sensor chamber were plotted in Figure 6.4.

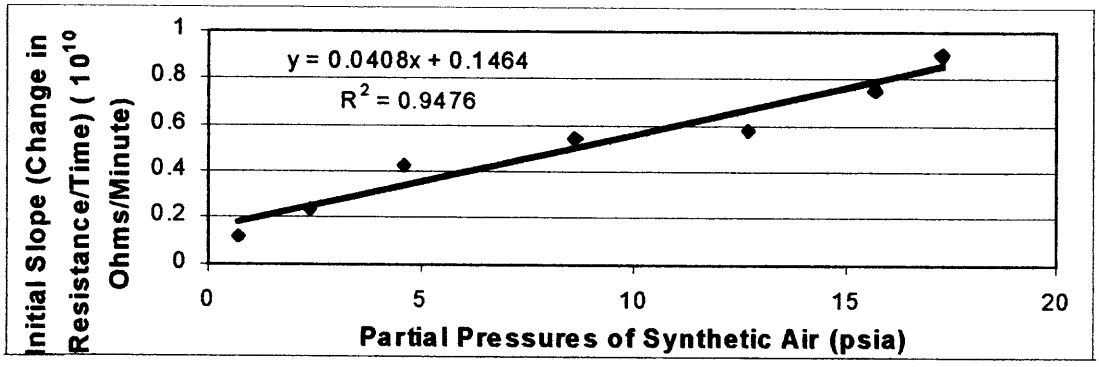

Figure 6.4 The initial slopes (first 2 minutes) vs. partial pressures of synthetic air.

Several experiments were undertaken to further examine the use of the sensor with a 0.5-micron cadmium sulfide layer on a glass substrate dyed in Rhodamine B dye as an oxygen sensor and the results from these experiments with synthetic air/nitrogen gas mixtures are outlined in sections 6.2.2.1 through 6.2.2.5.

6.2.2 The Response of the Sensor When the Amount of Oxygen in the Sensor Chamber Varied But the Total Pressure Remained Constant

6.2.2.1 Gas Mixture Prepared in a Sensor Chamber. The sensor being investigated was shown to be a relatively fast acting oxygen sensor from results obtained in the last section. An investigation was undertaken to determine if the sensor being studied would determine not only the presence of oxygen but also the concentration (partial pressure of oxygen if the total gas pressure was kept constant for each run) if the gas mixture used in the experiment was made-up directly in the sensor chamber. Complete experimental procedures for this experimental run are outlined in Section 4.6.

The data in Figure 6.5 show the results obtained when different partial pressures of synthetic air were admitted into the chamber. It can be seen that the sensor being studied, in addition to being able to detect oxygen, can also detect the quantity of oxygen present The photoresistance was shown to increase as the percentage of the oxygen increases.

When the data in Figure 6.5 is plotted in a different way, as the change in resistance versus the oxygen concentration (percentage) at various time intervals, Figure 6.6 resulted. The sensor response is close to equilibrium at 60 minutes of exposure time and the equilibrium curve is:

$$y = -0.0112\,x^2 + 0.3227x + 0.1659; \qquad R^2 = 0.9399;$$

where y is change in resistance in 10^{10} ohms and x is percentage of oxygen in the gas mixture.

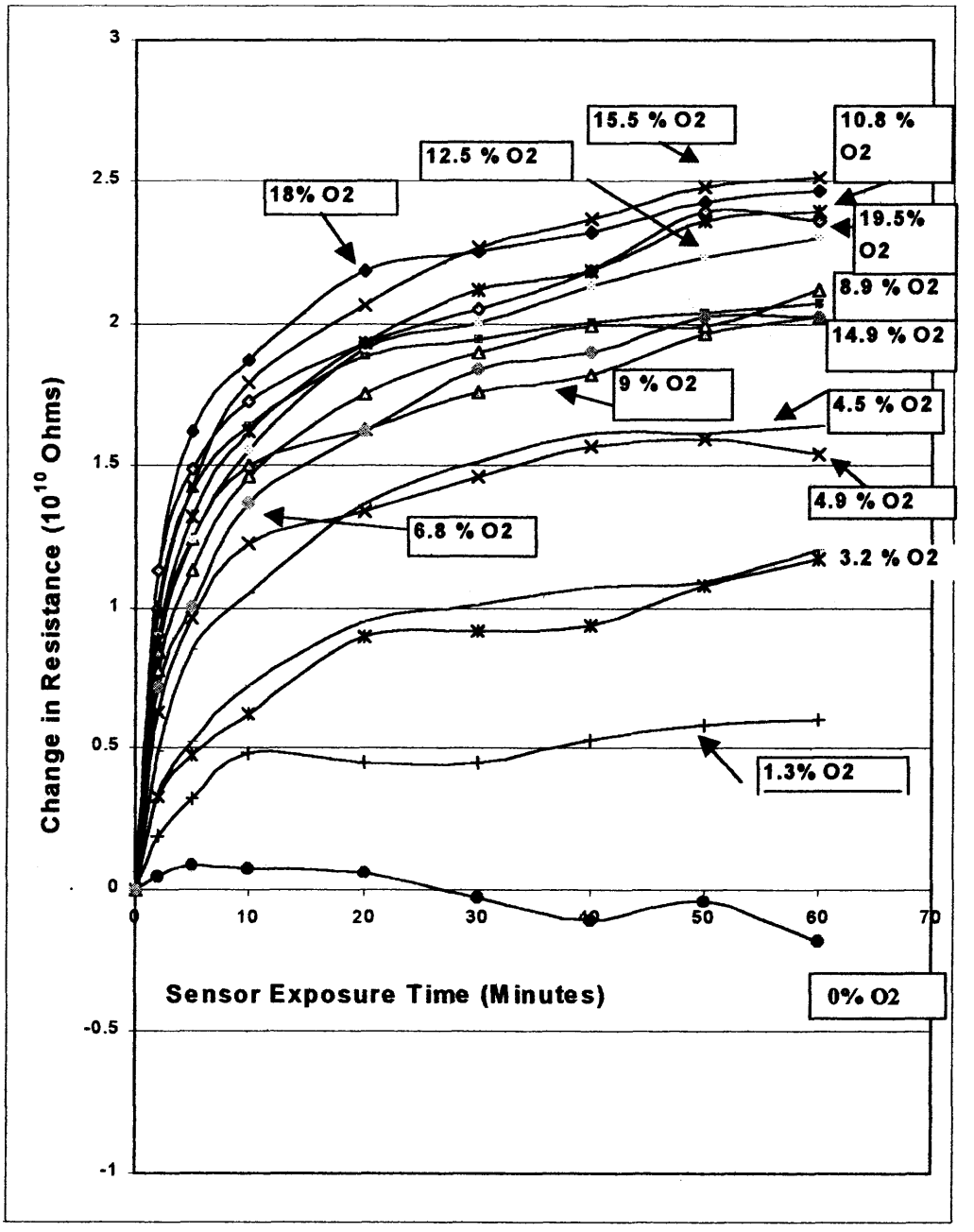

Figure 6.5 Resistances versus sensor exposure time for synthetic air containing various oxygen/nitrogen concentrations and a constant total pressure.

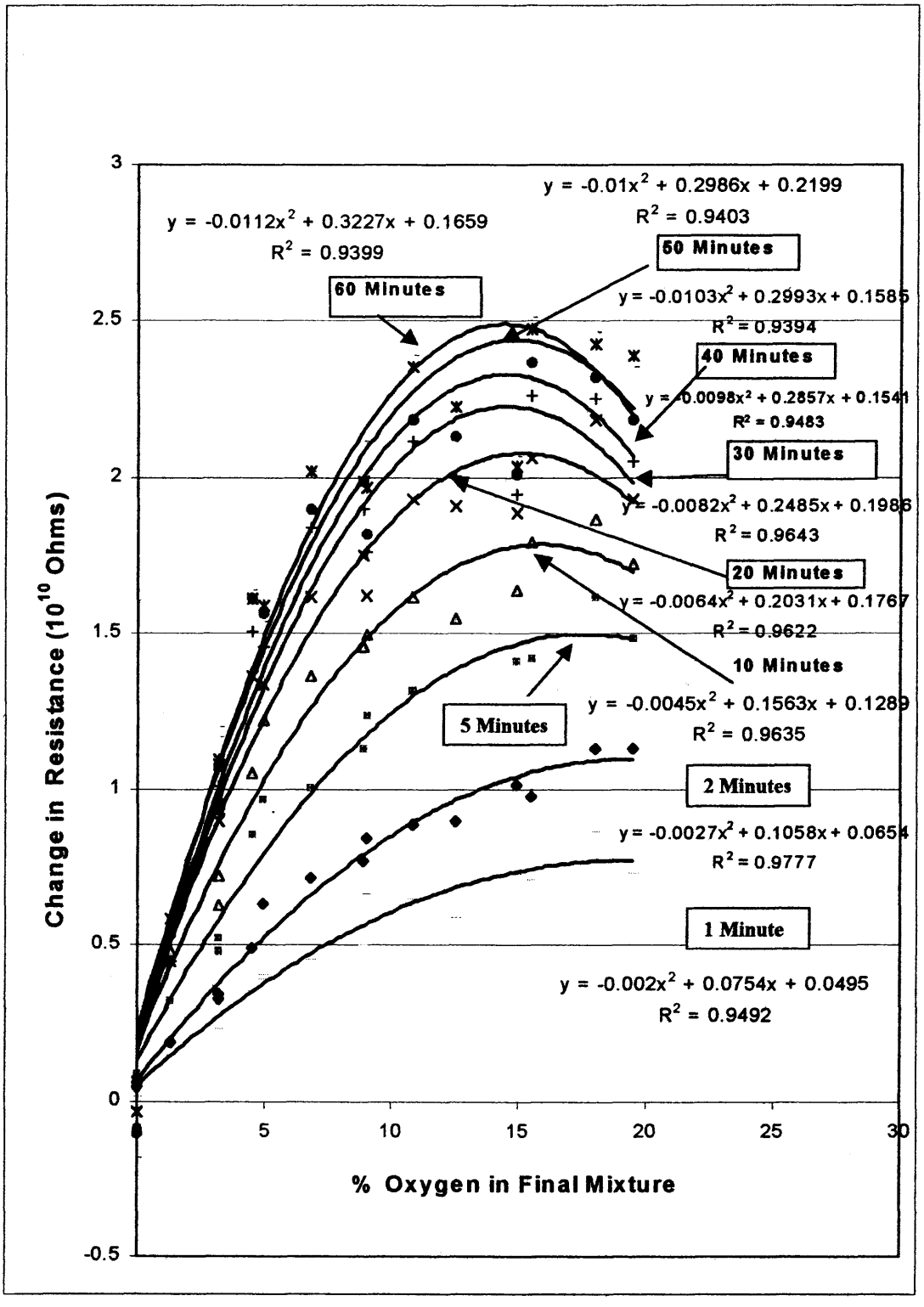

Figure 6.6 Sensor resistance versus percent oxygen at different exposure times using synthetic air with different oxygen concentrations at a constant total pressure.

The data in Figure 6.7 show that the initial slopes of the curves of resistance versus oxygen concentration in Figure 6.6 are linear when the gas mixture is not flowing through the sensor chamber.

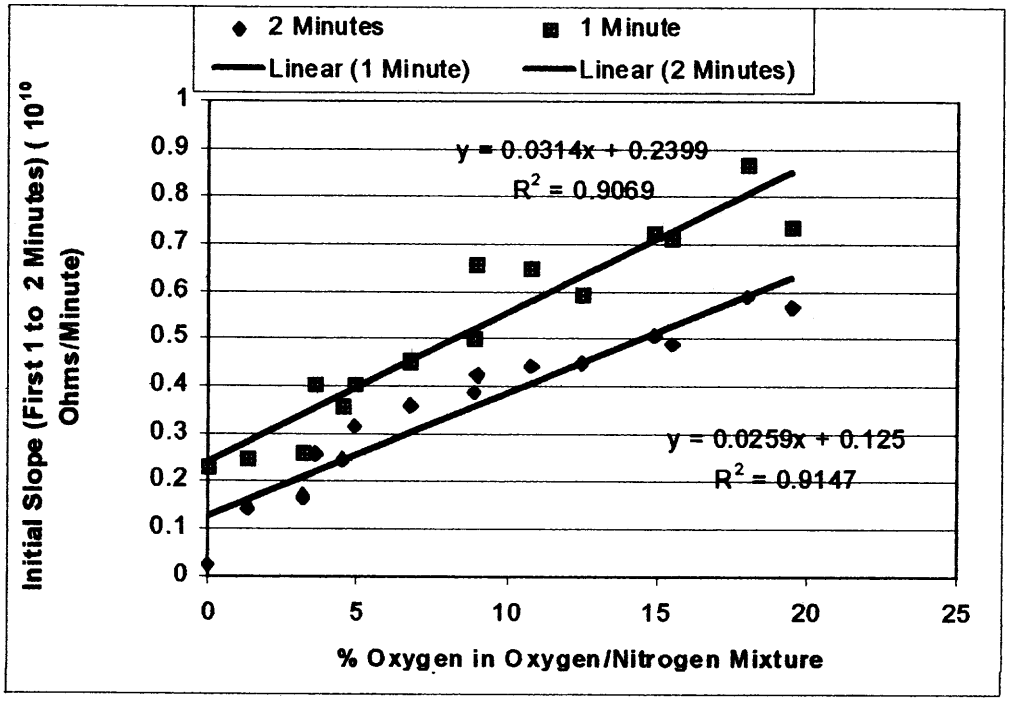

Figure 6.7 Initial slope (first 1 and 2 minutes) versus sensor exposure time.

6.2.2.2 Gas Mixture Made-Up in Tank. In a new experiment, the gas mixtures were made up in a tank and then sent to the sensor chamber, instead of making them up directly in the chamber as was done in experimental procedure 4.6. (The experimental procedure is described in experimental procedure Section 4.7). Several runs were made at various oxygen concentrations, so a comparison could be made between the two experiments. The data in Figure 6.8 shows the graphs obtained when the data points from several different oxygen concentration runs were plotted.

In Figure 6.8, the equilibrium resistances obtained by the synthetic air mixtures are not as high as those in Figure 6.5, but the curves show the same general trend.

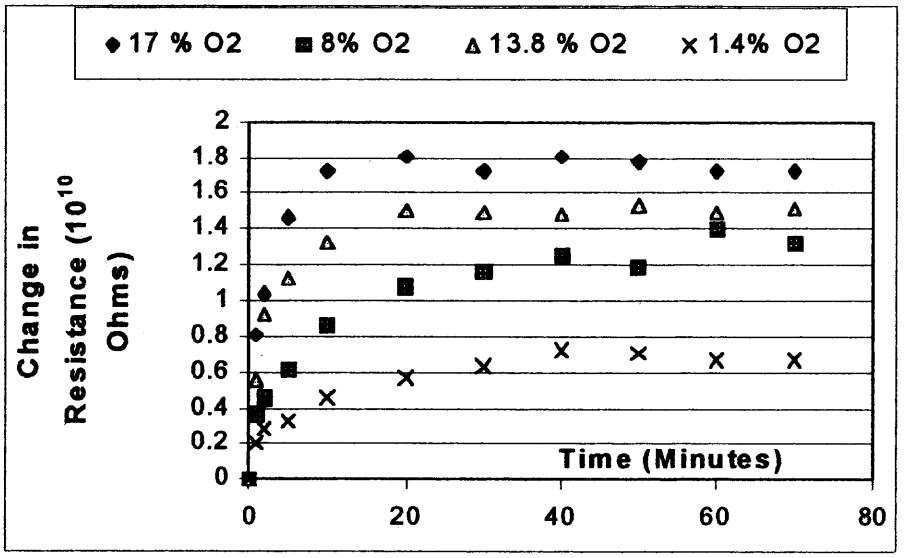

Figure 6.8 Change in resistances versus sensor exposure time for different synthetic air/nitrogen mixtures.

The data in Figure 6.9 show the initial slopes (change in resistance versus time) for this experiment. Comparison of Figures 6.7 and 6.9, show that at one-minute exposure time, the slope of the curve is linear.

The linear equation for 1 minute of exposure time from the experimental procedure described in Section 4.6 (Figure 6.7) was: $y = 0.0314 x + 0.2399$ and for the experimental procedure described in Section 4.7 (Figure 6.9) was: $y = 0.0365 x + 0.1185$; for 2 minutes of exposure time the equation for the experimental procedure described in Section 4.6 (Figure 6.7) was: $y = 0.0259 x + 0.125$ and for the experimental procedure described in Section 4.7 (Figure 6.9) was: $0.0258 x + 0.0789$, which are very similar.

These data show that the two experiments using synthetic air had very similar slopes for the first 2 minutes of sensor exposure time. Figure 6.10 contains the graph of change in resistance versus oxygen concentration (percent oxygen) for the second synthetic air experiment. Figures 6.6 and 6.10 contain graphs, which show similar equilibrium curves after 60 minutes of exposure time, but the curve in Figure 6.10 equilibrates at a lower resistance.

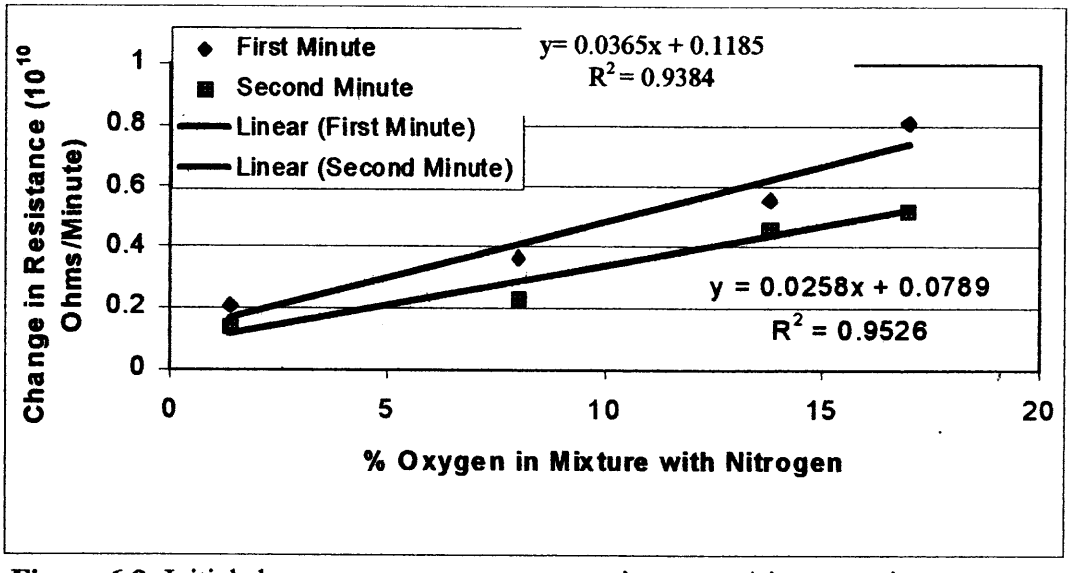

Figure 6.9 Initial slopes versus percent oxygen in oxygen/nitrogen mixture.

6.2.2.3 Gas Mixture Made-Up in Tank - Initial Purge (10 Seconds) of Sensor Chamber. The procedure for this experiment was different from the one described in Section 4.7, in that the integrator was now working and being used and the sensor chamber was also being purged for the initial 10 seconds of the sensor run. The purge valve was then closed and the mixture was allowed to fill the gas chamber to 15 psig. This was done to make sure that the GC would determine the concentration of a gas

mixture, which was the same as the one that the sensor was exposed to for the 70 minutes of sensor run time. (The procedure for these experiments is outlined in Section 4.8).

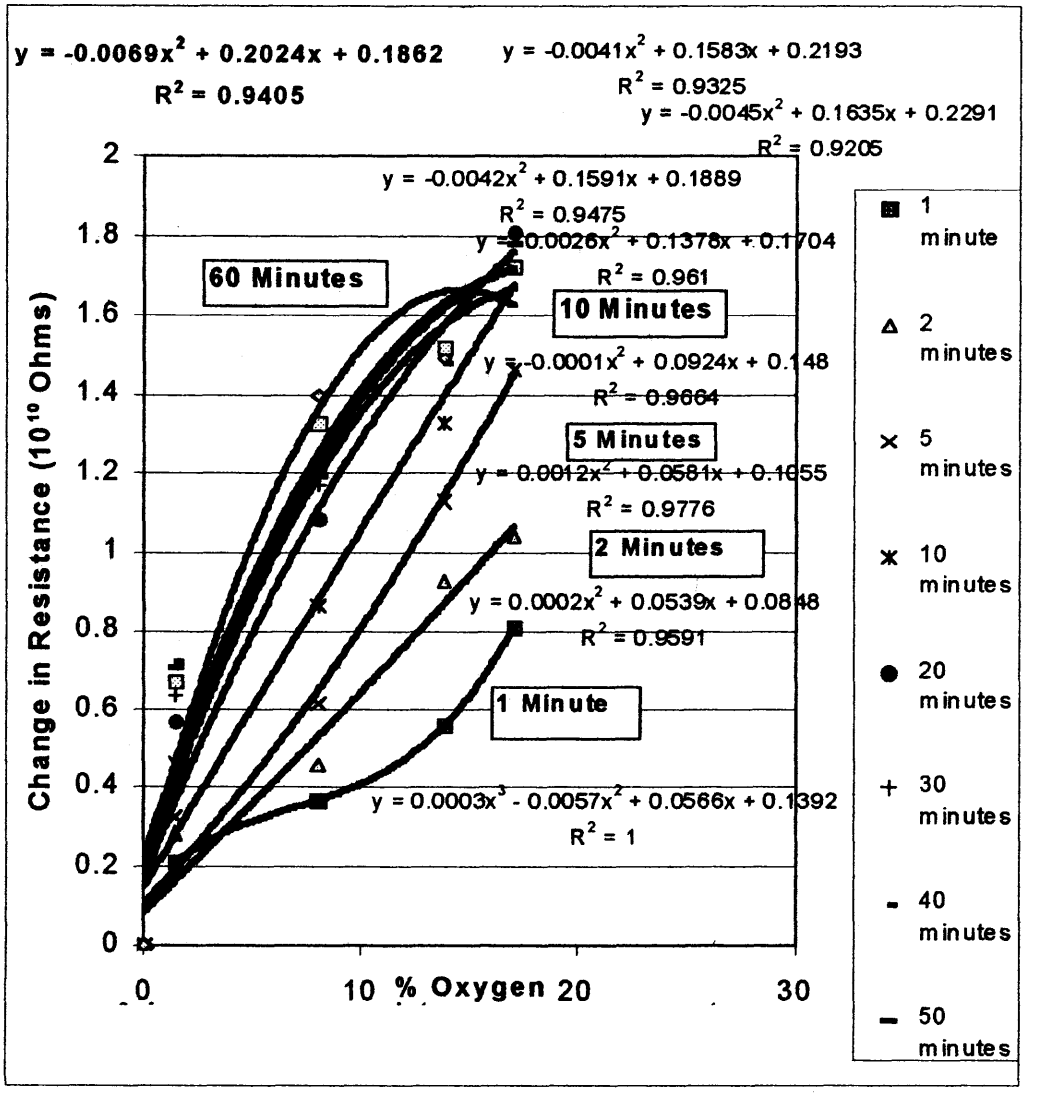

Figure 6.10 Change in resistance versus percent oxygen.

The change in resistance versus time graphs, resulting from this experiment, were similar to those obtained in the last two sections, as can be seen in Figure 6.11.

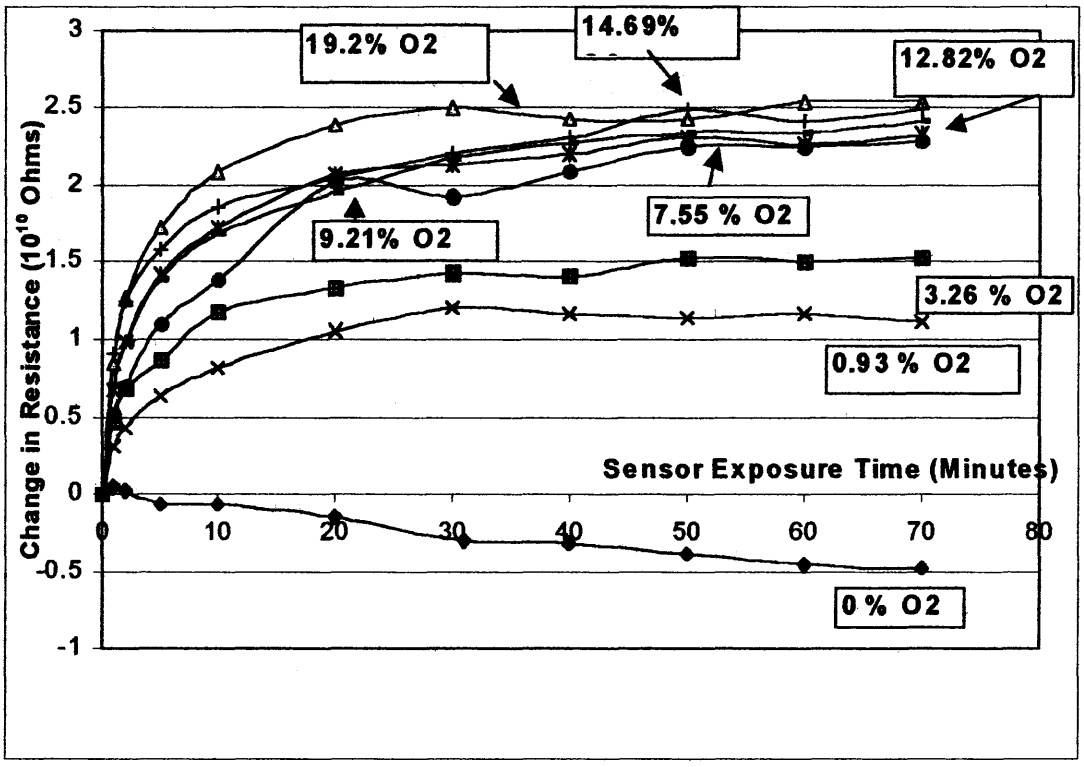

Figure 6.11 Resistances versus percent oxygen (determined by an integrator).

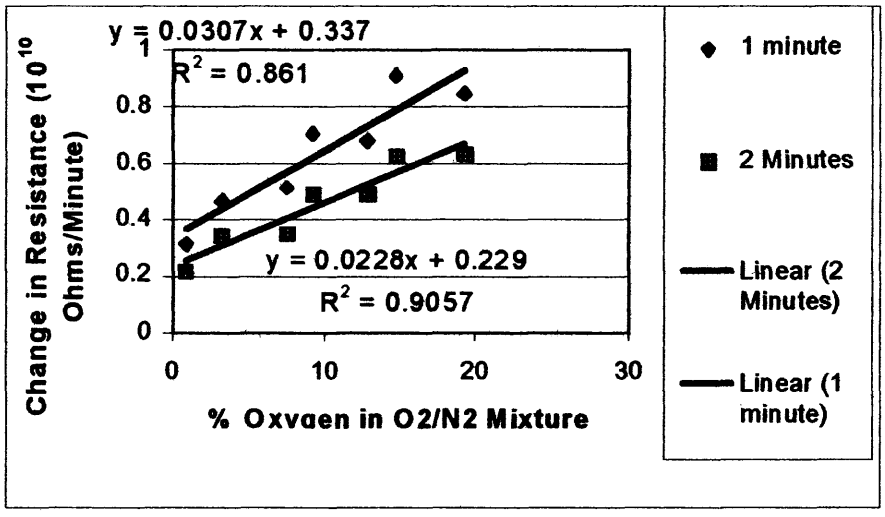

Figure 6.12 Initial slopes in Figure 6.11.

The initial slopes obtained for the results from the experiments described in the experimental procedure section 4.8 are graphed in Figure 6.12.

The experimental results from the last two sections plus this section suggest that the initial slopes of resistance versus oxygen concentration are linear. From literature research it was found that the kinetics of quenching of fluorescence ideally follows the Stern-Volmer law, which is linear:

$$R - 1 = K[Q] \tag{6.1}$$

Where:

R = the ratio of fluorescence intensity, without and with the quencher.

Q = the quencher (oxygen in this case) concentration

K = the Stern-Volmer constant. [72]

The above equation is derived in Section 6.3 of this report.

The current or millivolt potential data from this experiment were used to calculate the ratio of current intensity without oxygen over the intensity with oxygen at each oxygen concentration. It was assumed that the current ratio would be proportional to the fluorescence ratio. (See Subsection 6.3.1 for a further discussion of the energy transfer by the fluorescent dye. By conservation of energy, the absorption of energy by the dye molecules on the sensor surface is equal to the sum of the energy transferred by the dye into the cadmium sulfide layer plus the energy transferred into the fluorescent emission, so the fluorescence intensity ratio should be proportional to the energy absorption into the cadmium sulfide layer ratio and the resultant current ratio at the same quenching rate.)

The numbers that resulted were plotted as the y-axis in Figure 6.13, versus the oxygen concentration in percent oxygen as the x-axis (Q).

The slopes obtained in Figure 6.13 for 1 and 2 minute exposure times with synthetic air are the K or Stern-Volmer constant in the above equation. The graphed lines didn't go through one as the intersection point. So K must be divided by the intercept. K is equal to 0.0085 at a one-minute exposure time and 0.0124 at two minutes exposure time.

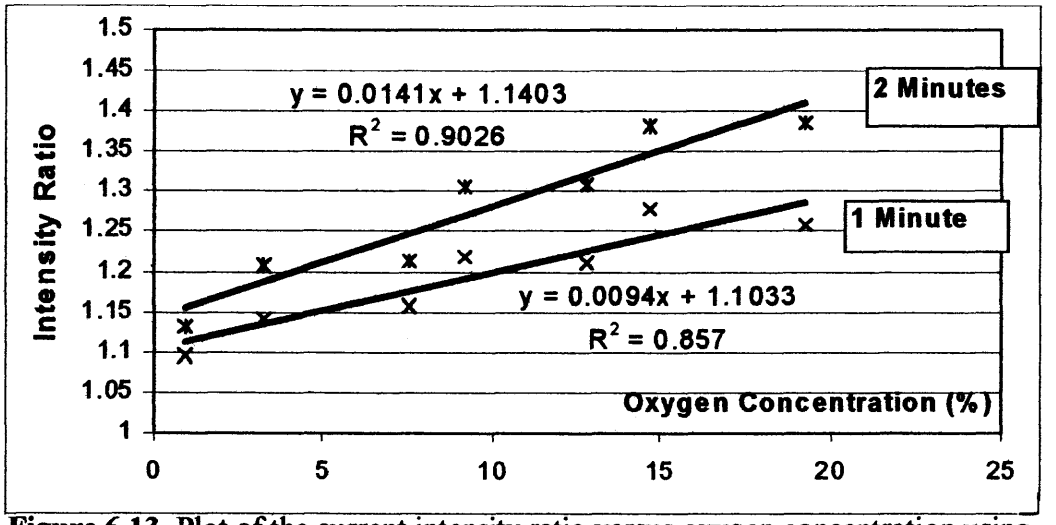

Figure 6.13 Plot of the current intensity ratio versus oxygen concentration using synthetic air.

The Stern-Volmer constant, K, is equal to the ratio of the rate constant for quenching divided by the rate constant for fluorescence.

The following table shows how similar the initial slopes of the three experiments were:

Table 6.1 The Equations of the Graphed Lines in Figures 6.7, 6.9 and 6.12

	After 1 Minute	After 2 Minutes
Experiment (Figure 6.7):	y = 0.0314x + 0.2399;	y = 0.0259x + 0.125
Experiment (Figure 6.9):	y = 0.0365x + 0.1185;	y = 0.0258x + 0.0789
Experiment (Figure 6.12):	y = 0.0307x + 0.337;	y = 0.0228x + 0.229

These results show that it did not make much of a difference in the initial equations, whether the gas mixtures were made-up in the sensor chamber or in the tank first. It also did not make much of a difference if there was an initial purge of the sensor chamber for 10 seconds.

Figure 6.14 contains plots of resistance versus oxygen concentration for this experiment. These types of plots were also similar for the three synthetic air experiments and resulted in similar equilibrium curves. Equilibrium curves are shown in Table 6.2.

Table 6.2 The Equations of the Graphed Lines in Figures 6.6, 6.10 and 6.14

Experiment (Figure 6.6), at 60 minutes: $y = -0.0112 x^2 + 0.3227x + 0.1659$
Experiment (Figure 6.10), at 60 minutes: $y = -0.0069 x^2 + 0.2024x + 0.1862$
Experiment (Figure 6.14), at 60 minutes: $y = -0.0115 x^2 + 0.3274x + 0.2841$
Experiment (Figure 6.14), at 70 minutes: $y = -0.0124 x^2 + 0.3472x + 0.2425$

6.2.2.4 Gas Mixture Made-Up in Tank (Gas Flowing First Minute). The nitrogen/oxygen gas mixtures used in the experiments described in experimental procedure Sections 4.6 through 4.8 were all admitted into the chamber and were stationary in the sensor chamber until equilibrium was reached. (In the experiment using the experimental procedure described in Section 4.8, the gas mixtures were purged through the sensor chamber for the initial ten seconds). The experimental procedure for this experiment is described in Section 4.9.

The purpose of this experiment was to determine if there would be the same sensor response to a nitrogen/oxygen gas mixture that was flowing instead of stationary, for the first minute.

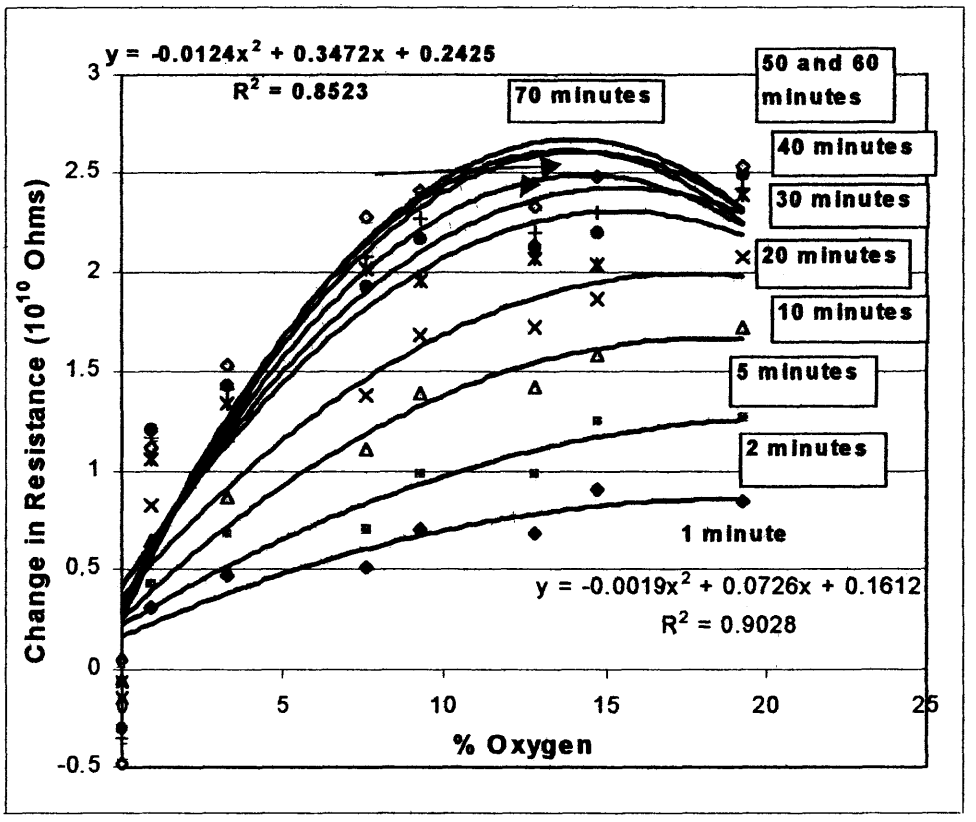

Figure 6.14 Resistance versus percent oxygen concentration for various sensor exposure times.

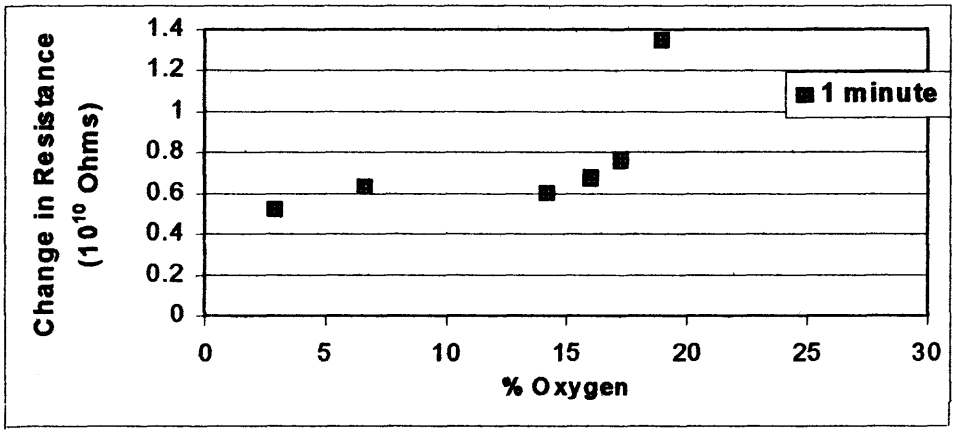

Figure 6.15 Change in resistance versus percent oxygen when the synthetic air was flowing for one minute.

Figure 6.15 contains data that shows that the sensor response was very different when the gas mixture containing synthetic air was flowing for the initial minute of exposure than when it was stationary in the sensor chamber.

Initially, if the gas is flowing through the sensor chamber, the amount quenching by the oxygen is higher with higher concentrations of oxygen, as shown in Figure 6.15.

6.2.2.5 Synthetic Air Flowing Through the Sensor Chamber for 25 Minutes.

In this experiment, synthetic air (18.93% O2) was allowed to flow through the sensor chamber for 25 minutes at 15 psig, and then the sensor was desorbed for another 225 minutes, using alternating applications of vacuum and nitrogen. The data in Figure 6.16 resulted. (The procedure for the experimental results covered in this section can be found in Section 4.10).

For 10 minutes during the desorption run, helium gas was used instead of nitrogen to see if it would be more efficient at clearing sorbed gases from the sensor and chamber than nitrogen. It was found that helium and nitrogen were comparable in their desorbing ability.

Figure 6.16 was divided up into two processes: the adsorption and desorption processes. The adsorption process was further divided into 2 sections. The three sections that resulted included the following areas:

Figure 6.17 – Quenching Section - First 1 minute of oxygen exposure (initial slope) - synthetic air flowing through the sensor chamber.

Figure 6.18 – The adsorption section from 2 to 25 minutes of oxygen exposure time - synthetic air flowing through the sensor chamber.

Figure 6.21 – The desorption section (25 to 250 minutes) - alternating vacuum and nitrogen application to desorb sensor surface.

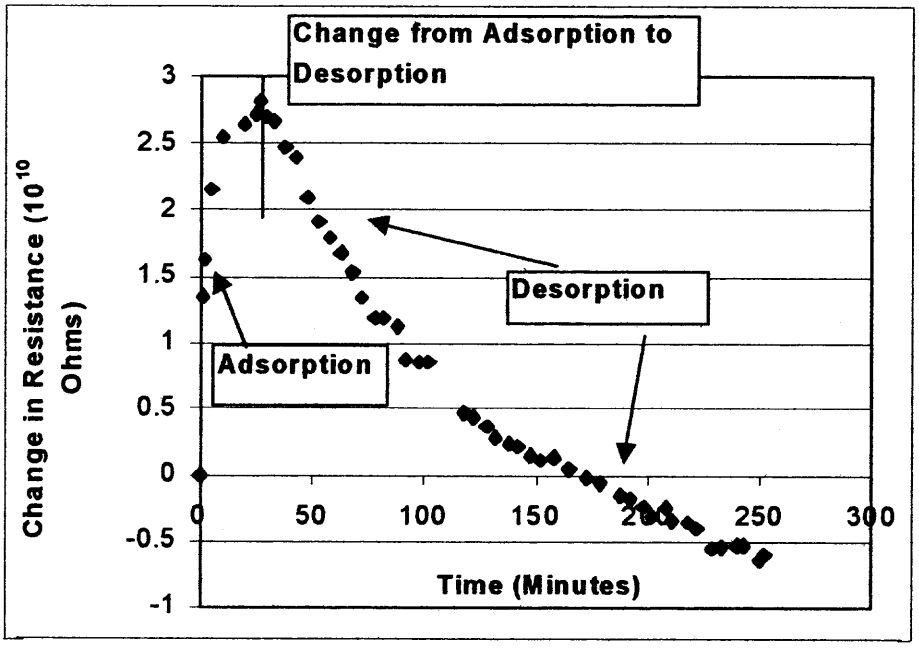

Figure 6.16 Resistance versus exposure time during synthetic air exposure involving oxygen adsorption and the subsequent desorption process.

Figure 6.17 contains the first two points of Figure 6.16.

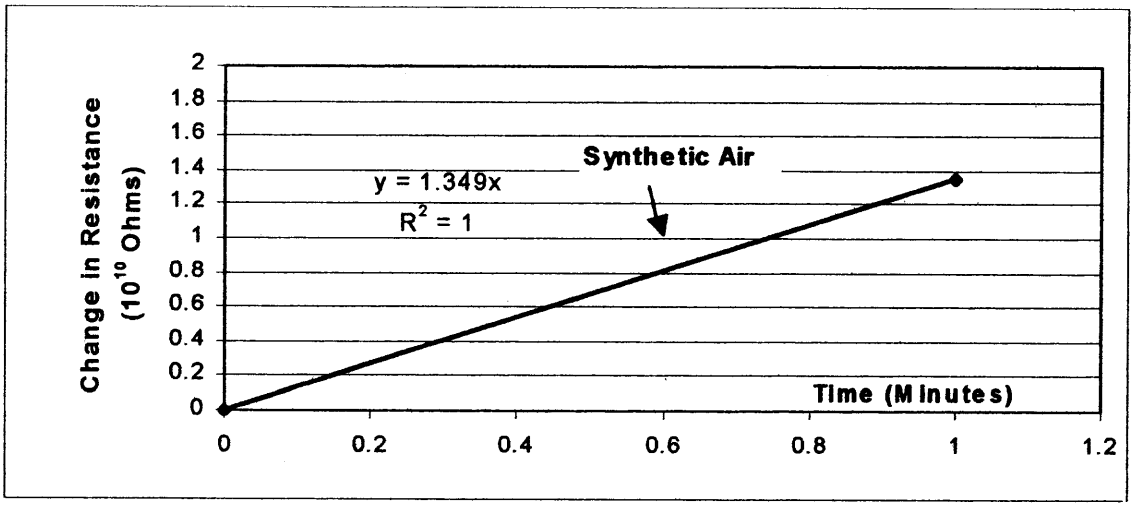

Figure 6.17 Change in resistance versus exposure time for the first minute of exposure to synthetic air (first section of Figure 6.16).

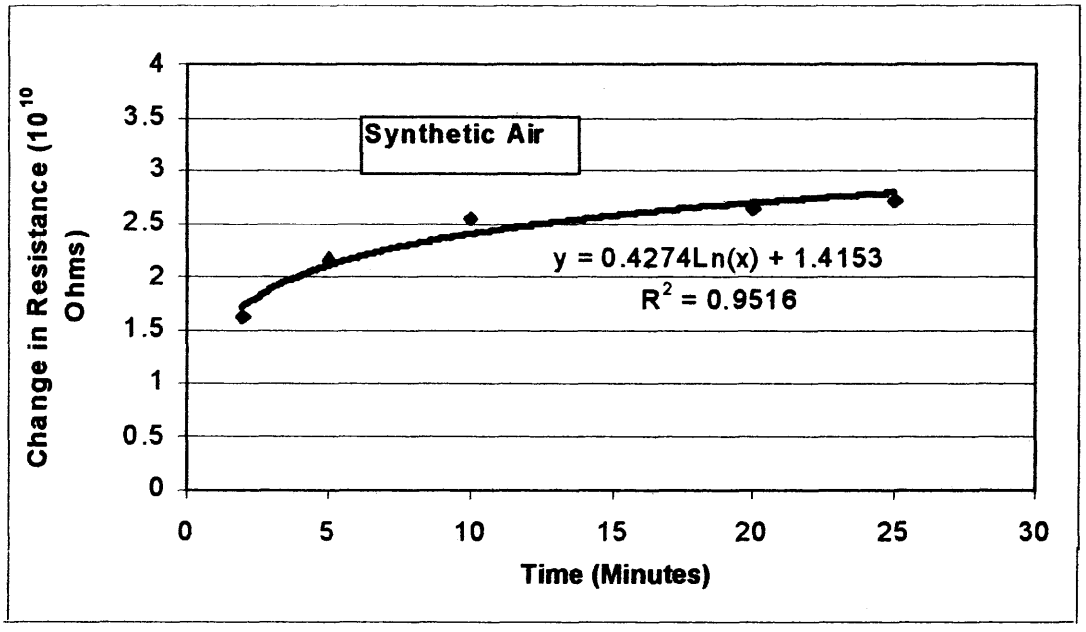

Figure 6.18 Resistance versus exposure time during 2 to 25 minutes of synthetic air exposure (second section of Figure 6.16).

The data in Figure 6.18 show the adsorption section of Figure 6.16 minus the first two minutes of exposure time.

The adsorption curve in Figure 6.19 follows the Elovich equation, which is:

$$\Delta I = I_S - I(t) = \lambda \ln[(t/t_o) + 1] \qquad (6.2)$$

Where:

t_o = 3 seconds

I = photocurrent

t = time (seconds)

I_s = photocurrent prior to adsorption (amps)

I(t) = photocurrent at time (t) (amps)

ΔI = change in photocurrent (amps) [41]

λ = slope

Figure 6.19 data follows the Elovich equation for exposure times from 2 to 12 minutes (indicated by the ♦ symbol). After 12 minutes the Elovich equation no longer applies (indicated by the x symbol).

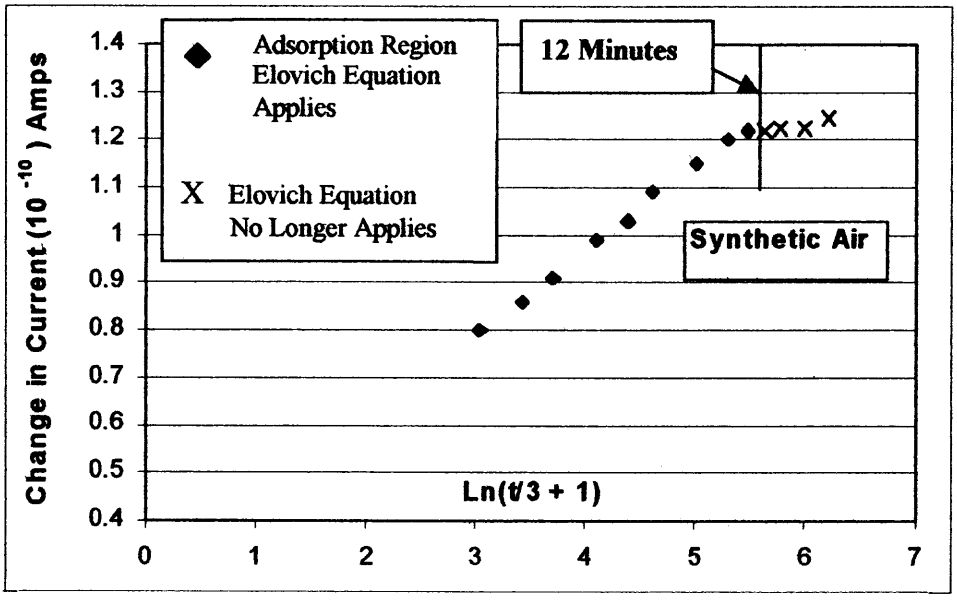

Figure 6.19 Figure 6.16 regraphed using the Elovich equation parameters.

According to References 41 and 42, during the initial portion of the adsorption curve shown in Figure 6.19, there is a steady-state build-up of adsorbed oxygen ions on the surface of the crystal.

Initially the CdS semiconductor material supplies electrons to the surface in the oxygen-free state. When oxygen is exposed to the surface, oxygen ions are formed and become chemisorbed ions. [41, 42]

At first, diffusion of electrons to the surface is the rate-determining step and the Elovich equation is obeyed. After a while, however, desorption limits the accumulation of surface ions, and a dynamic equilibrium is established involving the flow of charge to the surface from the bulk and the flow of gas to and from the surface. [41, 42]

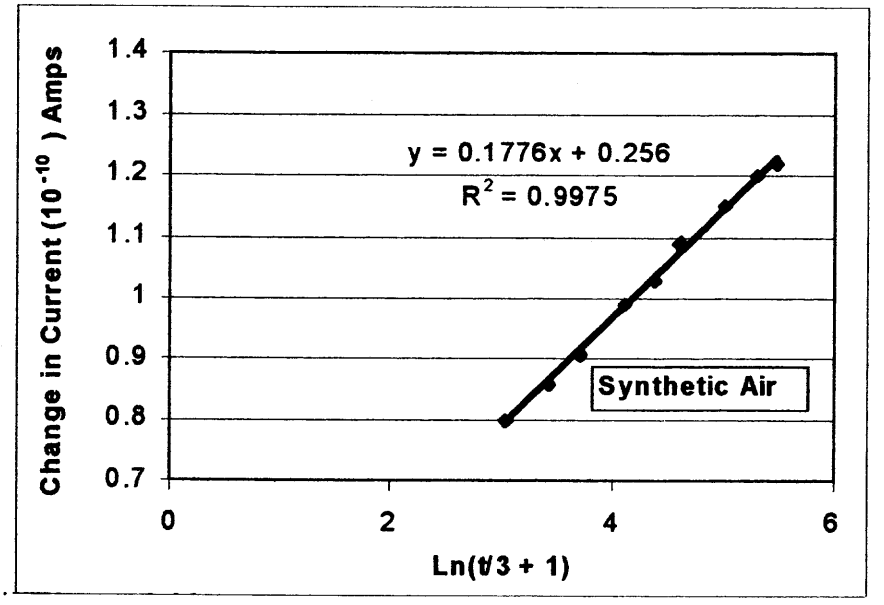

Figure 6.20 A graph of the initial linear portion of Figure 6.19.

If the initial linear portion of the curve in Figure 6.19 is extracted (corresponding to 1 to 12 minutes of oxygen adsorption), Figure 6.20 results.

The Elovich equation is only applicable over a finite interval because an assumption was made that the desorption could be neglected during the initial response, which is a physically reasonable assumption only in the initial stages of adsorption. [41, 42]

The desorption process under vacuum with several purges of nitrogen or helium gas is a logarithmic function as can be seen in Figure 6.21.

The desorption process is completed more rapidly when the oxygen concentration in the sampled gas was lower.

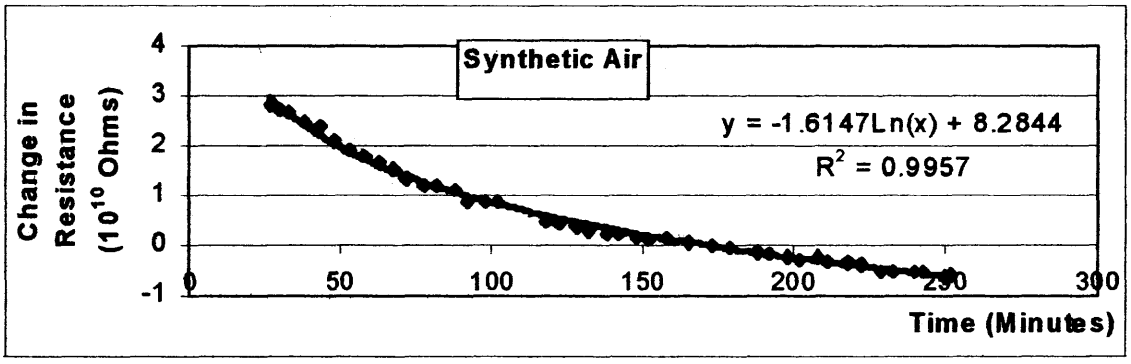

Figure 6.21 Resistance versus exposure time during the desorption process for synthetic air from 25 to 250 minutes (third section of Figure 6.16).

6.3 Theory Explaining the Sensor's Response to Oxygen

The gas sensor we tested in this experiment was made of a semiconductor crystalline material (cadmium sulfide) and was coated with a fluorescent dye (Rhodamine B) as developed by Dr. Zaitsev of the Moscow State University in Russia. The theoretical selectivity of the sensor to different hydrocarbons is due to the overlapping of rich vibrational spectra of gas molecules sorbed onto the surface (e.g. pollutant or VOC) with the adsorbed fluorescent dye. [27, 64]

It has been shown to be sensitive to organic vapors at low pressures under near vacuum conditions, but was not tested previously under ambient conditions to any great extent, hence the need for the experiments whose results were reported in the last two of this sensor to analyze. [27, 64]

6.3.1 The Effect of the Cadmium Sulfide Layer

The sensor, with the 0.5-micron cadmium sulfide layer used in this experiment, was prepared by Dr. Zaitsev at Moscow State University. A thin film of cadmium sulfide was deposited on a 2 mm thick glass substrate from a water solution of cadmium salt and

thiourea. [1, 73]

Cadmium sulfide is a semiconducting material, and as such, the electrons in the cadmium sulfide layer can become excited and be promoted into the conduction band where they are free to move throughout the crystal, including the surface of the sensor, as the material is subjected to an energy source such as the halogen lamp. When the charge covered surface is exposed to oxygen, oxygen anions are formed when oxygen sorbs to the surface and takes up an electrons. [3, 41]

Cadmium sulfide is both an insulating semiconductor and a crystal. From Reference 41, it has been found that negative ions, such as oxygen anions, can be reversibly adsorbed on insulating, crystalline photoconductors at room temperature under the action of bandgap light. In order to observe a large dependence on the photoconductivity by oxygen, it is necessary that the photoconductive channel be confined near the illuminated surface, so that the energy will be greatly affected by the formation of chemisorbed ions on the surface. [6, 41, 74]

Reference 75 describes the energy band diagram of a semiconductor. A semiconductor such as the cadmium sulfide surface used in this experiment has the following simplified energy band diagram taken from Reference 75, as shown in Figure 6.22.

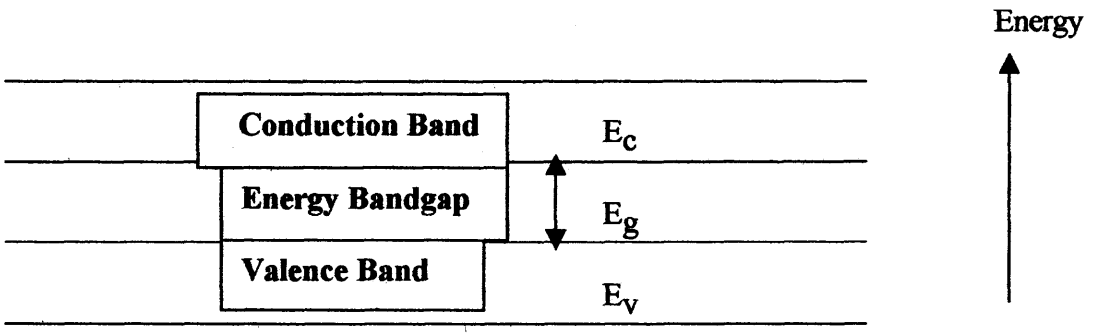

Figure 6.22 A simplified energy band diagram of semiconductors. [75]

Figure 6.22 depicts the valence band, where the valence electrons are situated in an atom, having a maximum energy of E_V. It also shows the conduction band having a minimum value of E_C. The energy difference between the valence band and the conduction band is E_g. [75]

An electron can get carried from the valence band to the conduction band due to light absorption if the photon energy is larger than the bandgap energy. If an electron does jump the bandgap, the photon energy is converted to kinetic energy. [75]

We have determined that the light from the halogen lamp in this study was 380 foot candles or 0.165 Lumens. The energy of the halogen lamp was approximately 4 X 10^{-19} Joules and the bandgap energy of the cadmium sulfide layer was 2.4 eV or 4 X 10^{-19} Joules, so there was sufficient energy for the electrons in the cadmium sulfide layer to jump the bandgap.

In a cadmium sulfide crystal, which is not photosensitive to red light, the photo-conducting channel depth is about one micron. [12, 41] For most of the experiments in this study, the thickness of the cadmium sulfide layer (CdS) was 0.5 microns. [73]

According to Reference 7, the thickness of the film of CdSe or CdS affects the sensor adsorption sensitivity. It was shown experimentally that the ratio of cation to anion, surface oxygen concentrations and film adsorption sensitivity all increased when the thickness of the film was changed from approximately 0.25 to 0.5 microns for CdSe sensors. [7]

The fluorescent dye on the surface of the sensor is a xanthene derivative containing large rings, and therefore provides a layer through which the oxygen must diffuse to get to the cadmium sulfide surface. [66]

Desorption of the oxygen can also occur with the subsequent loss of the electron back to the bulk of the cadmium sulfide material. According to Reference 41, a nitrogen atmosphere produces oxygen desorption of the sensor's surface. [41, 77]

As a dynamic equilibrium is reached the adsorption/desorption processes and the gain of electrons and loss of electrons by oxygen atoms process equilibrates. The process involving the gain of energy by electrons in the bulk of the cadmium sulfide layer, and then relocation to the cadmium sulfide layer surface also equilibrates with the loss of energy by the electron and their recombination back to the bulk of the cadmium sulfide as shown in Figure 6.23a. These processes result in an overall constant amount of oxygen ions and electrons on the sensor surface. [41]

Oxygen acts as a quencher in this experiment. According to Reference 77, "Molecular oxygen is a very effective quencher of some luminescent molecules. In the presence of oxygen the excited triplet state of the luminescent molecule may undergo collisional quenching with a singlet ground-state oxygen." [77]

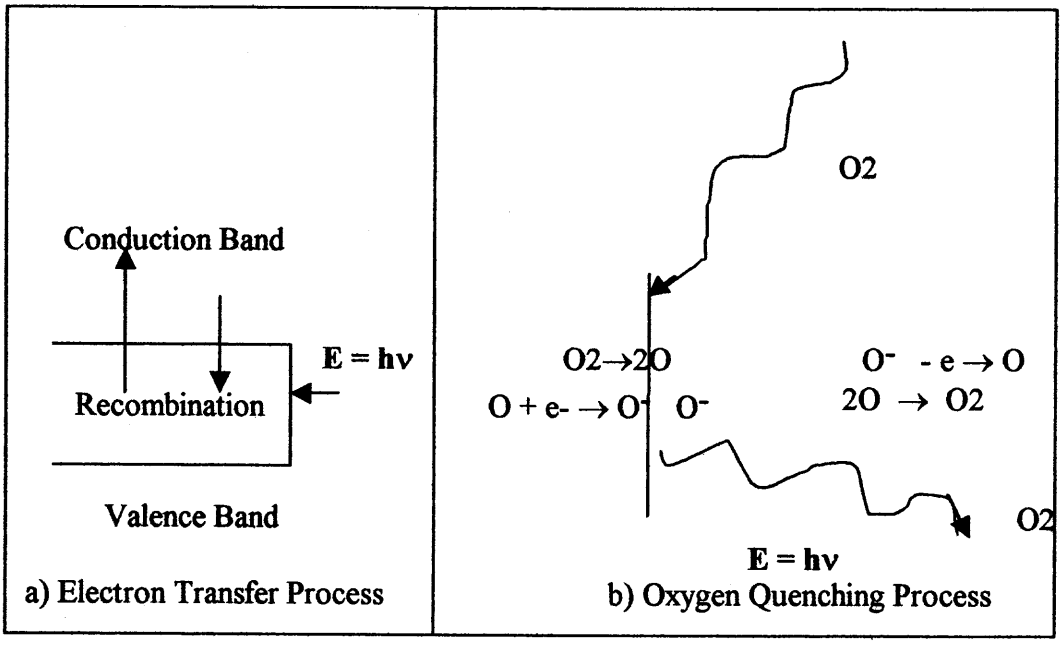

Figure 6.23 Model for photo-induced adsorption on CdS surface. [8, 41]

True quenching is a reversible process. If the quenching agent, in this case oxygen is removed from contact with the sensor, the original luminescent intensity is restored. For quenching to take place the quenching agent and the agent supplying the electron must collide.

A quencher molecule acts either by extracting an electron or supplying one to an excited molecule. After energy loss, the process is reversed. The process whereby oxygen acts as a quencher by extracting an electron from the surface and then returning it after energy loss is shown in Figure 6.23b. [41]

Figure 6.23b shows the electron transfer process. The thin cadmium sulfide layer, initially contains many electrons in the valence band. On exposure of the surface to a halogen lamp, the energy that is absorbed by the surface, [Energy (E) = Planck's constant (h) times the frequency of the light (ν)] is absorbed by the electrons and they become excited and enter the conduction band, where they can be quenched by the oxygen

molecules. [41] Oxygen has an electron valence configuration of $1s^2\ 2s^2\ 2p^4$ and an orbital diagram of the valence configuration (where circles represent orbitals and arrows represent electrons) is shown in Figure 6.24.

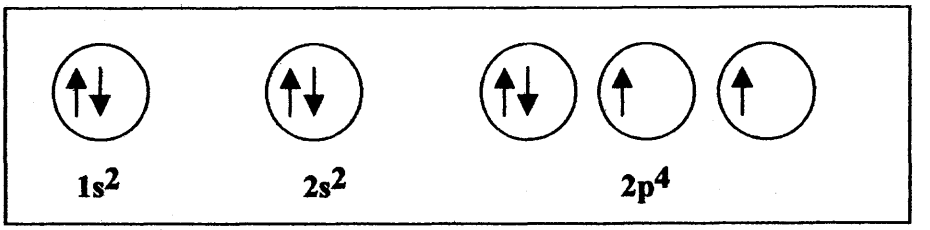

Figure 6.24 The electronic configuration of oxygen.

The arrows are in opposite directions in the same orbital to represent two electrons that have opposite spin. It can be seen from this orbital diagram of an oxygen atom that there are two orbitals that are not filled and can pick up an additional electron. [79]

Reference 8, contains data from a surface spectroscopic study of CdSe and CdS thin-film oxygen sensors. This study showed that two principal forms of oxygen are chemiadsorbed onto the sensor surface (O2- at a binding energy of 531.8 +/- 0.2 eV and O- at a binding energy of 531.1 +/- 0.2 eV). More oxygen was adsorbed when the surface was enriched with cadmium and it was the metal atoms that were determined to be the basic centers of oxygen chemiadsorption. [5, 8]

In Reference 80, Sootha et. al. report detecting the formation of oxygen radicals in CdS, so adsorption of oxygen on the surface of CdS is in the form of radicals. [8, 80] Reference 81 states that there are at least two types of adsorbed oxygen species present on CdSe surfaces. [81]

Figure 6.25 depicts the semiconductor, cadmium sulfide surface gaining energy from light application, which is resulting in an increase in current on the surface.

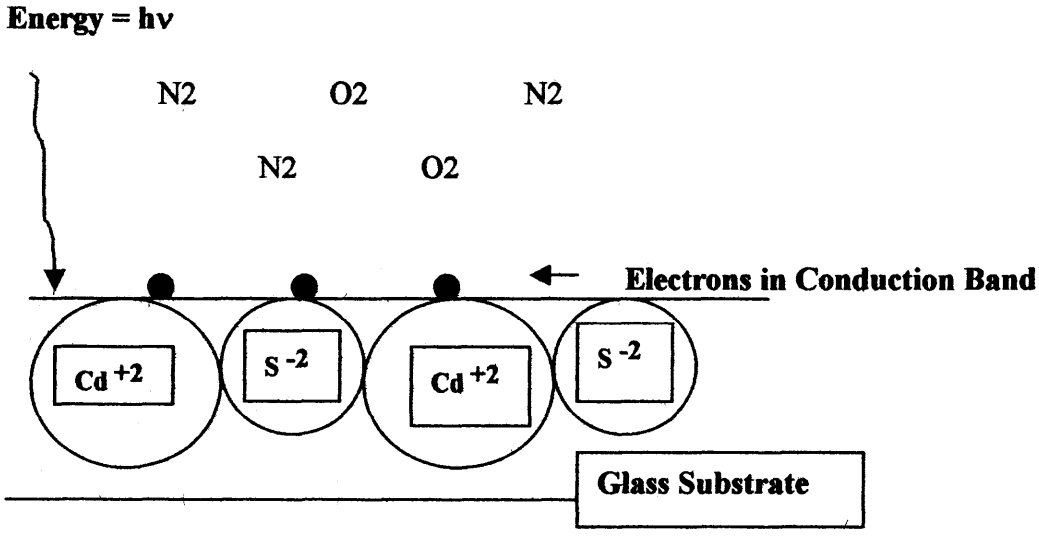

Figure 6.25 Depiction of surface current on the cadmium sulfide surface, during initial exposure to an oxygen/nitrogen environment.

Figure 6.25 shows the glass substrate on which the cadmium sulfide thin layer was formed. It is interesting to note that one of the basic components of glass is sodium (Na), which has a high mobility in the semiconductor CdS. The glass can enrich the CdS surface layer with Na, so it may have more cationic centers for oxygen chemiadsorption._[4] Na+ cations that migrate from the glass substrate layer to the CdS sensor layer offer more cationic sites for the oxygen radicals to chemiadsorb to. [4]

Figure 6.26 shows a simplified theory of the O^- and O^{-2} radicals being chemi-adsorbed onto the CdS surface. CdS is an ionic crystalline material composed of Cd^{+2} and S^{-2} ions. The oxygen radicals are negatively charged and are attracted to the Cd^{+2} cations on the surface of the sensor.

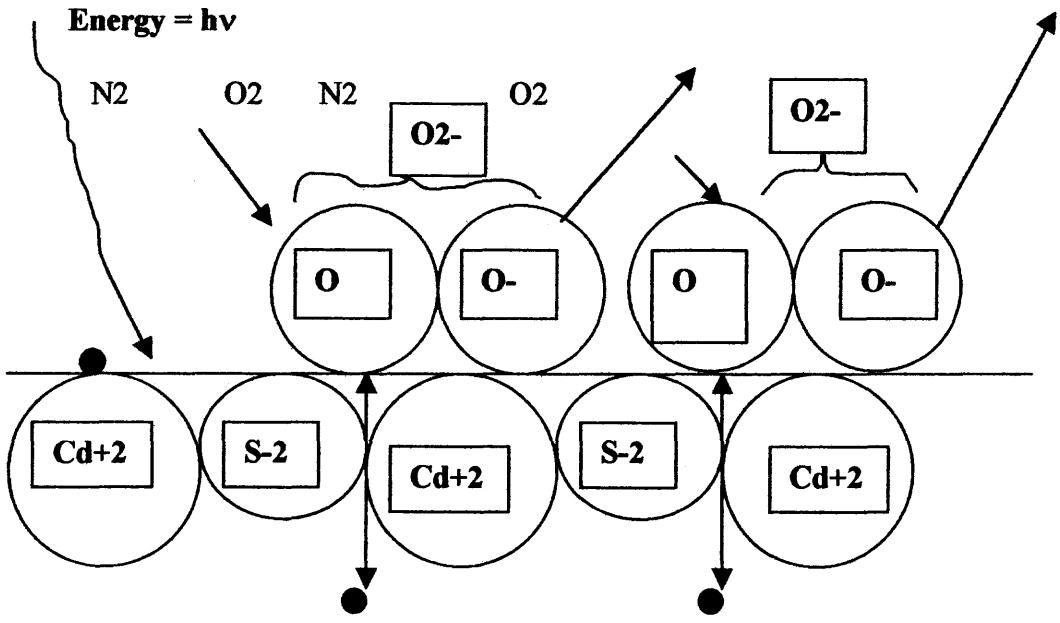

Figure 6.26 Depiction of the establishment of equilibrium, while light is being applied and synthetic air is in the sensor chamber (showing two oxygen molecules that have each picked up an electron and become an ion, adsorbing to the cadmium sulfide surface).

6.3.2 The Effect of the Rhodamine B Fluorescent Dye Layer

Rhodamine dyes, such as the one used in this experiment, are xanthene derivatives and have high fluorescent quantum yields, and therefore are widely used in technological applications.

The principle of fluorescent sensors, according to Reference 78, is that the intensity of the fluorescence from a dye is dependent on the concentration of oxygen present. [78]

Thin films of cadmium sulfide are highly sensitive to oxygen chemisorption and can act as oxygen sensors without a fluorescent dye, however. The oxygen atom picks up an electron from the CdS crystal and becomes negatively charged and then chemically bonds to the cadmium cation. The amount of electrons picked up (or the reduction in current) is directly proportional to the concentration of oxygen molecules present. [6, 82]

The principle of fluorescent sensors, according to Reference 78, is that the intensity of the fluorescence from a dye is dependent on the concentration of oxygen present. Each oxygen molecule can pick up energy, so the fluorescence intensity measured is proportional to the inverse of the oxygen concentration (the lower the fluorescence, the higher the oxygen concentration). [78]

The diagram in Figure 6.27 is from Reference 83, and will be used to explain the reason why the sensor has a huge response to the oxygen in air. It is difficult to detect toluene or other organic gases in air with the sensor, due to this large response to oxygen. In Figure 6.27, S_0 is the singlet ground state and S_1, S_2, and S_3 are the singlet excited states. T_1 is the triplet excited state. The straight arrows represent radiative processes and the curved arrows represent nonradiative processes.

The triplet states contain electrons that are not paired, while the singlet states contain paired electrons. The absorption of energy by a diamagnetic molecule (substances for which the magnetization is opposed to the field) usually changes its state from a singlet ground state to a singlet excited state. Depending on how much energy is absorbed, the molecule in the singlet ground state S_0 can jump to the energy level excited states of either S_1, S_2, or S_3.

The processes labeled in Figure 6.27 as internal conversion or intersystem crossing correspond to nonradiative losses in energy between states and are fast processes, and occur so rapidly that they precede fluorescence, phosphorescence, and chemical reactions. (Fluorescence is the radiation emitted between the same type of states such as singlet-singlet transitions, while phosphorescence is between different states such as triplet-singlet transitions). [83]

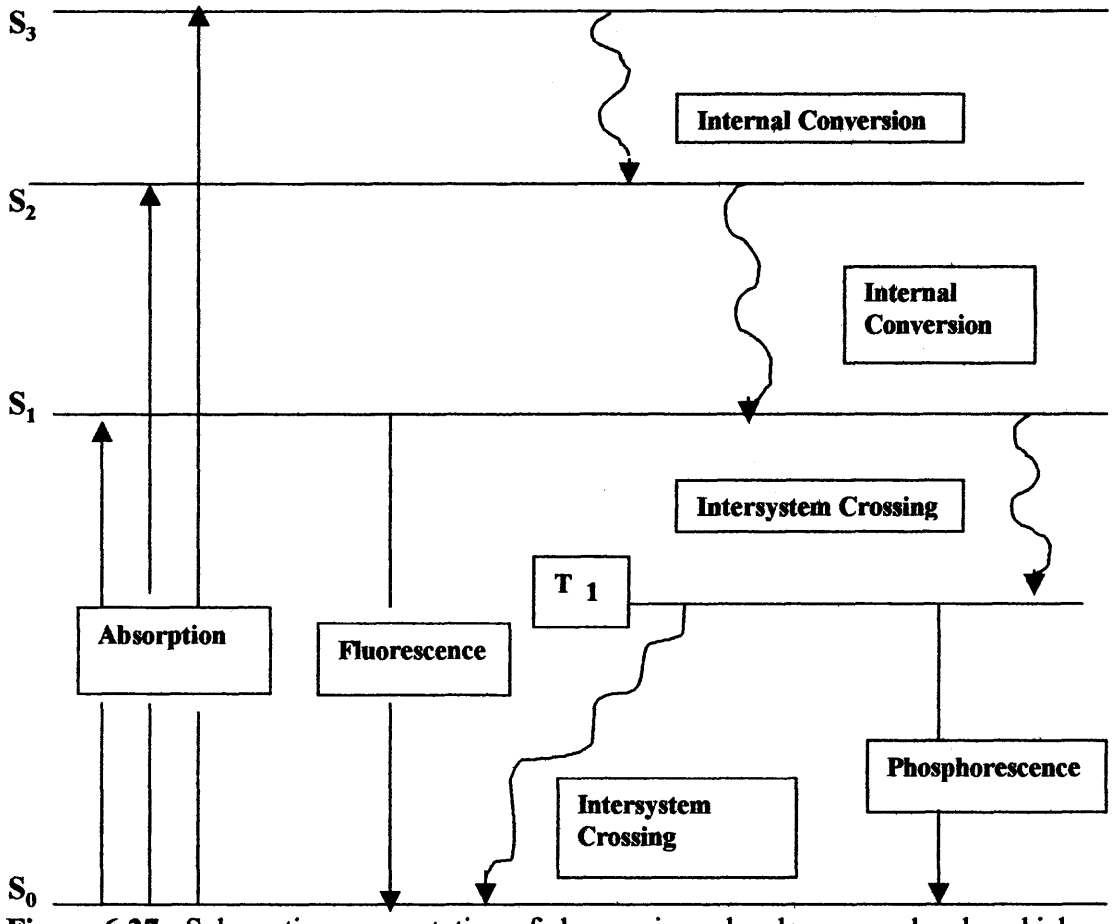

Figure 6.27 Schematic representation of changes in molecular energy levels, which may occur upon absorption of radiation. [83]

According to the theory on which this gas sensor was developed, the adsorbed dye molecules experience a singlet-singlet $S_0 \rightarrow S_1$ transition induced by the halogen lamp. This means that the dye molecules go from a ground state singlet molecule to an excited state singlet molecule due to the absorption of energy from the light. Energy can then be transferred through five different channels:

1. Luminescence (Fluorescence)
2. Nonradiative energy transfer to near adsorbed molecules through the Forster-Dexter induction-resonance mechanism (Intersystem Crossing)

3. Intermolecular singlet-triplet transfer (Phosphorescence)
4. Electron-vibrational coupling (Internal energy conversion to vibrational modes)
5. Nonradiative energy transfer to the solid (Intersystem Crossing) [64]

A reference has been found, which describes a new type of laser-scanning. A reference has been found, which describes a new type of laser-scanning spectroscopy process which can be used to determine the photophysical and photochemical properties of electronically excited fluorescent dyes, such as the Rhodamine B dye used in this experiment. This reference is listed as Reference 66 in this report. [66]

The triplet oxygen molecule, which is always present in air, frequently acts an efficient intermolecular quencher for excited singlet and triplet states. The Rhodamine dye is in the excited singlet state after it absorbs energy from the halogen lamp. [66] It is believed that this quenching of the excited singlet state of the dye molecules to their ground state, and the subsequent addition of energy and electrons to the oxygen molecule is the reason that the photoresistance of the sensor increases so rapidly when air is emitted into the sensor chamber.

The process that takes place during this quenching by triplet oxygen molecules is due to intersystem crossing, which is a much more rapid process than the fluorescence, or phosfluorescence processes. [83]

It appears that this intersystem crossing may predominate the energy transfer to such a great extent that channel number two (Nonradiative energy transfer to near adsorbed molecules through the Forster-Dexter induction resonance mechanism) is the

only reaction that really needs to be looked at. The rate constant for the Forster-Dexter mechanism is given by:

$$k_{FD} = [(R_o/R)^6]/\lambda_o \qquad (6.3)$$

R = the distance from donor to acceptor,

R_o = the critical radius (approximately five nanometers),

λ_o = the excited state lifetime of the isolated dye molecule.

k_{FD} = rate constant for the Forster-Dexter mechanism [27, 64]

The equation for the rate constant of the Forster-Dexter mechanism was taken from References 27 and 64. This equation contains the excited state lifetime of the isolated dye molecule as a denominator, and so the rate constant is inversely proportional to it. Since the excited state lifetime of the dye molecule is so short the rate constant is a very large number, and this fact explains why the photoresistance of the sensor increases so rapidly due to the introduction of air (oxygen).

Another reference was found which reported the same results as our experiment but with another dye (ETHT 3001). The luminescence of this dye was quenched by oxygen, as shown in Figure 6.28. [84]

Figure 6.28 shows the photon of light energy equal to hν being absorbed by the dye molecule, when it is in its ground state. (h is equal to Planck's constant and ν is the frequency of the light shining on the dye molecule). When the dye molecule absorbs the light, it increases in energy and becomes an excited state, symbolized by the square brackets and the asterisk.

After it reaches an excited state it can either release its photon of energy as luminescence or can become quenched by the oxygen molecules, and no luminescence

will occur. The theory described in this section is the basis for a luminescence-based oxygen sensor and it appears that the applications for which this sensor was developed would be pertinent for the sensor described in this report as well. [84]

The quenching mechanism occurs when the oxygen molecule collides with a dye molecule and absorbs the energy from the excited dye molecule. The oxygen molecule then undergoes a triplet-to-singlet transition and the dye molecule experiences a nonradiative relaxation and there is no fluorescence. [85]

Reference 85 describes an optical oxygen sensor, which has been developed based on this technology using a silica aerogel. [85]

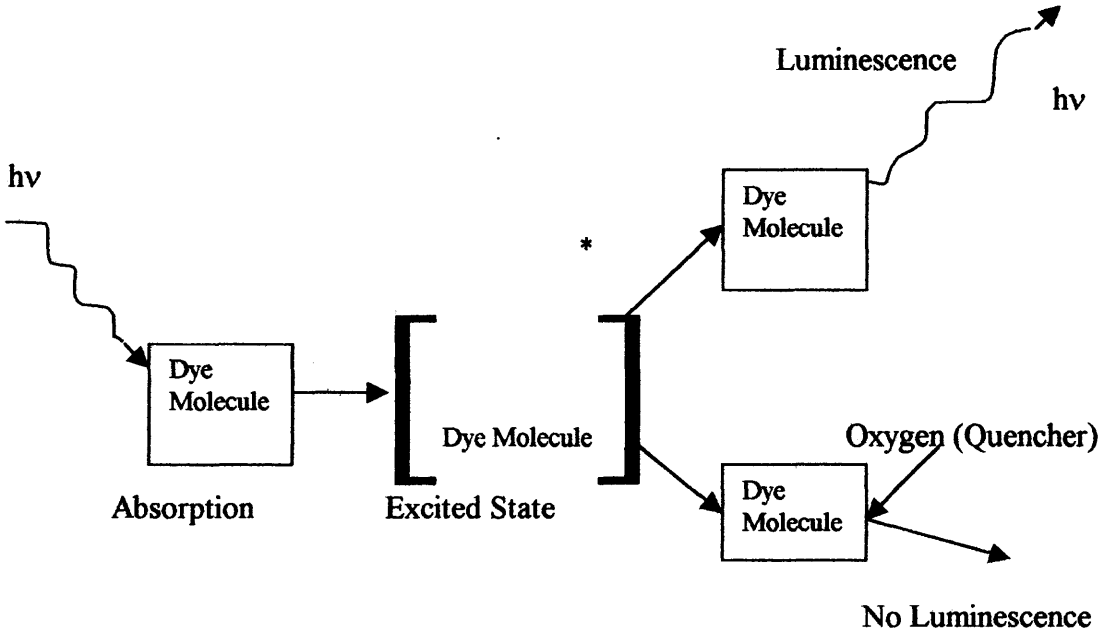

Figure 6.28 A pictorial depiction of the absorption of light energy by a dye molecule and the subsequent luminescence or oxygen quenching process. [84]

Another reference refers to a new product developed as an oxygen sensor for respiration monitoring by Ocean Optics, Inc. and can be found on the website listed in Reference 86.

It was determined by experimentation that an oxygen-free surface responds ideally to oxygen according to the Stern-Volmer law for quenching, during the first minute or two of oxygen exposure when using either synthetic or atmospheric air. The response of the surface to oxygen quenching is enhanced by the use of the fluorescent dye. [78, 86]

With a certain fluorescent dye such as Rhodamine B, optical excitation elicits fluorescence of a specific wavelength. The amount of luminescence energy transferred to the oxygen is dependent on the concentration of oxygen present. This relationship is described by the Stern-Volmer equation:

$$I_0 / I = t_0 / t = 1 + K_{sv} [O_2] \tag{6.4}$$

Where:

I_0 = Luminescent intensity with no oxygen present

I = Luminescent intensity at time, t, with a particular oxygen concentration

t_0 = time with no oxygen concentration

t = time of the I measurement

K_{sv} = the Stern-Volmer constant [78]

The Stern-Volmer law, states that the fluorescence intensity ratio is linearly based on two competing reactions: a unimolecular light emission and a bimolecular quenching encounter. This law applies as long as quenching is entirely diffusional. [15, 72]

Reference 72 describes how the Stern-Volmer equation was derived. For a fluorescence quenching process, the simplest process involves:

1) *Absorption* – The absorption of energy (hν) by A, an electron in the cadmium sulfide layer in this case, to become an excited (*) electron involves the following kinetics equation:

$$A + h\nu \xrightarrow{k_i} A^* \tag{6.5}$$

Where k_i is the rate constant for the absorption kinetics equation. [72]

2) *Quenching* – The next kinetics equation in the process is for quenching, a pick-up of an electron and energy by the quencher (oxygen in this case).

$$A^* + O_2 \xrightarrow{k_q} A + O_2 \tag{6.6}$$

Where k_q is the rate constant for the quenching kinetics equation. [72]

3) *Fluorescence* – The last kinetics equation in the process is for fluorescence, a loss of energy by the electron.

$$A^* \xrightarrow{k_r} A + h\nu \tag{6.7}$$

Where k_r is the rate constant for the quenching kinetics equation. [72]

If the symbol, I, is used to represent the absorbed light intensity and [A] represents the concentration of electrons, [A^*] represents the concentration of excited electrons and [O_2] represents the concentration of oxygen, then:

$$I\,(\text{Absorption}) = k_i\,[A] \tag{6.8}$$

$$I\,(\text{Quenching}) = k_q\,[O_2]\,[A^*] \tag{6.9}$$

$$I\,(\text{Fluorescence}) = k_r\,[A^*] \tag{6.10}$$

By conservation of energy over species A:

$$I\,(\text{Absorption}) = I\,(\text{Quenching}) + I\,(\text{Fluorescence}) \tag{6.11}$$

If both sides of the above equation are divided by I (Fluorescence), then it becomes:

$$\frac{I\,(Absorption)}{I\,(Fluorescence)} = \frac{I\,(Quenching)}{I\,(Fluorescence)} + 1 \qquad (6.12)$$

And replacing the I (Quenching) and I (Fluorescence) by their kinetic equations in the term after the equal sign yields:

$$\frac{I\,(Absorption)}{I\,(Fluorescence)} = (k_q\,[O_2]\,[A^*])/(k_r\,[A^*]) + 1 = (k_q\,[O_2])/k_r + 1 \qquad (6.13)$$

$$\frac{I\,(Absorption)}{I\,(Fluorescence)} = K[O_2] + 1 \qquad (6.14)$$

Where: K (The Stern-Volmer constant) = k_q / k_r (6.15)

If the intensity ratio is graphed versus the oxygen concentration, the ratio of slope to intercept will be K , regardless of the units used for measuring the intensity. (The resistance of the cadmium sulfide surface was used in this study). [72] This is the same as the Stern-Volmer equation, given above from Reference 78.

After the initial exposure of the oxygen-free sensor to oxygen, the response no longer can be described by the Stern-Volmer law, because the chemiadsorption of the oxygen ion to the sensor surface becomes the dominant step. It was found that the next 10 to 11 minutes of exposure time, instead follows the Elovich equation for chemi-adsorption for the determination of the photocurrent as a function of time. The Elovich equation can only be used for a finite time however, because it neglects the desorption of the oxygen ion from the surface, which becomes more predominant as an equilibrium is reached. [41]

6.4 Response of the Sensor to the Oxygen in Atmospheric Air Versus Synthetic Air

6.4.1 Response of the Sensor to the Oxygen in Atmospheric Air

Experiments were also performed with atmospheric air instead of synthetic air to determine the practicality of the sensor by studying its response in an ambient environment. Figures 6.29 and 6.30 resulted. (The procedures for these experiments are described in Section 4.10).

Sensor resistance data versus sensor exposure time to different concentrations of atmospheric air and nitrogen were graphed in Figure 6.29. The curves in Figure 6.29 are similar in shape to those in Figure 6.5.

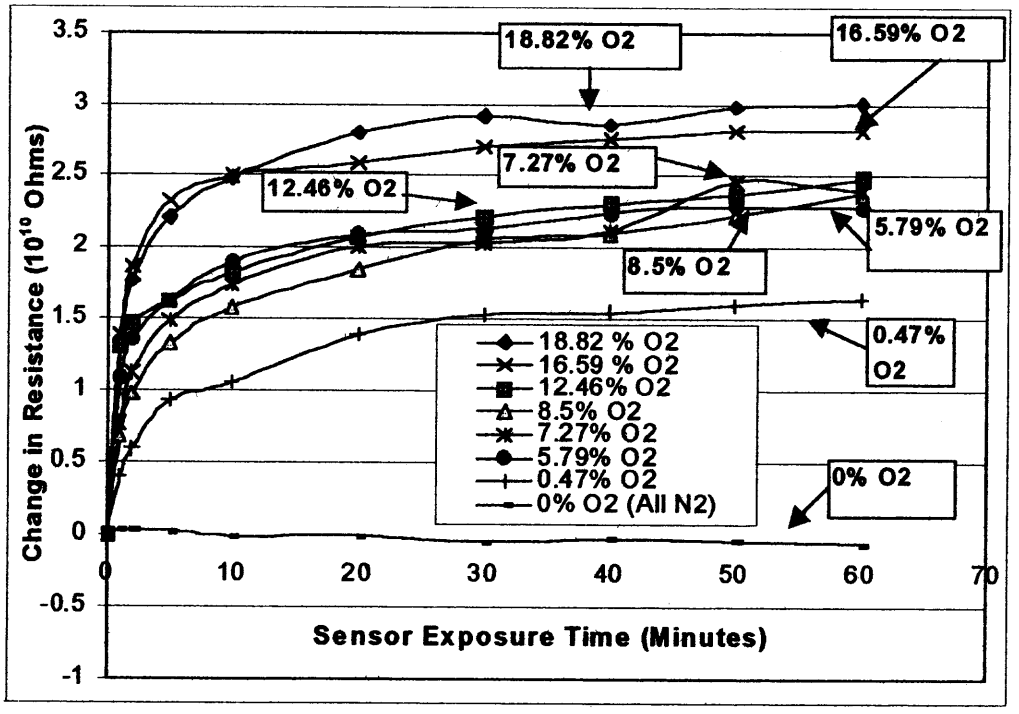

Figure 6.29 Resistance versus sensor exposure time for atmospheric air at various oxygen concentrations.

The initial slopes of each of the curves in Figure 6.29 are plotted in Figure 6.30. The initial change in resistance versus percent oxygen data given in Figure 6.30 are linear

when using atmospheric air as they were with synthetic air (Figure 6.12) when using the desorption equilibrium potential value as the initial resistance value.

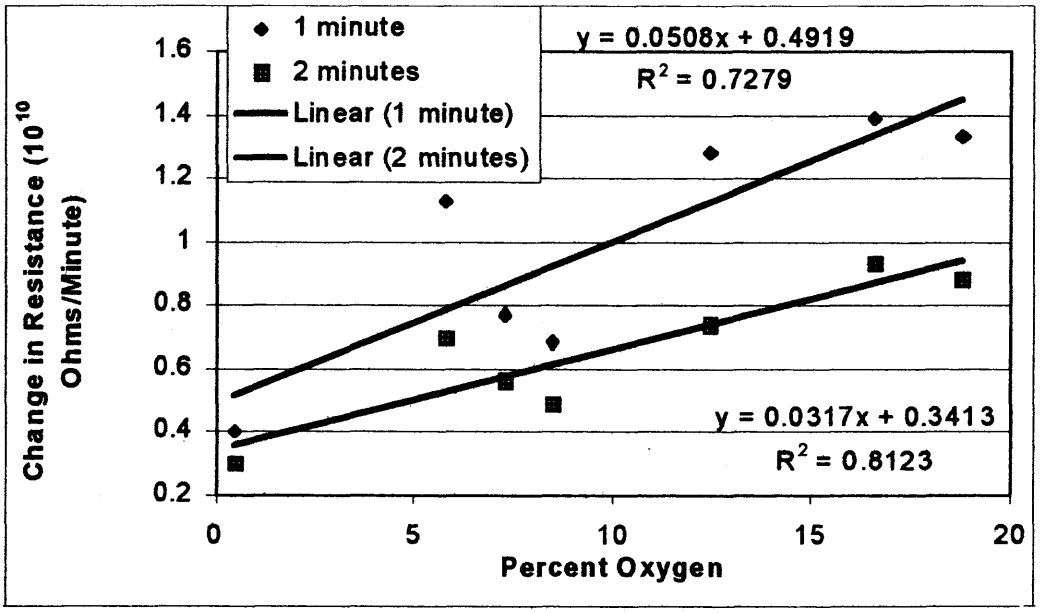

Figure 6.30 Initial slopes of the curves in Figure 6.29 using atmospheric air.

A comparison of the initial slope equations obtained in Figure 6.30 for atmospheric air versus those obtained with synthetic air in Figure 6.12 is as follows:

Table 6.3 A Comparison of the Linear Equations in Figures 6.12 and 6.30

	Synthetic Air (Figure 6.12)	Atmospheric Air (Figure 6.30)
During the First Minute	$y = 0.0307\,x + 0.337$	$y = 0.0508\,x + 0.4919$
During the Second Minute	$y = 0.0228\,x + 0.229$	$y = 0.0317\,x + 0.3413$

The atmospheric air caused a larger response than the synthetic air during both the first and second minutes of oxygen exposure.

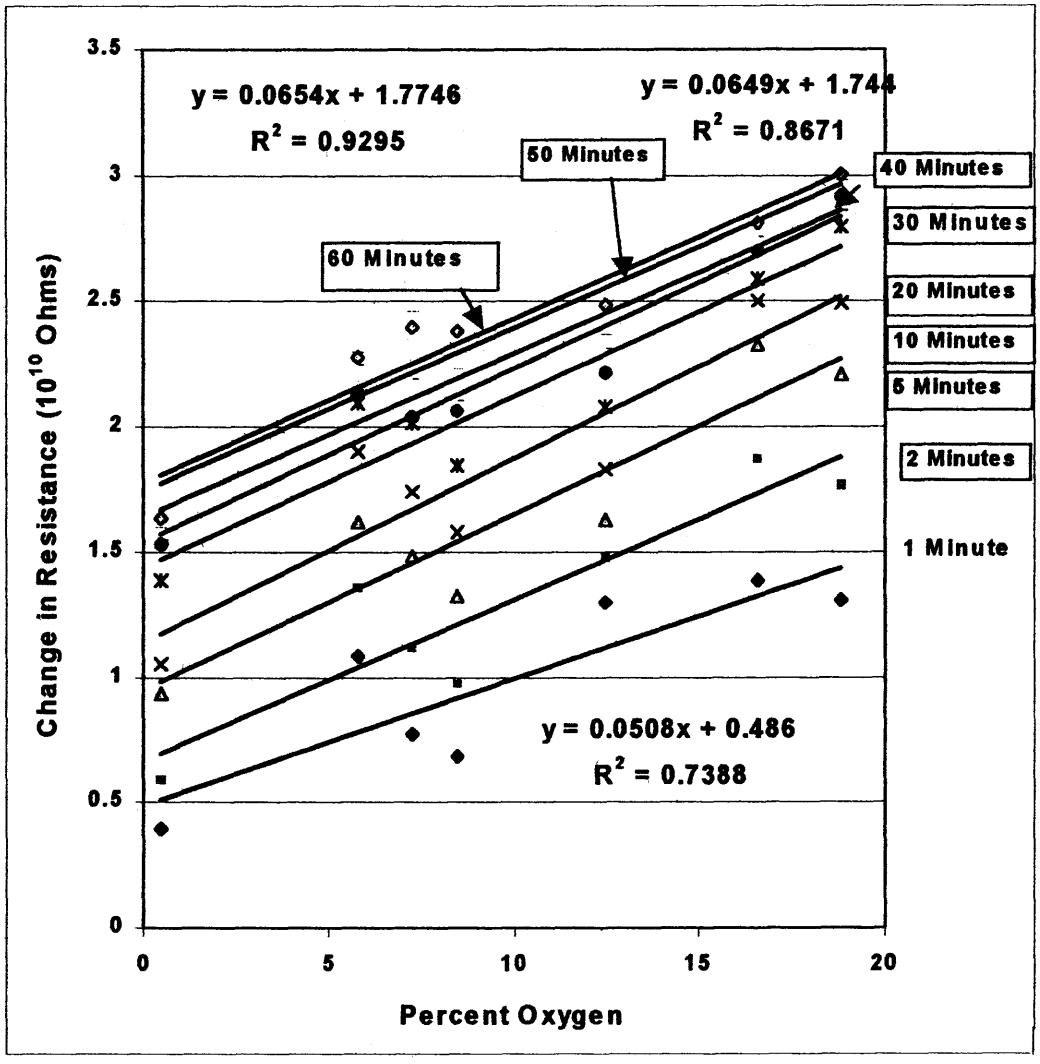

Figure 6.31 Resistance versus percent oxygen in atmospheric air mixtures at different sensor exposure times.

The resistance versus percent oxygen concentration data in Figure 6.31 for atmospheric air are very different from similar data for synthetic air shown in Figure 6.14.

The atmospheric air curves can be represented by linear equations for the entire range of one minute to 60 minutes of exposure time, whereas the synthetic air curves are

represented by second order polynomials except for the first or second minutes of exposure, which may be represented as a linear function.

In Figure 6.14, the equilibrium curve at 60 minutes for synthetic air is:

$$y = -0.0112\,x2 + 0.3227x + 0.1659 \qquad (6.16)$$

and from Figure 6.31, the equilibrium line at 60 minutes for atmospheric air is:

$$y = 0.0654\,x + 1.7746 \qquad (6.17)$$

This shows that the Stern-Volmer law of quenching, which states that the fluorescent intensity is linearly proportional to the quencher concentration, is obeyed from the start of the run until the finish at 60 minutes, only when atmospheric air is used.

Additional experimentation was undertaken to understand why this difference occurred.

Table 6.4 Graphical Equations Shown in Figure 6.31

Sensor Exposure Time (Minutes)	Equation	R squared
1	y = 0.0508x + 0.4860	0.7388
2	y = 0.0641x + 0.6689	0.8354
5	y = 0.0701x + 0.9489	0.8522
10	y = 0.0732x + 1.1398	0.8463
20	y = 0.0681x + 1.4354	0.8779
30	y = 0.0690x + 1.5390	0.9334
40	y = 0.0647x + 1.6410	0.9087
50	y = 0.0649x + 1.7440	0.8671
60	y = 0.0654x + 1.7746	0.9295

Figure 6.32 gives the results of plotting the ratio of the current or millivolt potentials minus one versus the % oxygen concentration after 1 and 2 minutes of atmospheric air sensor exposure, which represent the parameters of the Stern-Volmer equation.

A comparison of equations obtained with synthetic air, as graphed in Figure 6.13, with the equations obtained with atmospheric air in Figure 6.32, yields Table 6.5.

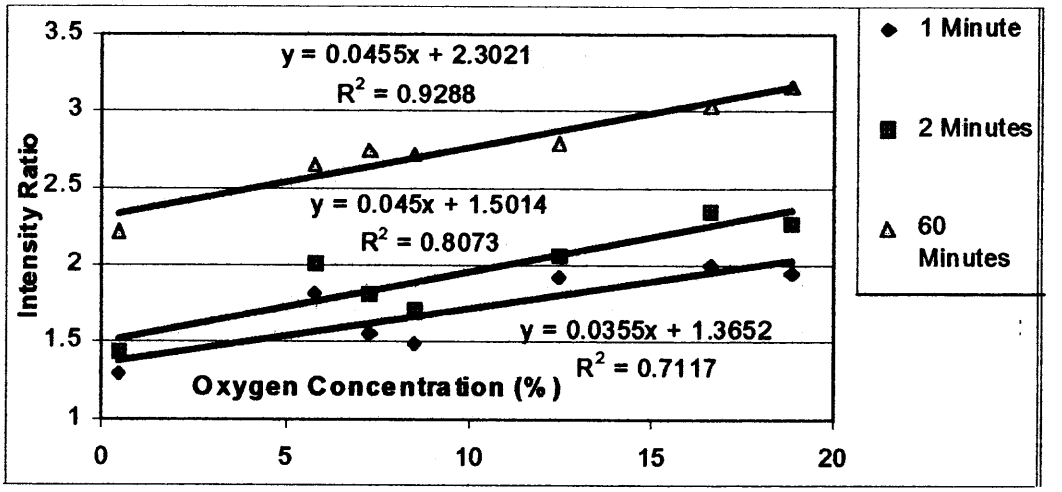

Figure 6.32 A plot of the Stern-Volmer equation for atmospheric air after 1 and 2 minutes of oxygen exposure.

Table 6.5 A Comparison of the Linear Equations in Figures 6.13 and 6.32

	Synthetic Air (Figure 6.13)	Atmospheric Air (Figure 6.32)
During the First Minute	y = 0.0094 x + 1.1033	y = 0.0355 x + 1.3652
During the Second Minute	y = 0.0141x + 1.1403	y = 0.045 x + 1.5014

The atmospheric air response is about four times that of the synthetic air, meaning that the resistance increases faster with synthetic air during the first one to two minutes of exposure time.

The value of the Stern-Volmer constant, K, for atmospheric air is the slope over the intercept from Figure 6.32. The values for 1 minute, 2 minutes and 60 minutes of sensor exposure time to atmospheric air as compared to synthetic air are given in Table 6.6.

Table 6.6 The Stern-Volmer Constant for Atmospheric Air and Synthetic Air Exposure at 1, 2 and 60 Minutes of Exposure Time

	Atmospheric Air	Synthetic Air
1 minute	K = 0.0260	K = 0.0085
2 minutes	K = 0.0300	K = 0.0124
60 minutes	K = 0.0198	Doesn't Apply

The Stern-Volmer constant is the ratio of the quenching rate constant over the fluorescence rate constant. The Stern-Volmer constant for the sensor using synthetic air is less than it is with atmospheric air during the initial exposure times, meaning that ratio of the quenching rate over the fluorescence rate is less with synthetic air initially.

6.4.2 Atmospheric Air Versus Synthetic Air Using the Same Initial Resistance Value for Each Run

This experiment was the same as the experiment described in experimental procedure Section 4.10, except that the air used was atmospheric air (using a compressor) instead of synthetic air. (The procedure for this experiment is described in Section 4.11).

The sensor was exposed to atmospheric air instead of synthetic air, using the same initial resistance value (baseline) as had been used for the synthetic air run. The results shown in Figure 6.33 were obtained. (In both runs, vacuum was applied for ten minutes followed by nitrogen application at 15 psig for ten minutes, to desorb the sample gas, and this procedure was repeated numerous times prior to and after air exposure).

The difference between desorption in the two runs, was that helium gas was used for a short time, from approximately 35 to 45 minutes during the synthetic air run, to see if it performed the same as the nitrogen, and in the atmospheric air run, nitrogen was used throughout.

It can be seen from Figure 6.33 that the atmospheric air produces a lower resistance versus time than synthetic air, although the two adsorption/desorption curves are similar in shape.

The reason for the difference in resistance is that polar gases, such as H2O, can be reversibly adsorbed on the sensor surface as well as O2. [41]

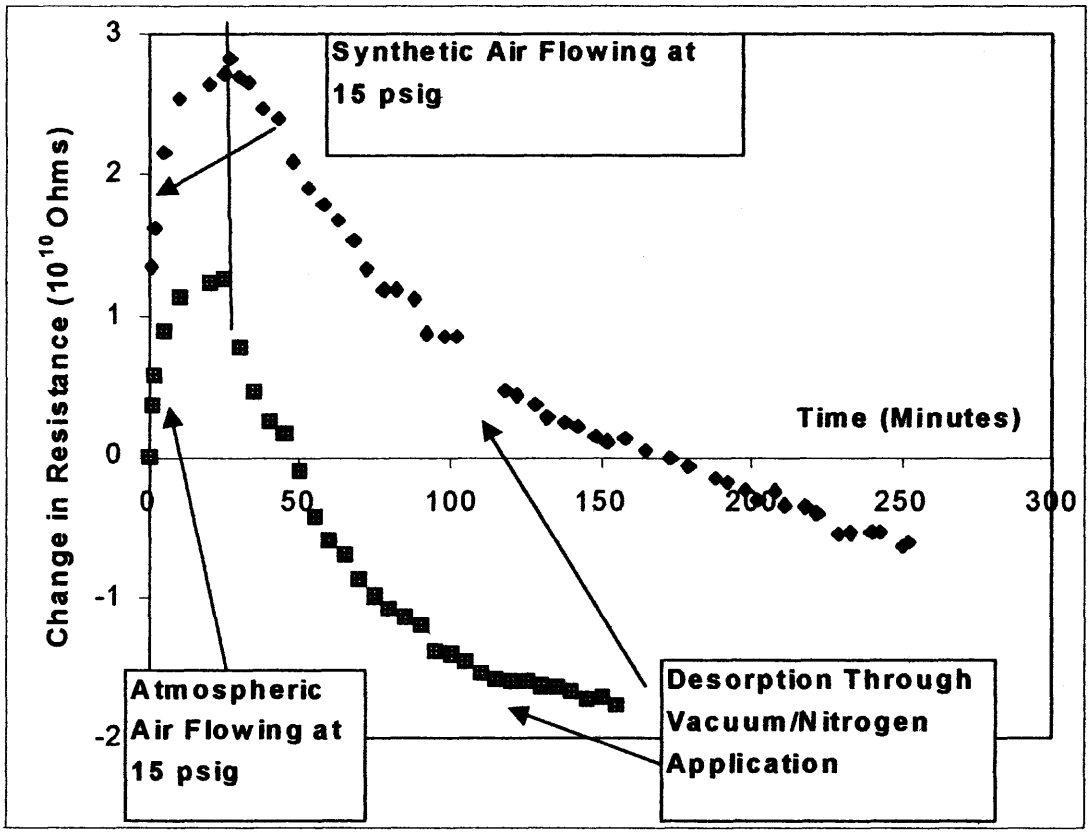

Figure 6.33 Resistance versus exposure time after air exposure and the subsequent desorption process for synthetic versus atmospheric air using the same initial resistance value.

Other sorbed gases compete with oxygen for sorption sites, which explains the lower response of the sensor to atmospheric air versus synthetic air.

In Reference 41, N2O adsorbed on the CdS surface, and this adsorption resulted in a smaller sensor equilibrium resistance value than with the adsorption of oxygen.

Reference 41 states that electronegative gases like N2O can be reversibly adsorbed on insulator surfaces such as CdS. [41]

According to Reference 3, CdS sensors are sensitive to carbon monoxide, CO, and Reference 4 showed that CdS sensors are sensitive to microconcentrations of SO2 in atmospheric air. [3, 4]

Adsorption of water instead of oxygen ions on the sensor surface causes a higher flow of current because water cannot pick up electrons to lower the current flow like oxygen can, and this leads to a lower response (resistance) of the sensor with atmospheric air than with synthetic air. [41]

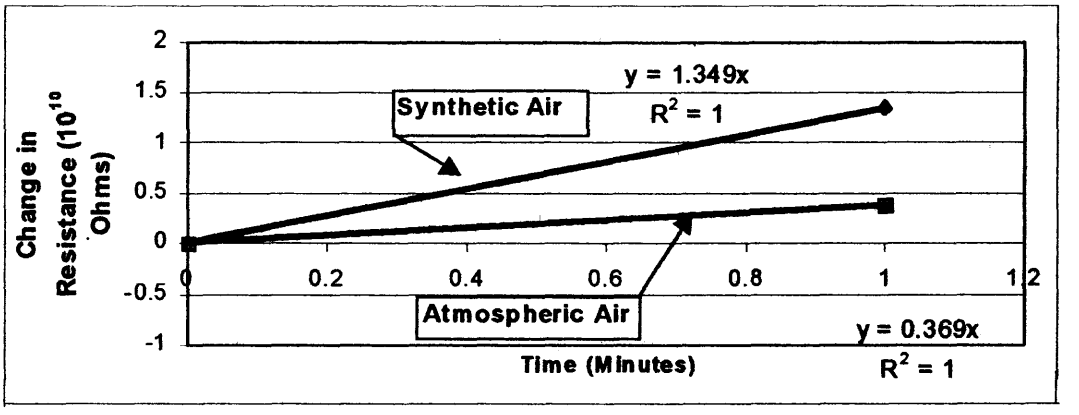

Figure 6.34 Resistance versus exposure time during the first minute of air exposure for atmospheric and synthetic air using the same initial resistance value (first section of Figure 6.33).

In order to be able to compare initial slopes of atmospheric air data with synthetic air data, the initial resistance of the atmospheric air experiment, will need to be lowered to around 1.5 x 10^{10} ohms instead of around 3.3 x 10^{10} ohms, which was used with the synthetic air. This was done so that the initial starting points of both runs with the two types of air were at their respective equilibrium desorption resistance values.

Data from Figures 6.17, 6.18 and 6.21 were replotted with the atmospheric air data in Figures 6.34, 6.35 and 6.36 for comparison purposes.

Figures 6.34, 6.35 and 6.36 indicate that atmospheric air consistently produces a much lower resistance and consequently a higher current or potential than synthetic air throughout the adsorption and desorption sections of their curves, even though the runs were started at the same initial resistance values.

The curves are very similar in the desorption, but dissimilar in the initial minute of the run. The synthetic air showed a slope that was approximately four times greater than the atmospheric air did, as shown in the graphs in Figure 6.34.

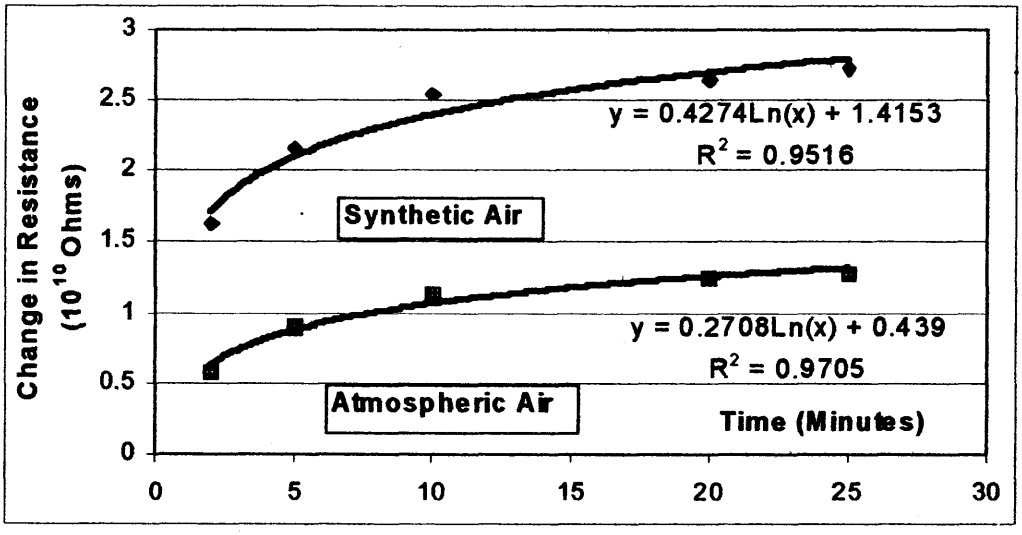

Figure 6.35 Resistance versus exposure time during 2 to 25 minutes of air exposure for both synthetic and atmospheric air using the same initial resistance value (second section of Figure 6.33).

Figure 6.35 contains data that shows that the synthetic air and atmospheric air curves had fairly similar logarithmic shapes in the 2 to 25 minute section of the runs, and the desorption curves in Figure 6.36 are very similar.

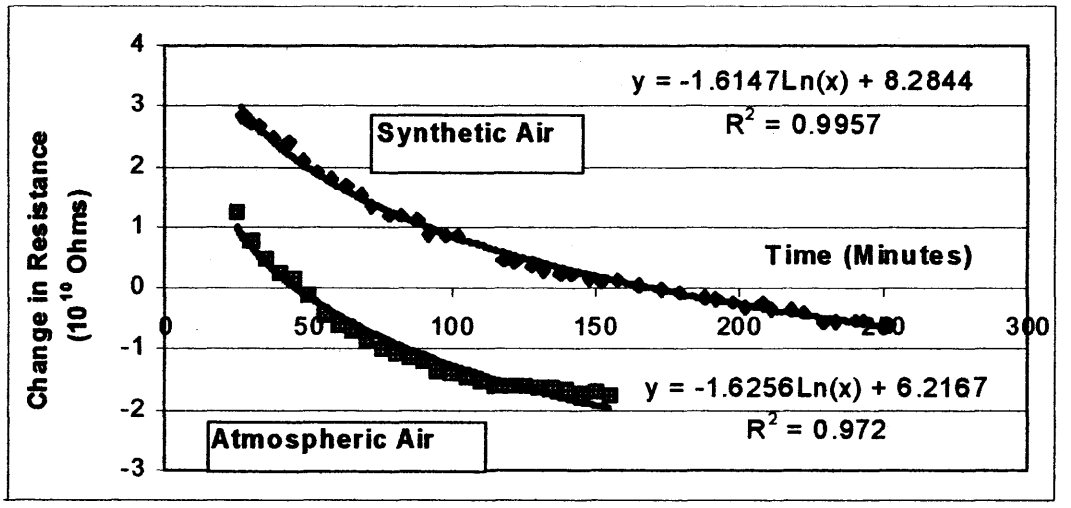

Figure 6.36 Resistance versus exposure time during the desorption process for both synthetic and atmospheric air using the same initial resistance value (third section of Figure 6.33).

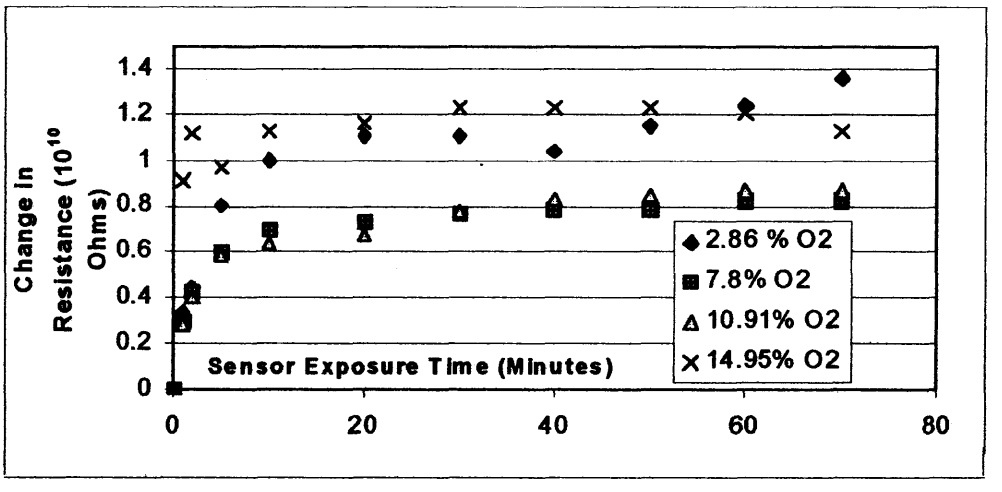

Figure 6.37 Resistance versus sensor exposure time using atmospheric air.

Figure 6.37 contains a graph of resistance versus sensor exposure time for four different atmospheric air/nitrogen mixtures. (The 2.86% oxygen curve appears to be off compared to other data).

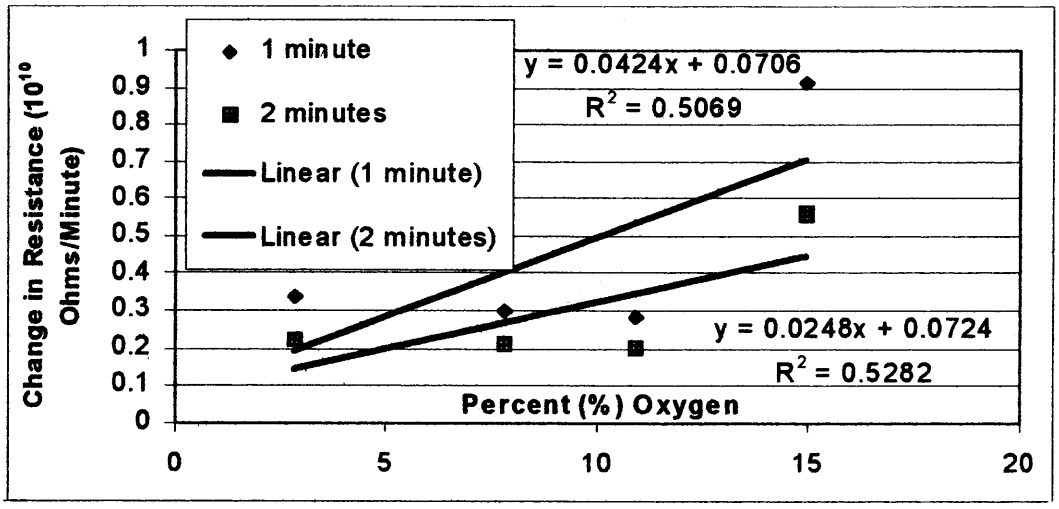

Figure 6.38 Initial slopes using atmospheric air and the same initial resistance value as the synthetic air.

The data in Figure 6.38 show the initial slopes obtained during the first minutes of oxygen exposure. The slopes were not linear like those obtained with the synthetic air, so it was assumed that this was due to the fact that the baseline was not the equilibrium resistance obtained after desorption like the synthetic air had been.

This run was then repeated so that the two different air types would not have the same initial resistance value (baseline), but would instead both have initial resistance values corresponding to their equilibrium desorption values.

6.4.3 Atmospheric Air Versus Synthetic Air Using Different Initial Resistance Values for Each Run

The atmospheric air curve was redone using a different and much lower initial resistance value, to better correspond with the equilibrium resistance value obtained with the desorption portion of the curve for atmospheric air. Results are shown in Figure 6.39. (The details of the experimental procedures are described in Section 4.13).

A potential of 64.5 millivolts was used as the baseline with the atmospheric air instead of 27.3 millivolts, which had been used for both the synthetic and atmospheric air in Figure 6.39.

Subsequently, Figures 6.34, 6.35 and 6.36 were redone with the new data graphed in the atmospheric air curve in Figure 6.39. Figures 6.40 and 6.41 compares the initial slopes of the atmospheric air versus the synthetic air while they were flowing through the sensor chamber at 15 psig at the one and two minute exposure marks.

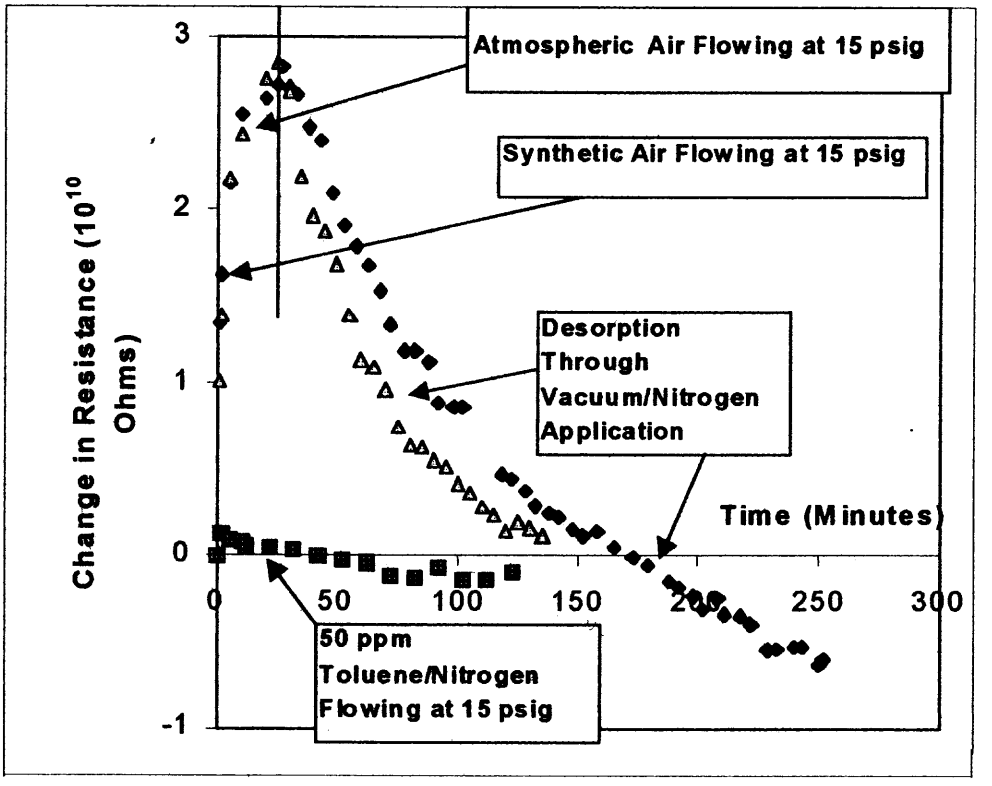

Figure 6.39 Resistance versus exposure time after air exposure and the subsequent desorption process for synthetic versus atmospheric air using different initial resistance values equal to the desorption equilibrium resistance values for each run.

The data in Figure 6.40 show the slope after the first minute of exposure and Figure 6.41 shows the initial slope during the first 2 minutes of exposure of the change in resistance versus time of sensor exposure.

Figures 6.40 and 6.41 contain graphs that show that the initial slope of the synthetic air and atmospheric air curves are much more similar, when a different initial resistance value or potential value corresponding to the equilibrium desorption potential value was used, than when the same potential or resistance baseline was used as shown in Figure 6.33.

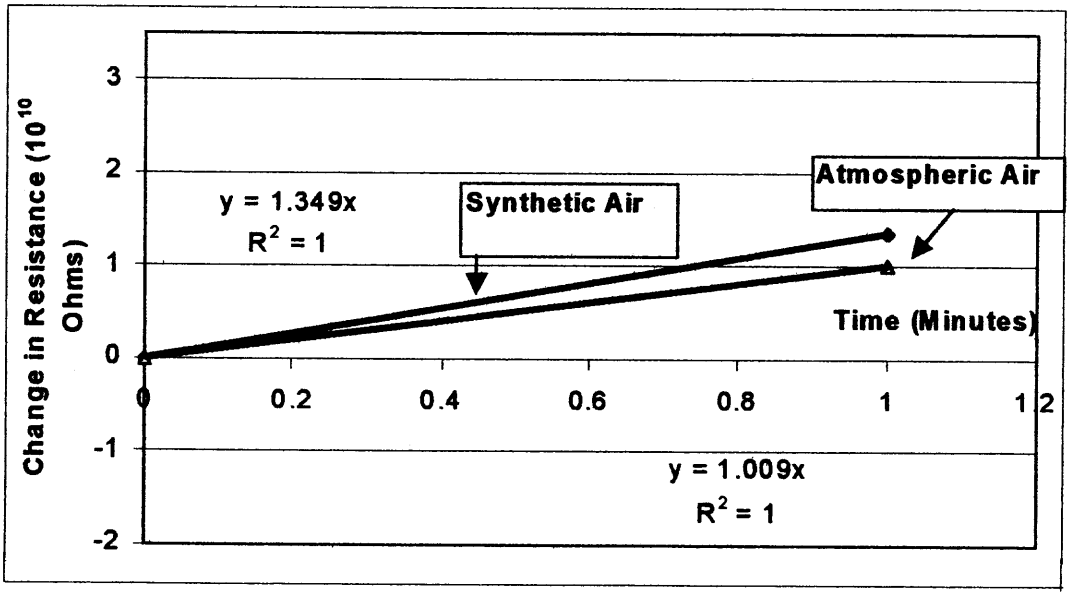

Figure 6.40 Resistance versus exposure time during the first minute of air exposure for atmospheric and synthetic air using different initial resistance values (first section of Figure 6.34).

Table 6.7 A Comparison of the Linear Equations in Figures 6.34 and 6.40

	Linear Equation for Initial Slope (First Minute of Run)	
	Synthetic Air	Atmospheric Air
Same Baseline (Figure 6.34)	y = 1.349x	y = 0.369x
Different Baselines (Figure 6.40)	y = 1.349x	y = 1.009x

The curves for the synthetic air versus atmospheric air runs during the 2 through 25-minute exposure period (using different baselines for each corresponding to their equilibrium adsorption baselines) are shown in Figure 6.42.

These adsorption section of the curves were slightly more similar when different initial resistance values were used as in Figure 6.41, than they were when the same initial resistance value was used, as was shown in Figure 6.35.

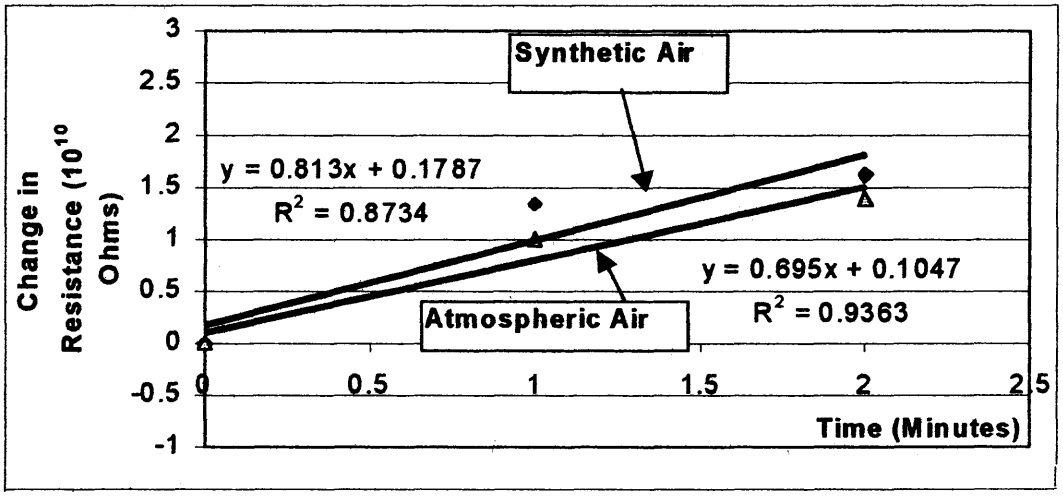

Figure 6.41 Resistance versus exposure time during the first 2 minutes of air exposure for atmospheric and synthetic air using different initial resistance values (first section of Figure 6.39).

Table 6.8 A Comparison of the Linear Equations in Figures 6.35 and 6.42

	Synthetic Air	Atmospheric Air
Same Baseline (Figure 6.35)	y = 0.4274 Ln(x) + 1.4153;	y = 0.2708 Ln(x) + 0.4390
Different Baselines (Fig. 6.42)	y = 0.4274 Ln(x) + 1.4153;	y = 0.5559 Ln(x) + 1.1193

Figure 6.43 contains Figure 6.42 data when it is plotted as change in current versus a natural logarithmic function of time in seconds, which are the parameters used in the Elovich adsorption equations. The data in Figure 6.43 show that the adsorption

section follows the Elovich equation from 2 to 12 minutes. After 12 minutes, the curve no longer follows the linear Elovich equation, because desorption also starts to become a prominent part of the process.

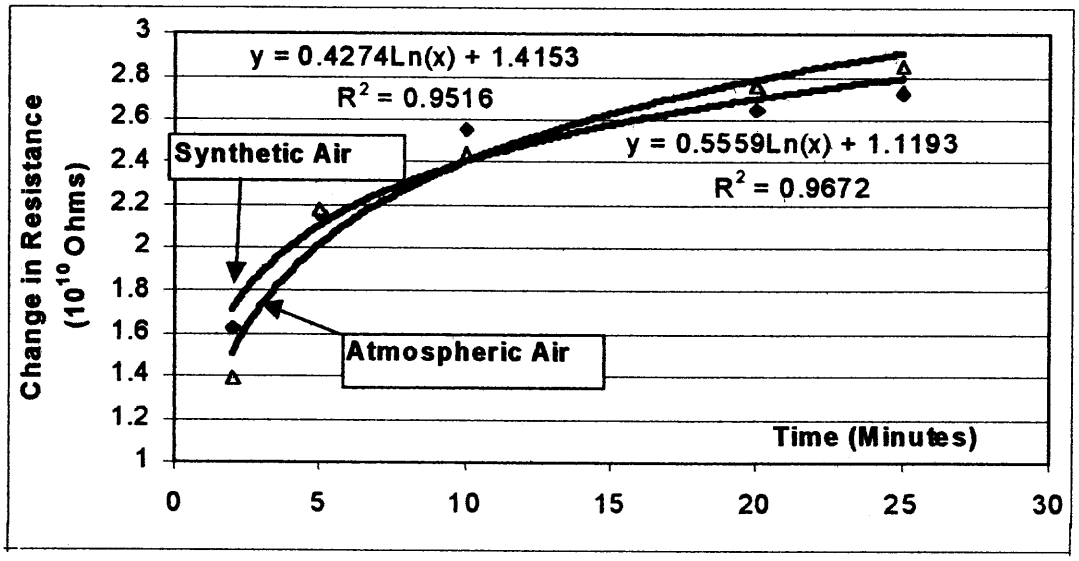

Figure 6.42 Resistance versus exposure time during 2 to 25 minutes of air exposure for both synthetic and atmospheric air using different initial resistance values (second section of Figure 6.39).

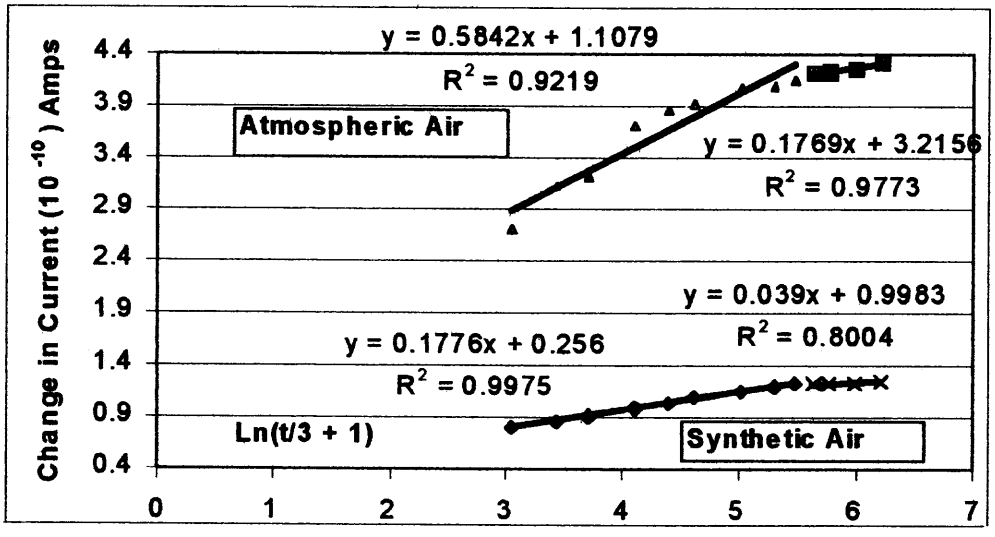

Figure 6.43 The graphing of the adsorption section of Figure 6.42 using the Elovich Equation.

If just the initial linear part of both the synthetic and atmospheric air curves are regraphed from Figure 6.43, then Figure 6.44 results. Figure 6.44 curves show that the adsorption sections give quite different slopes depending on the type of air being used and this would be expected, because the atmospheric air contains oxygen-containing contaminants such as water and carbon dioxide molecules. These molecules have oxygen atoms, which are more electronegative than the other atoms in the molecule and therefore have a slight negative charge and can be adsorbed to the cadmium sulfide surface.

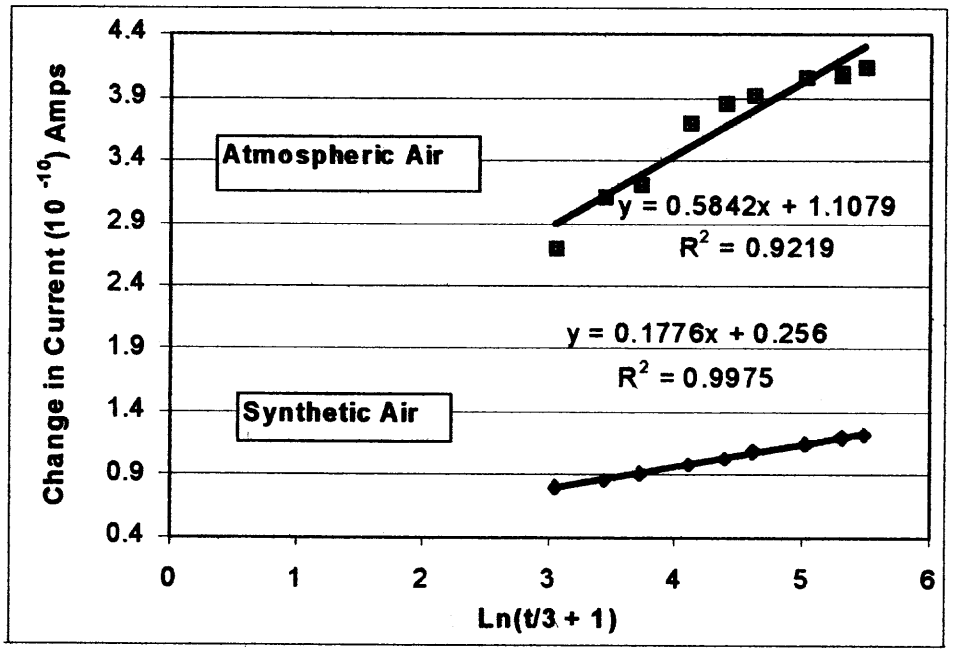

Figure 6.44 The graphing of the adsorption section of 2 to 12 minutes of Figure 6.37 using the Elovich equation.

However they do not affect the sensor as the oxygen molecules do by picking up electrons, but compete with oxygen by occupying bonding sites on the cadmium sulfide surface. [41, 74]

Figure 6.45 contains the desorption section of the curves in Figure 6.39 for both synthetic air and atmospheric air, when different initial resistance values were used. The

data in this figure shows that the desorption rates of synthetic air and atmospheric air are very similar for both synthetic air and atmospheric air.

The resistance of the sensor when exposed to synthetic air is always higher though, due to a lower resultant current with synthetic air since there are no other oxygen containing molecules that can interfere with the adsorption of oxygen and its acceptance of an electron which decreases the current.

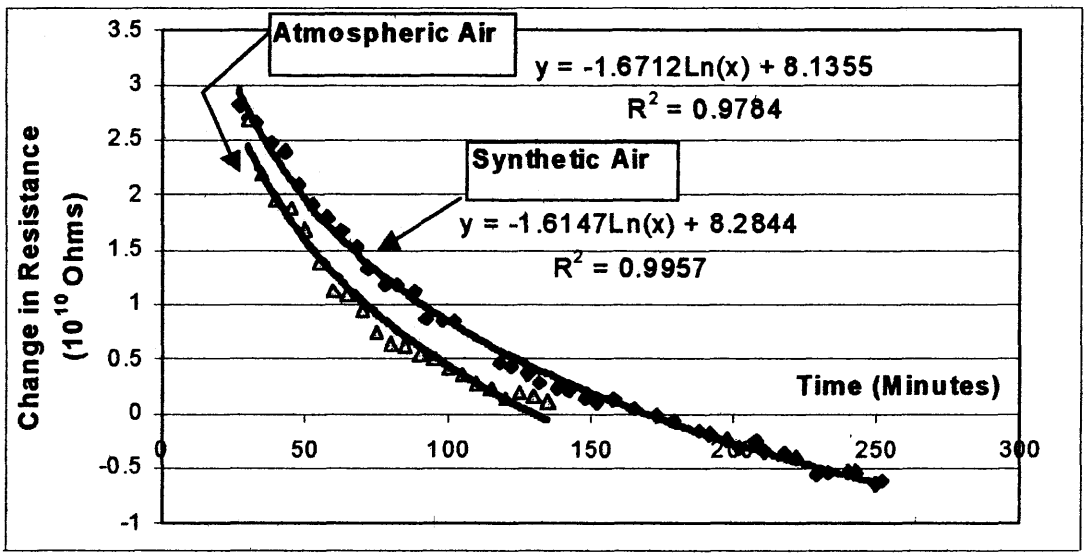

Figure 6.45 Resistance versus exposure time during the desorption process for both synthetic and atmospheric air using different initial resisstance values (third section of Figure 6.39).

Comparison of the synthetic air versus the atmospheric air logarithmic desorption curves at the same and different initial resistance values (baselines) are as follows:

Table 6.9 A Comparison of the Linear Equations in Figures 6.36 and 6.45

	Synthetic Air	Atmospheric Air
Same Baseline (Figure 6.36)	y = -1.6147 Ln(x) + 8.2844;	y = -1.6256 Ln(x) + 6.2167
Different Baselines (Fig. 6.45)	y = -1.6147 Ln(x) + 8.2844;	y = -1.6712 Ln(x) + 8.1355

The graphs in Figure 6.46 show the slope of the lines obtained when the change in resistance data is graphed versus percent oxygen for atmospheric air versus synthetic air (zero grade air from cylinders) after 30 minutes of sensor exposure time. These data were from runs where the intial resistance was the equilibrium desorption resistance value for that type of air. It can be seen that the slopes of the two lines in Figure 6.46 are very similar.

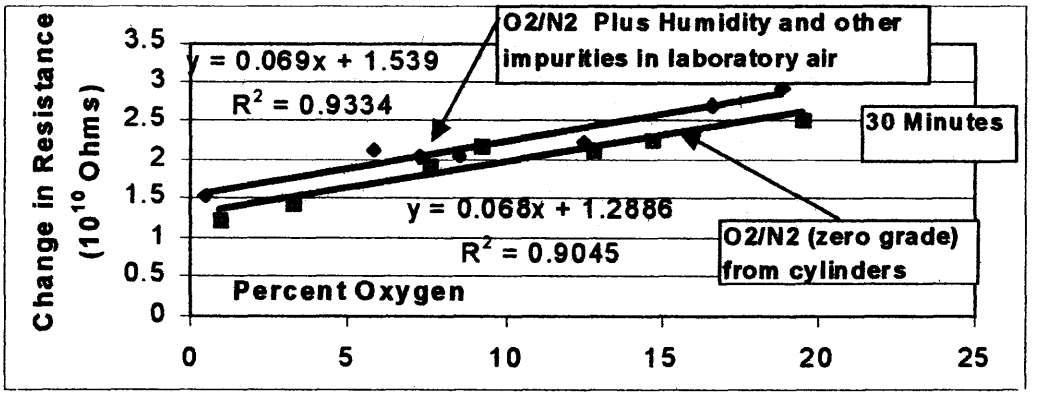

Figure 6.46 Change in resistance versus percent oxygen for atmospheric versus synthetic air after 30 minutes of exposure time.

6.5 Response of the Sensor to Humidity

The resistance across the sensor was shown to be less with atmospheric air than with synthetic air, containing approximately the same oxygen content and at the same total pressure, as was discussed in the last four sections.

In order to determine the effect of the moisture/oxygen combination on the sensor, synthetic air was bubbled through various saturated salt/water solutions, in order to obtain a known level of relative humidity (RH) in the synthetic air. Nitrogen was

also bubbled through the same salt solutions to determine the effect of humidity alone on the sensor (since nitrogen has little effect on the resistance of the sensor).

It appears that, as expected, water sorption reduces the amount of sorbed oxygen and therefore reduces the sensor response to the oxygen. The resistance decreases with nitrogen containing water vapor, which suggests that the conductivity of the sensor surface actually increases with a high concentration of water. This suggests that at some point moisture absorption may predominate and prohibit all but the very initial quenching by the oxygen.

Figure 6.47 contains change in resistance data versus sensor exposure time for different levels of humidified synthetic air. This figure generally shows a definite decrease in resistance with increased moisture levels.

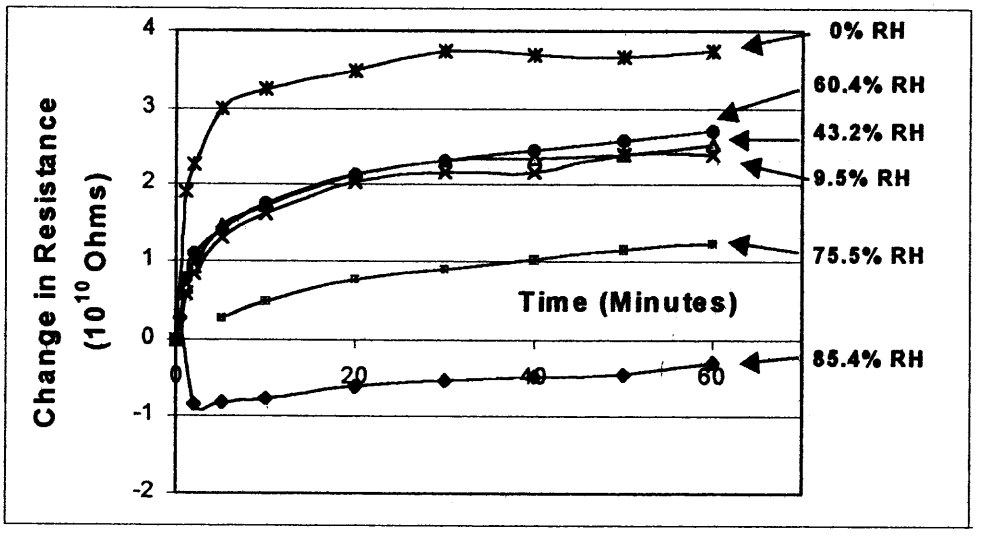

Figure 6.47 The effect of various levels of water vapor on the resistance of the sensor versus time during synthetic air exposure.

Figure 6.48 contains change in resistance versus sensor exposure time for different levels of humidified nitrogen, which again shows a decrease in resistance with increasing moisture levels, except for the 9.6% RH value.

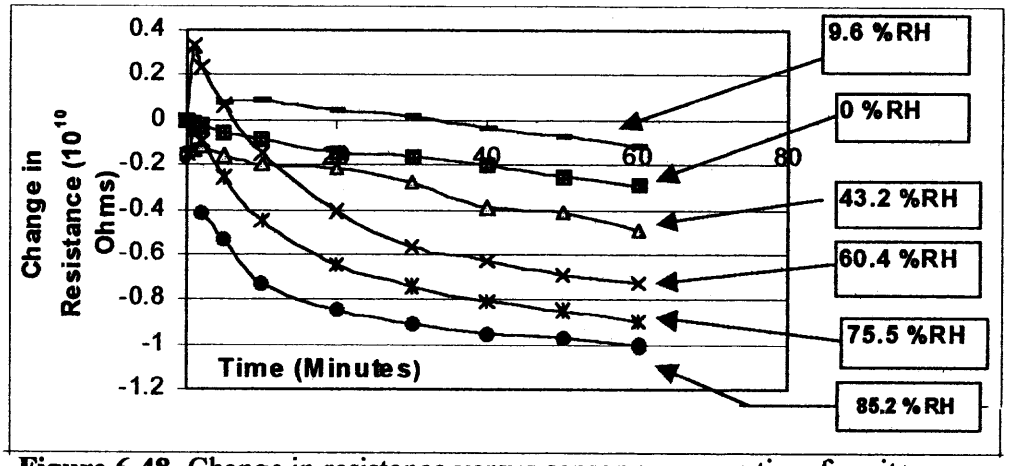

Figure 6.48 Change in resistance versus sensor exposure time for nitrogen with different amount of water vapor content.

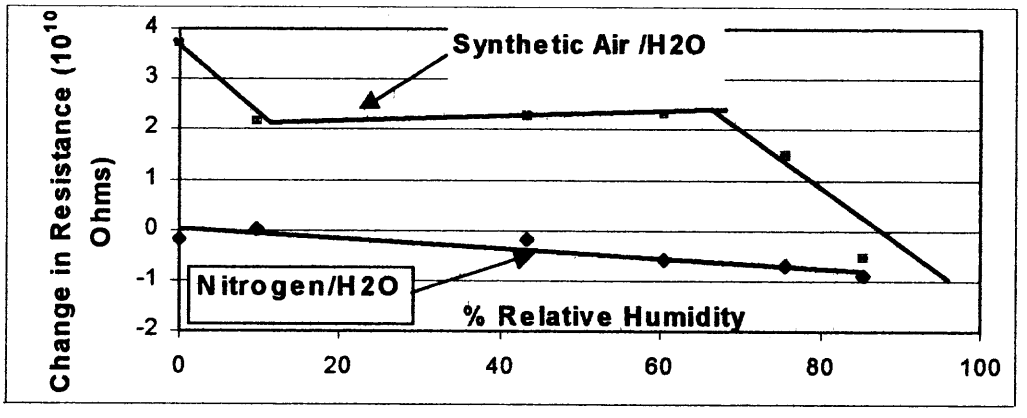

Figure 6.49 Change in resistance versus time for nitrogen and synthetic air containing various amounts of humidity after 30 minutes of sensor exposure time.

The presence of a small amount of water vapor in nitrogen causes a slight increase in resistance, when there is no interference from oxygen. The presence of moisture at a level of 43.2% RH and above effects the sensor, causing a reduction in resistance, and the resistance continues to decrease as the humidity increases. The reduction in resistance with humidity occurs as the surface conductivity increases presumably because the water

sorbed water provides an alternate pathway for electrons on the surface, once enough molecules are adsorbed on the sensor surface.

Figure 6.49 contains data from Figures 6.47 and 6.48 at the 30 minute exposure time interval. The resistance of the humidified nitrogen gas mixture and synthetic air mixture both generally decrease as the amount of gaseous water in the mixture increases from 0 to 80% relative humidity. The synthetic air/water gaseous mixture shows an initial decrease in resistance from 0 to 10% relative humidity but doesn't experience a decrease in resistance over the 10 to 60 % relative humidity range. Resistance for synthetic air/water gaseous mixtures above 60% show marked decreases in resistance.

Both curves cross at about 90% relative humidity, showing that oxygen can no longer quench when there is that level of water vapor present, because the air and nitrogen both have the same effect on the sensor response at that level of humidification.

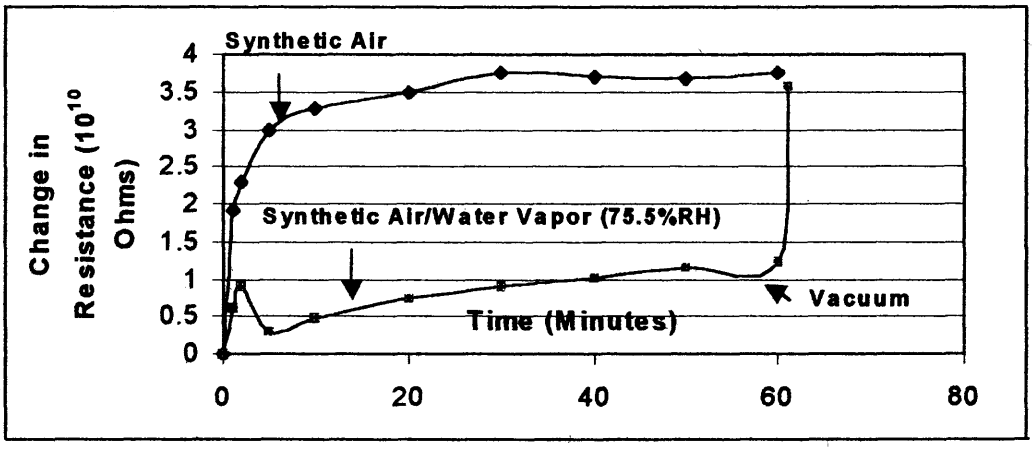

Figure 6.50 Change in resistance versus sensor exposure time synthetic air versus humidified synthetic air (75.5% RH).

Figure 6.50 contains a resistance versus time curve for synthetic air, plus synthetic air that has been humidified to the 75.5% relative humidity level. At the end of the 60-

minute exposure test, vacuum was applied to the humidified air and the resistance increased rapidly to the synthetic air level, indicating that the moisture may be adsorbing to the surface with weak Van der Waals forces. [11]

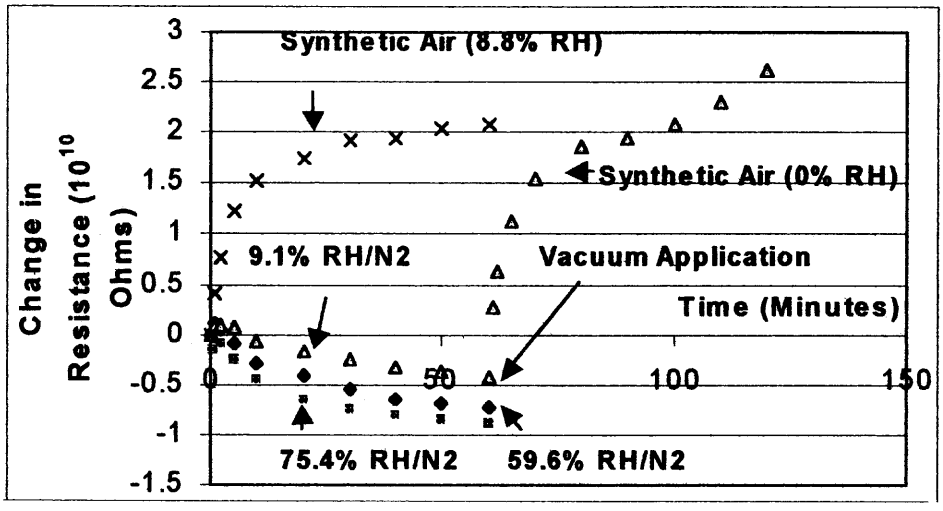

Figure 6.51 Change in resistance versus sensor exposure time for various humidified nitrogen mixtures and synthetic air.

Three different runs were made with different humidification levels in nitrogen gas (9.1%, 59.6% and 75.4% RH). The graphs from the resultant data from these runs are shown in Figure 6.51. The change in resistance was shown to decrease versus sensor exposure time as the humidification level of the nitrogen gas increased.

Vacuum was applied for 15 minutes (from 60 minutes to 75 minutes of sensor exposure time) during the 9.1% RH nitrogen run after 60 minutes of exposure time. Vacuum application led to an increase in the resistance of the sensor. After 15 minutes of vacuum application, synthetic air at a pressure of 4.5 psi was admitted into the sensor chamber. Figure 6.51 also shows the results from when humidified synthetic air (8.8%

RH) was admitted into the sensor chamber at 4.5 psi pressure for comparison with the 9.1% RH nitrogen run.

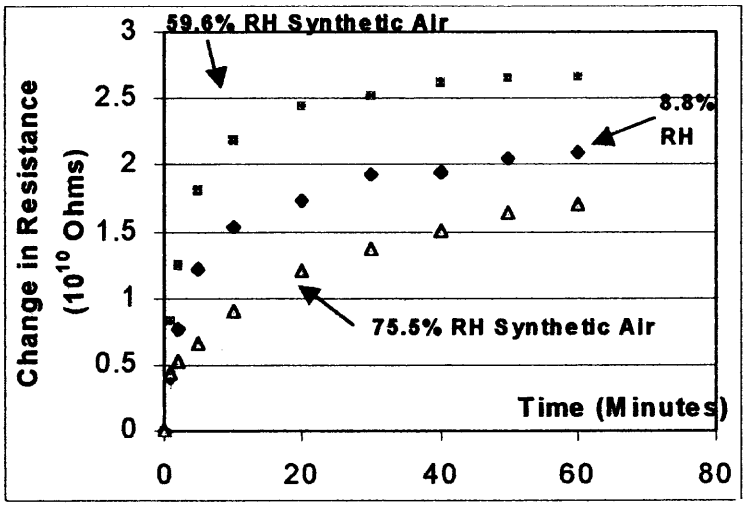

Figure 6.52 Change in resistance versus sensor exposure time for humidified synthetic air.

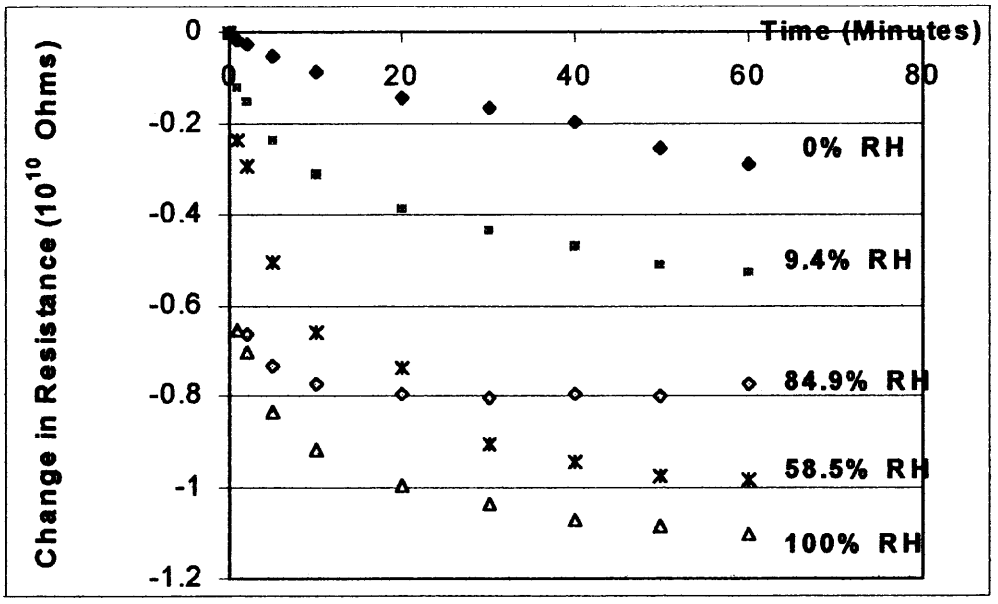

Figure 6.53 Change in resistance data versus sensor exposure time for four different humidity levels in nitrogen.

Additional runs were made containing various amounts of humidification of nitrogen and synthetic air and the curves resulting from these runs are contained in Figures 6.52, 6.53 and 6.54. These figures show that the sensor may not always work perfectly as a humidity detector, as evidenced by the 8.8% relative humidity curve in Figure 6.52, the 9.6% relative humidity curve in Figure 6.48 and the 9.1% relative humidity curve in Figure 6.54. The sensor can, however, generally detect higher humidity levels.

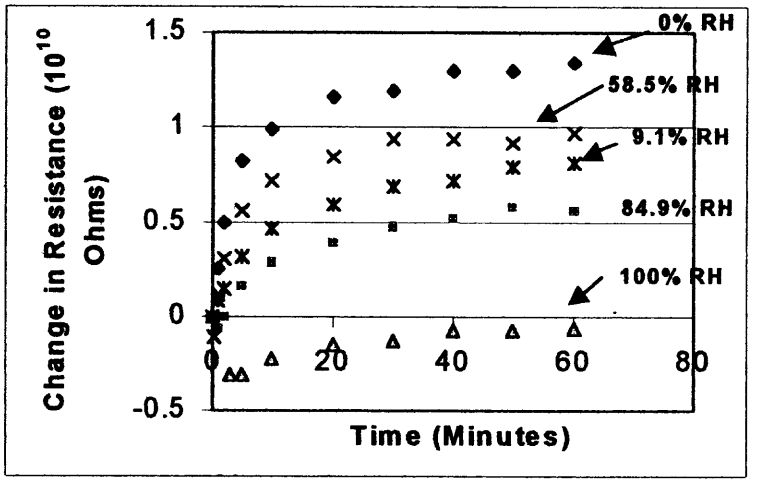

Figure 6.54 Change in resistance versus sensor exposure time for four different humidity levels in synthetic air.

6.6 Theory Explaining the Sensor's Response to Humidity

This section will focus on explaining the response of the sensor to water vapor.

Figure 6.55 depicts the sensor surface composed of cadmium sulfide at time zero when the surface has been illuminated for some time and atmospheric air or humidified synthetic air has been admitted into the sensor chamber. The cadmium sulfide layer is crystalline and composed of cadmium cations (Cd^{+2}) and sulfide anions (S^{-2}). The anions and cations are bonded together by ionic bonds. [81]

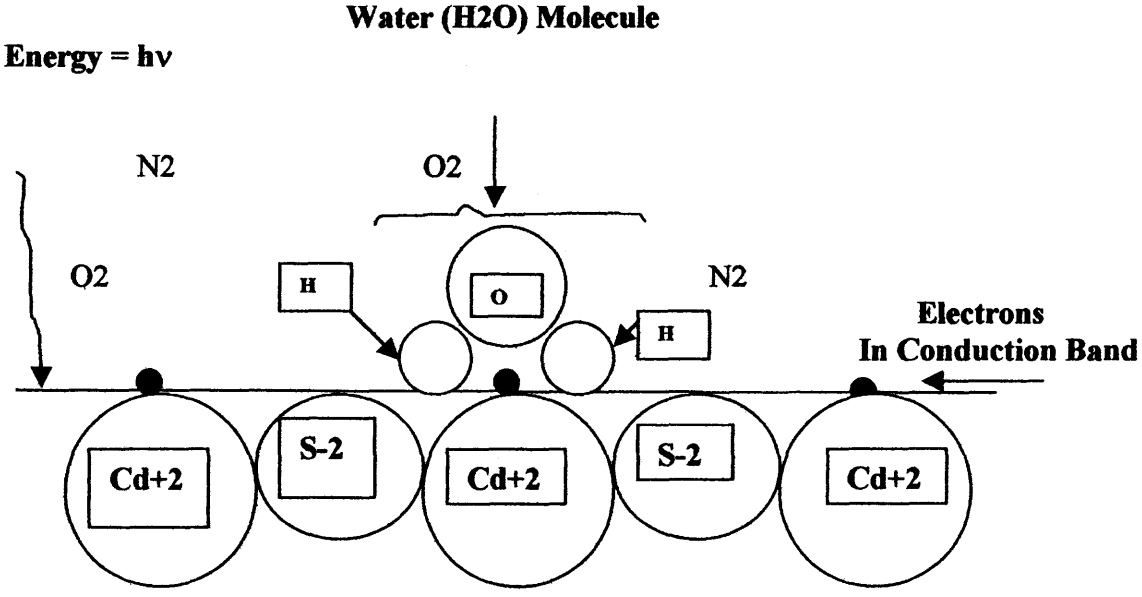

Figure 6.55 Depiction of the sensor upon exposure to atmospheric air in the sensor chamber (showing a water molecule which has become chemiadsorbed to the cadmium sulfide surface).

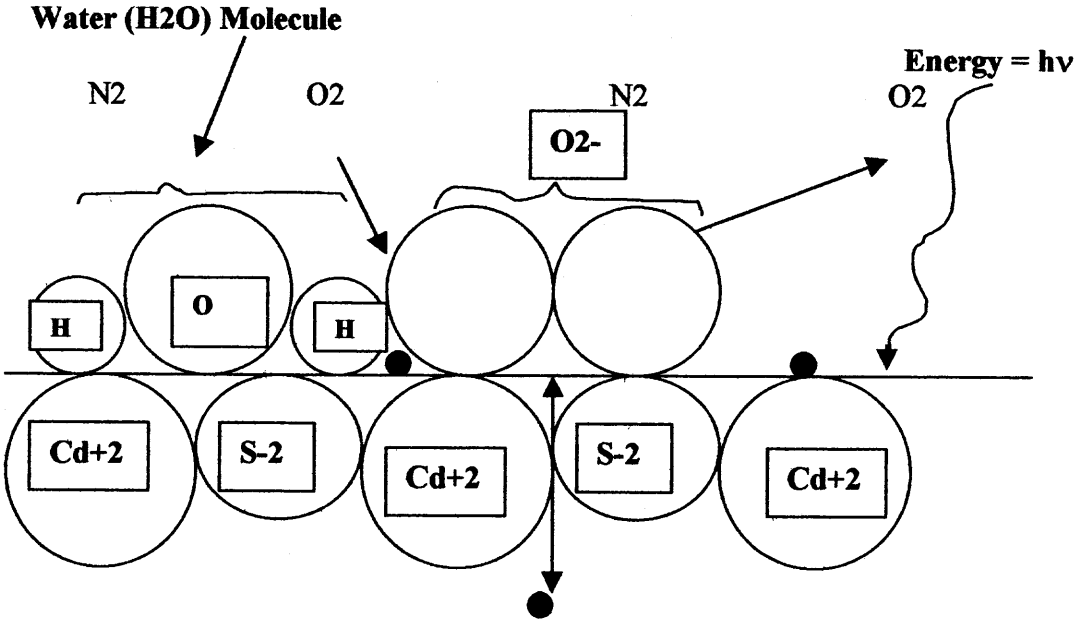

Figure 6.56 Depiction of the sensor upon exposure to atmospheric air in the sensor chamber (showing a water molecule and an oxygen molecule which has picked up an electron and become chemiadsorbed to the CdS surface).

The electrons shown as small, black filled-in circles have gained energy from the light [Energy = h (Planck's constant) multiplied by ν (the frequency of the light)]. The excited electrons, having gained this energy, have jumped up in energy levels to the conduction band from the valence band and are can travel to the surface of the sensor. [41, 74]

The synthetic air is composed of only nitrogen and oxygen gases, which are both symmetrical and nonpolar. Oxygen, however, can become an ion, as shown in Figure 6.56 and become bonded to the ionic cadmium sulfide surface.

Figures 6.55 and 6.56 both show atmospheric air in the sensor chamber, which contains other molecules besides nitrogen and oxygen, such as water and carbon dioxide.

Water is a polar molecule. The oxygen atom is more electronegative than the hydrogen atoms, and therefore the electrons in the hydrogen-oxygen bonds spend more time closer to the oxygen atom than the hydrogen atoms, making the oxygen atom partially negatively charged and the hydrogen atoms partially positively charged. The polar water molecule is therefore, somewhat attracted to the ionic cadmium sulfide surface as shown in Figure 6.55. Figure 6.55 shows the water molecule already on the surface at time zero. [79]

Figure 6.56 shows how the water molecules can actually prevent the oxygen molecules from picking up as many electrons as they do with synthetic air. The larger concentration of electrons on the sensor surface with atmospheric air as opposed to synthetic air, leads to a larger current at a particular oxygen concentration and a correspondingly lower resistance.

This water blocking of the positive Cd^{+2} sites, is probably also the reason that the Stern-Volmer equation for quenching is observed throughout the 60-minute atmospheric air run but for only one or two minutes in the synthetic air run. It may be that with the water blocking the positive sites for oxygen adsorption, the oxygen can still collide with the surface and obtain electrons, but doesn't have enough room on the surface to do a sufficient amount of energetically favorable ionic bonding (due to negative to positive attraction). If this is the case, then the predominant process would be the diffusion of the oxygen to the surface and the picking up of an electron, without much adsorption of the oxygen ion to the surface. The reduction in current or increase in fluorescent ratio would then be linearly dependent on the oxygen concentration.

The reason for the large difference between the sensor's response to atmospheric air and synthetic air is that the sorbed water (and possibly other gases in the atmospheric air) tends to interfere with oxygen sorption.

Initially, the surface will adsorb water first. The oxygen ion and polar water molecules vie for the same cationic sites, with atmospheric air exposure. The oxygen ion has a stronger charge than the oxygen in the water molecule, but the oxygen ion can lose energy and its electron and be desorbed from the surface, whereas the water molecule stays absorbed to the surface during the run.

As the humidity increases, a water layer forms on the surface inhibiting the ability of the oxygen ion to adsorb to the ionic cadmium sulfide surface. The oxygen can still quench, however, because the electrons are taking an alternative pathway through the water molecules on the surface. As the humidity increases, the number of water layers also increase and at a certain point, the oxygen can no longer quench.

6.7 Photoresistance of Toluene Gas Mixtures

6.7.1 Photoresistance of Toluene/Nitrogen Gas Mixtures

A thin-film sensor, composed of a 0.5 micron thick layer of cadmium sulfide on a glass substrate and coated with Rhodamine B fluorescent dye, was tested for changes in photo-conductivity due to exposure to different concentrations of gaseous toluene in the parts-per-million (ppm) range.

It was theorized that the gaseous toluene molecules would adsorb to the dyed semiconductor surface and that some energy would be transferred to the adsorbed toluene molecules rather than to the cadmium sulfide semiconductor layer through the

dye, thereby decreasing the photoconductivity of the surface in an amount proportional to the toluene concentration to which the sensor was exposed. [1]

When different concentrations of toluene/nitrogen gas mixtures were tested with the sensor, the photoresistance of the sensor was shown to increase as the concentration of the toluene/nitrogen gas mixture increased up to a certain point, where the photo-resistance was then seen to equilibrate.

Figure 6.57 is a graph of the change in photoresistance of various concentrations of toluene/nitrogen gas mixtures from their initial nitrogen levels versus the toluene gas concentration in ppm.

The data in Figure 6.57 shows that the change in photoresistance continues to climb until a concentration of about 20 to 25 ppm of toluene/nitrogen gas mixture is reached. At that point the change in photoresistance begins to level off at an equilibrium value of about 3.5 x 10^9 ohms.

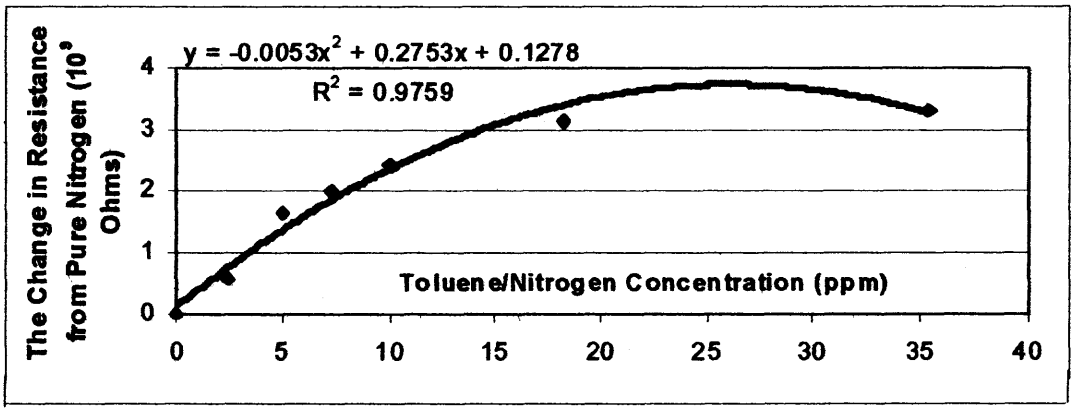

Figure 6.57 The change in resistance from pure nitrogen for various toluene/nitrogen concentrations.

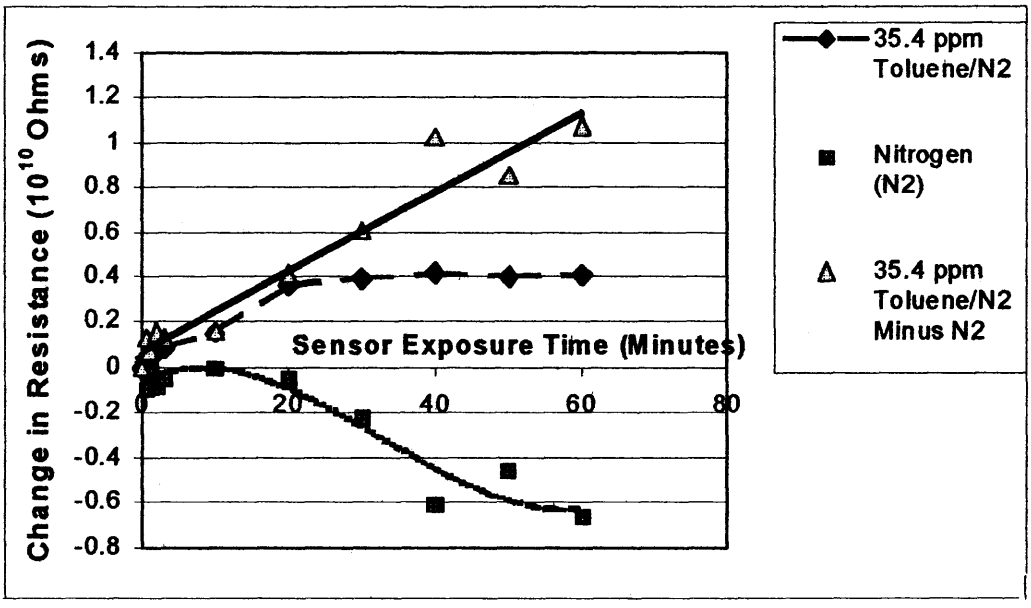

Figure 6.58 Comparison of the resistances obtained with nitrogen, 35.4 ppm toluene/nitrogen and when the two effects are subtracted.

Figure 6.58 shows the graph of the change in the photoresistance obtained when nitrogen gas was exposed to the sensor, along with two other curves. One curve shows the results of the exposure of the sensor to 35.4-ppm toluene/nitrogen, and the other

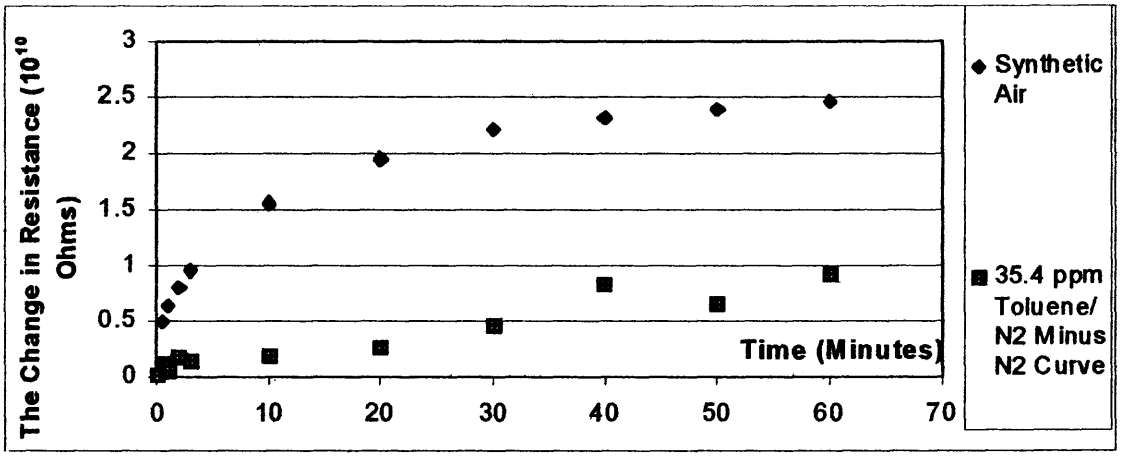

Figure 6.59 The change in resistance versus time with synthetic air exposure and 35.4 ppm toluene/N2 minus the nitrogen (N2) curve.

shows this same curve after the effects of the pure nitrogen on the sensor have been subtracted from it.

The effects of a toluene/nitrogen mixture on the sensor's photoresistance versus time is compared with the effect of a gas mixture of 35.4 ppm of toluene in nitrogen when the effect of the nitrogen gas on the resistance has been subtracted. Figure 6.59 is a comparison of the photoresistance of the sensor with exposure to synthetic air versus exposure to the toluene vapor in a 35.4 ppm toluene/nitrogen gas mixture.

Air has a much faster and stronger impact on the change of the sensor photo-resistance than the nitrogen does, as shown in Figure 6.59. From Figure 6.59, it can also be determined that a gas mixture of a small amount of toluene also has a much slower and weaker impact than air alone does on the photoresistance value, although this impact is greater than that of the nitrogen gas.

6.7.2 Photoresistance of Toluene/Air Gas Mixtures

The figures that appear in this section are given as representative examples of the results

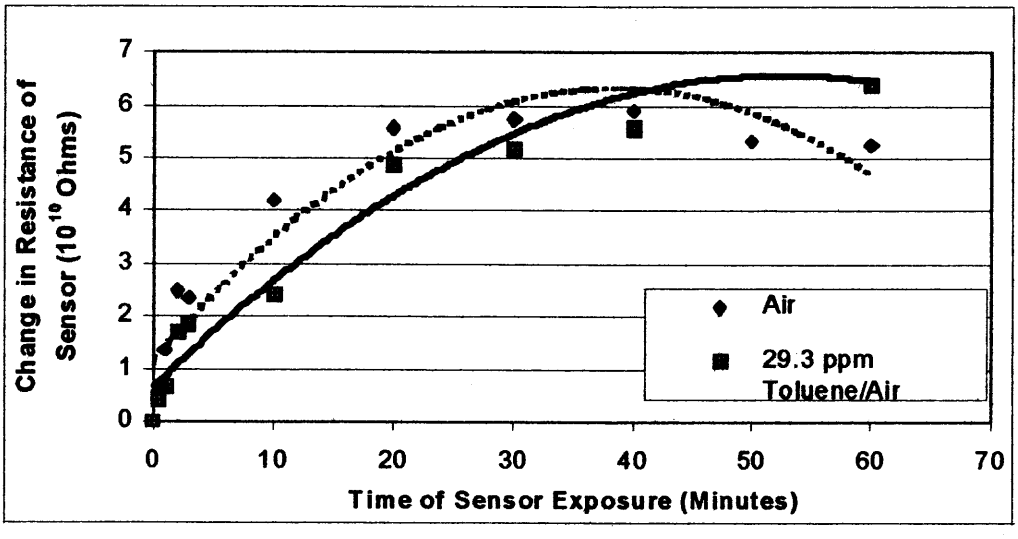

Figure 6.60 The resistances of 29.3 ppm toluene/air and air versus time of sensor exposure (method II).

that were obtained with exposure of the sensor to toluene/air gas mixtures.

When the sensor was primed so that the 29.3 ppm toluene/air and air alone runs were begun at the same initial resistance value, the results shown in Figure 6.60 were obtained. The data in Figure 6.60 show that the synthetic air curve had a steeper initial slope with corresponding resistances that were slightly higher than the 29.3 ppm toluene/air mixture, but both curves intersected at approximately 45 minutes of sensor exposure time.

After 45 minutes, the resistance of the sensor with the toluene/air mixture was slightly higher than the synthetic air. It can be concluded from Figure 6.60 that the photoresistance values of the sensor to either 29.3 ppm toluene/air gas mixture or just synthetic air were so similar over a period of 60 minutes as to be indistinguishable.

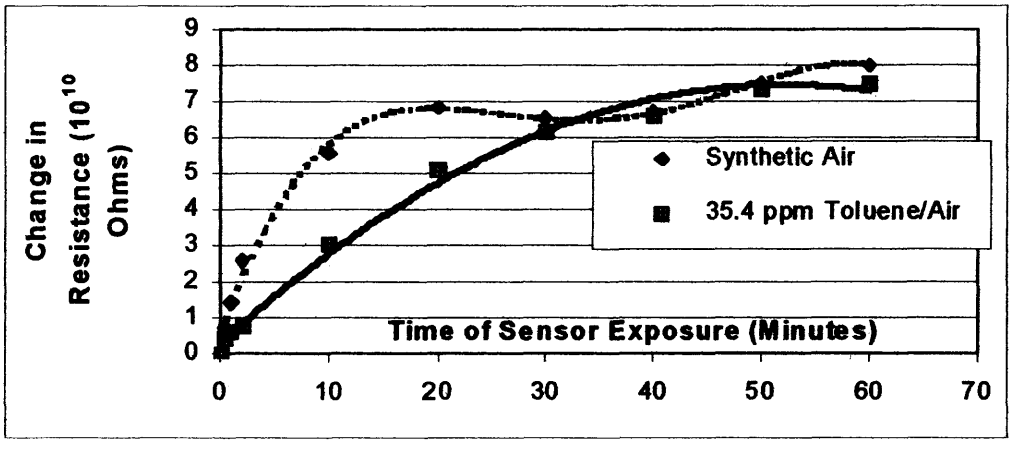

Figure 6.61 The change in resistance of a 35.4 ppm toluene/air gas mixture versus sensor exposure time.

In Figure 6.61, this same experiment was repeated for a slightly higher concentration of toluene (35.4 ppm toluene/air) and again the two curves converged at a sensor exposure time of approximately 40 minutes.

Figure 6.62 contains the results of the experiments where four different concentrations of toluene/synthetic air gas mixtures (10 ppm, 20 ppm, 29.3 ppm, 35.4 ppm toluene in synthetic air) were each started at a similar initial resistance value reading. The change in photoresistance of each run as compared to the original value, was plotted versus sensor exposure time.

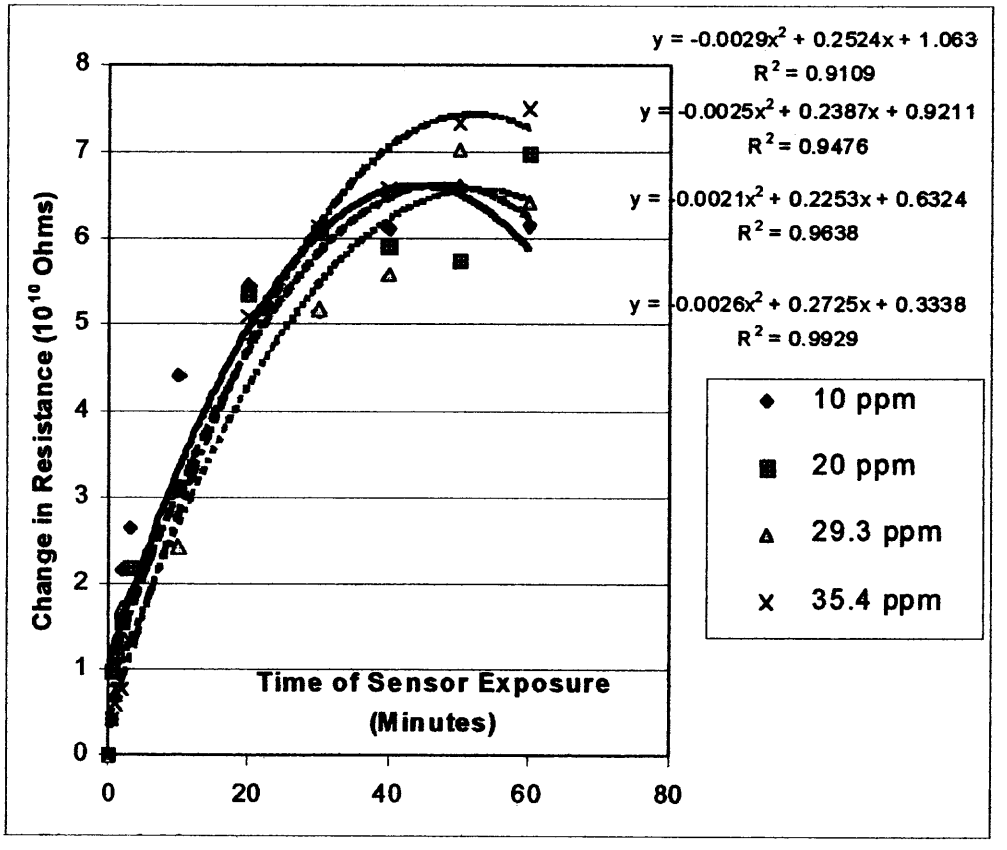

Figure 6.62 Change in resistance versus sensor exposure time for 10 ppm, 20 ppm, 29.3 ppm, 35.4 ppm of toluene/air gas mixtures.

The data from each run was fitted to a second powered polygram graph, and the equation for each of the curves is listed consecutively in Figure 6.62 for the 10 ppm, 20 ppm, 29.3 ppm, and 35.4 ppm toluene/air mixtures. The equations and the curves came out to be so similar as to be almost indistinguishable.

6.8 The Effect of the Cadmium Sulfide Layer Thickness on the Sensor's Response

All of the data shown in section 6.1 through 6.7 were collected from experiments utilizing a sensor with a 0.5 micron thick cadmium sulfide layer.

A new sensor chip was fabricated with a thicker cadmium sulfide layer (4.5 microns) and was dyed in the same way as the first with Rhodamine B dye. It acted as an oxygen sensor, just like the sensor with the 0.5 micron thick cadmium sulfide layer had, although the change in resistance values were at least ten times higher with the new thicker sensor presumably due to an increased porosity and the resultant increased surface area.

The new sensor also responded to oxygen much more than nitrogen, as the original sensor had. It showed a positive response to toluene at room temperature

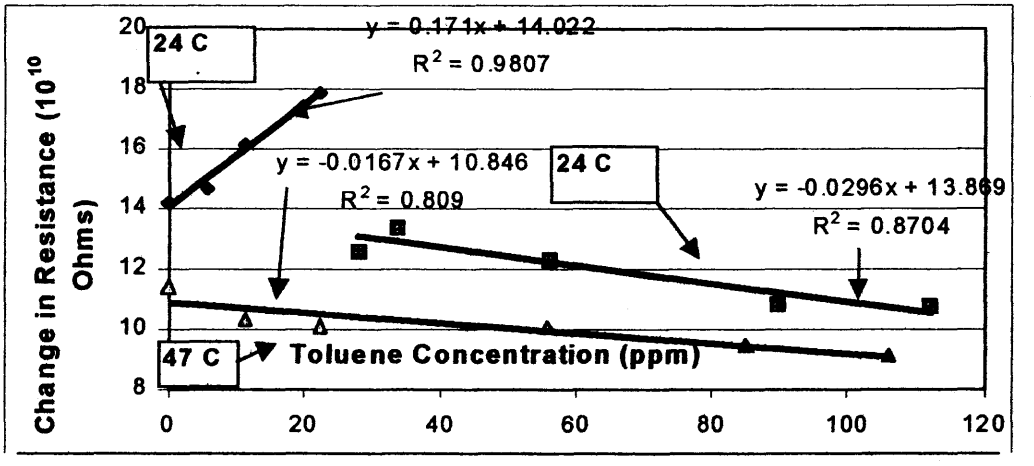

Figure 6.63 Change in resistance versus toluene concentration data for the 4.5 micron thick cadmium sulfide sensor (side 1) after 30 minutes exposure time

between the 0 to 20 ppm concentration range of toluene in a 20% oxygen/80% nitrogen gas mixture as shown in Figure 6.63 for side 1 of the sensor and Figure 6.64 for side 2. This increase in resistance was due to the absorption of energy by the toluene on the CdS

surface from the halogen lamp. The energy absorbed by the toluene was not available to overcome the bandgap energy, and thus corresponded to a reduction in current and an increase in resistance. (At room temperature (21°C), the wall temperature of the sensor chamber was 24°C due to a slight increase in temperature from the halogen lamp). [1, 87]

When the 30 ppm toluene concentration level was reached at room temperature, a large decrease in resistance occurred as shown in Figure 6.63 for side 1 of the sensor and Figure 6.64 for side 2. This decrease in resistance was believed to be due to the adsorption of enough toluene molecules on the surface of the sensor at this concentration to provide an alternative pathway for electrons, which was much more energetically favorable and thus lower in resistance.

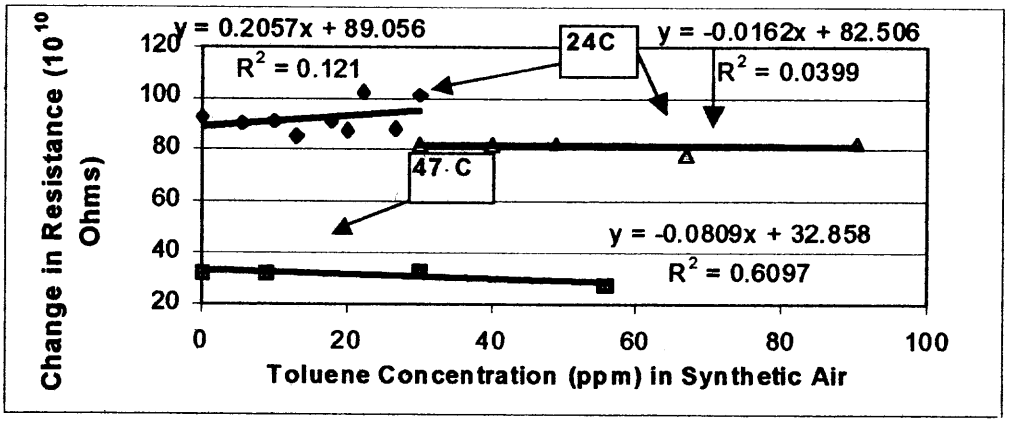

Figure 6.64 The change in resistance versus toluene concentration for the sensor with the 4.5 micron thick cadmium sulfide layer (side 2) after 30 minutes.

At a higher temperature (47 °C), the sensor with the thicker cadmium sulfide layer had lower resistances even with no toluene present, presumably due to the desorbing of gases from the sensor surface plus an increased ability of electrons to

partially overcome some of the intergrain resistance at the polycrystalline grain boundaries in the cadmium sulfide layer due to the presence of the heat energy. [2]

The sensor chip with the thicker cadmium sulfide layer (4.5 microns) was also tested to see if it could pick up different partial pressures of synthetic air. The results are shown in Figure 6.65. The sensor could detect the different partial pressures of synthetic air as shown by the curves in Figure 6.65.

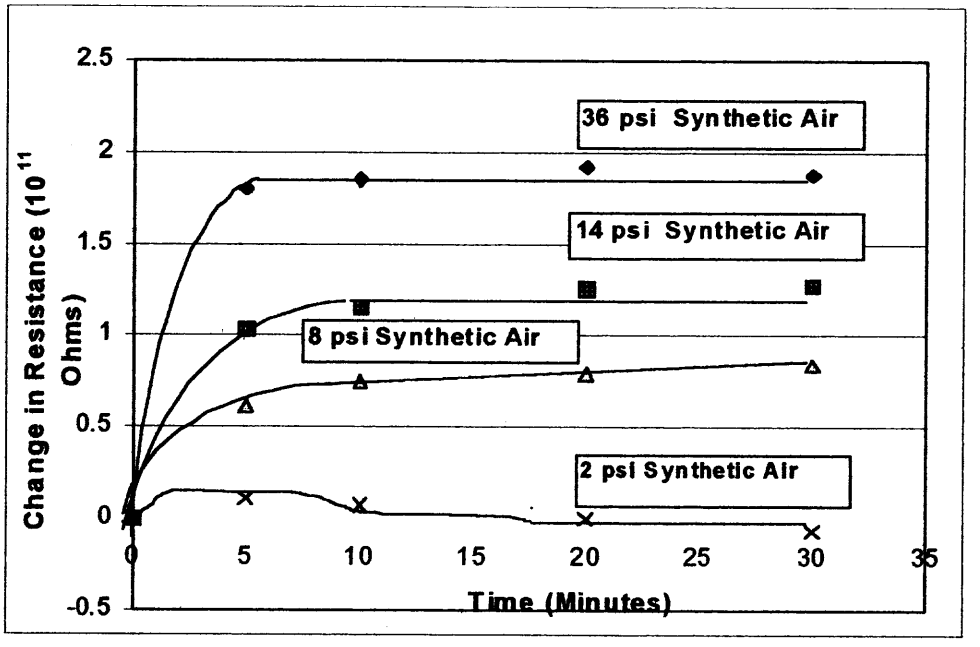

Figure 6.65 Change in resistance versus sensor exposure time using the NJIT lab-made sensor and the same amount of nitrogen in each run.

Various experiments were performed to see if the thicker sensor was as sensitive to humidity and it was not, since a 100% relative humidity/synthetic air graph turned out to be approximately the same as a synthetic air curve, when no water vapor was present in the sensor chamber.

6.9 Effect of Heating on the Sensor

All of the data up to this point in this report was taken at room temperature. It was desired to see what effect heating had on the sensor surface.

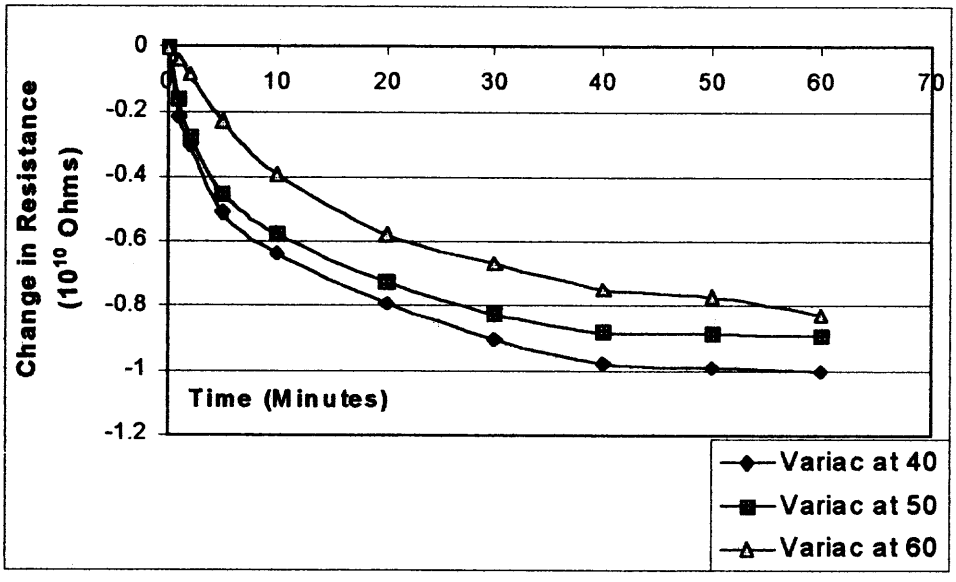

Figure 6.66 Desoprtion curves using heating tape at various variac settings.

Figure 6.66 resulted from the first experiment using the heated chamber. The variac was set at three different settings for each run (40, 50 and 60). The reduction in resistance versus time was very similar for each run, which resulted from the oxygen desorption of the sensor surface.

A mixture of synthetic air and nitrogen was admitted into the sensor chamber and allowed to equilibrate. Before any heat was applied, the temperature of the chamber registered at 25°C and had 11.5 % oxygen in it (as measured by a gas chromatograph).

After the variac connected to the heating tape was turned on, readings were taken at various intervals for the next 40 minutes and the graph in Figure 6.67 resulted, showing an overall increase in the oxygen concentration in the sensor chamber versus

heating time.

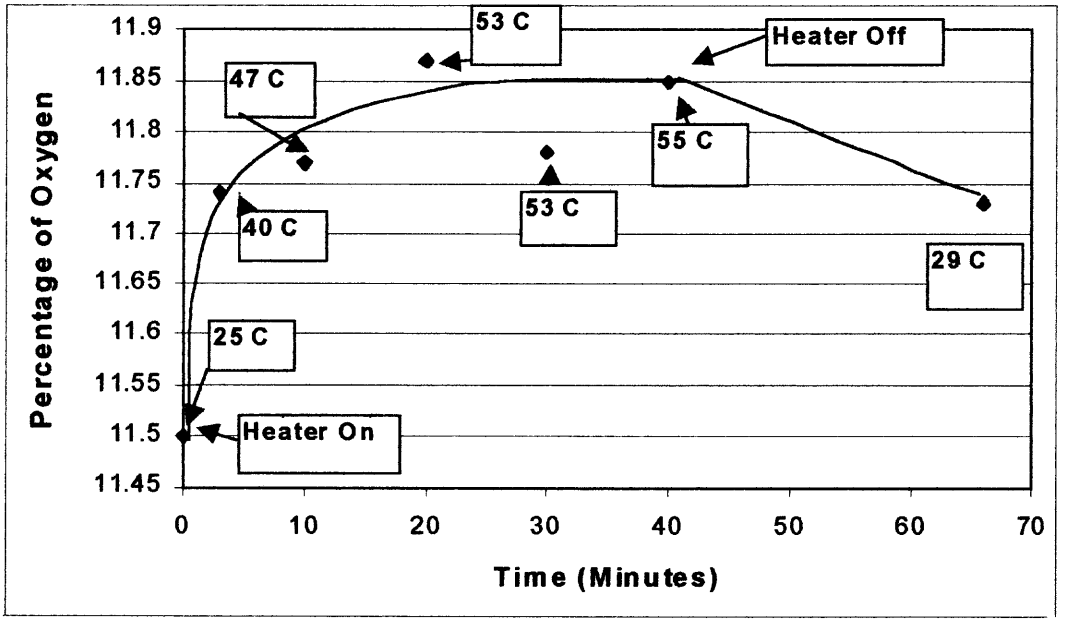

Figure 6.67 Percentage of oxygen in the sensor chamber versus heating time.

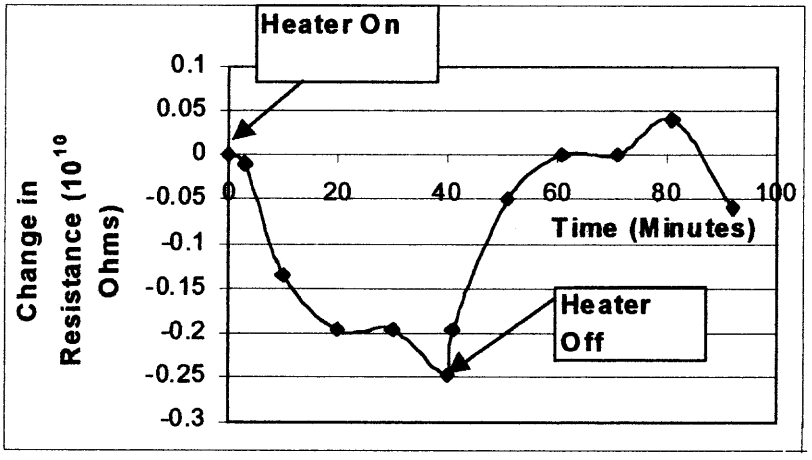

Figure 6.68 Resistance versus sensor exposure time to synthetic Air when the heater is turned on or off.

When the heater was turned off, the percentage of oxygen in the sensor chamber started to decline.

The data in Figure 6.68 shows how the resistance decreased when the heater was turned on due to the desorption of the oxygen off the sensor surface as well as the interior

of the chamber and the subsequent increase in current due to the loss of electrons by the oxygen molecules. The resistance then increased when the heater was turned back on due to readsorption of the oxygen and its subsequent quenching.

6.10 Sensor Results Without the Rhodamine B Dye

The same sensor chip that had been used for the experiments discussed in Sections 6.1 through 6.7 and Section 6.9 was rinsed with ethanol to remove the Rhodamine B dye and then reconnected to the electrical system on the same side of the chip. This undyed chip was then retested to see what the effect of the dye had been on the previous experiments.

The experimental runs graphed in Figure 6.3, using a sensor chip with dye and different partial pressures of synthetic air were rerun with the undyed chip and are graphed in Figure 6.69. Both experiments used approximately the same starting potential (resistance) and gain.

The graphs in Figure 6.69 for an undyed sensor chip show a smaller change in resistance and photosensitivity than those in Figure 6.3 for the dyed sensor chip and for the same partial pressures of synthetic air, but in general the shape of the curves are the same. The graphs in Figure 6.69, also show that the undyed sensor was able to detect different concentrations of oxygen, similar to the graphs in Figure 6.3.

The theory of using the Rhodamine B fluorescent dye in this study was as stated in Reference 1: "An organic dye rhodamine G (RhG) is deposited on the CdS films from an ethanol solution over a period of 15 minutes. The surface concentration of the RhG is determined by the solution molar concentration, which was chosen to be 10-3M/l to provide a surface concentration of about 2 X 10^{13} molecules/cm^2. This surface

concentration was estimated by the microbalance method and gives the best results for the spectral sensitization of the CdS film with the dye molecules. When the film with deposited RhG molecules is illuminated with light, it shows a new spectrum of photoconductivity. It consists of an "old" CdS photoconductivity band and a new additional wide peak of photoconductance with a maximum at about 530 nm.

This new peak lies in the region where the initial film was not light sensitive and it is due to the light absorption by the RhG molecules and energy transfer from the molecules to the CdS film. To trigger the photosensitization, the specimens are illuminated with monochromatic light. In these experiments, a xenon lamp and monochromator are being used to obtain the proper wavelength." [1]

When measuring the effect of the dye on the sensor, it was determined that there was more of an increase in current flow (proportional to the potential) on the surface of the sensor with the dye than without the dye.

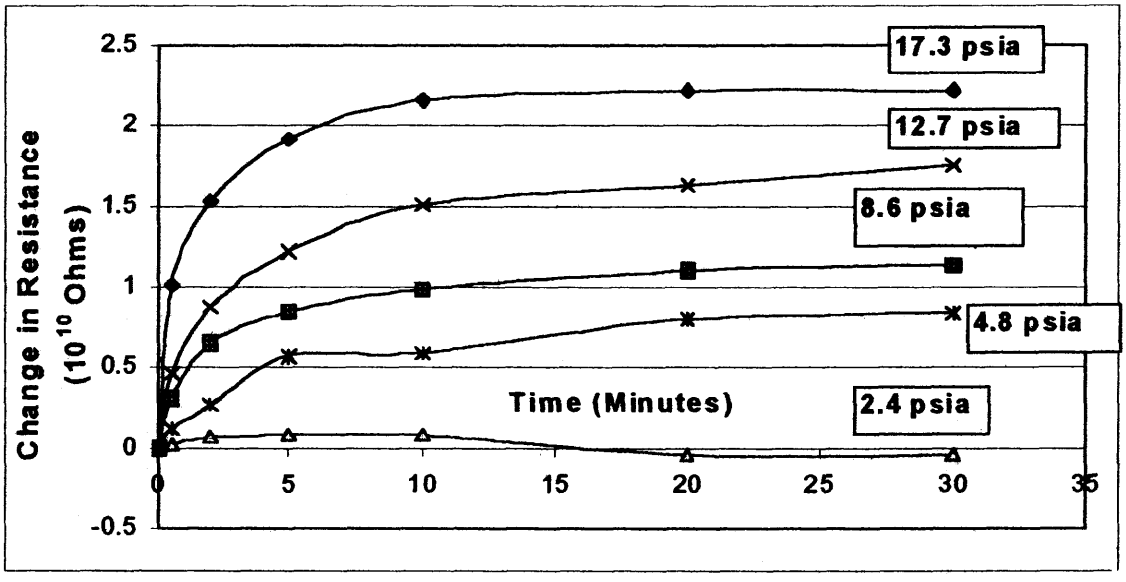

Figure 6.69 Change in resistance versus an undyed sensor's exposure time to various amounts of synthetic air.

Table 6.10 Differences in Potential Between the Dyed and Undyed Sensor Chip

	With Light	Without Light	Change in Potential
Sensor With Dye	59.2 mV	14.6 mV	44.6 mV
Sensor Without Dye	53.0 mV	14.8 mV	38.2 mV

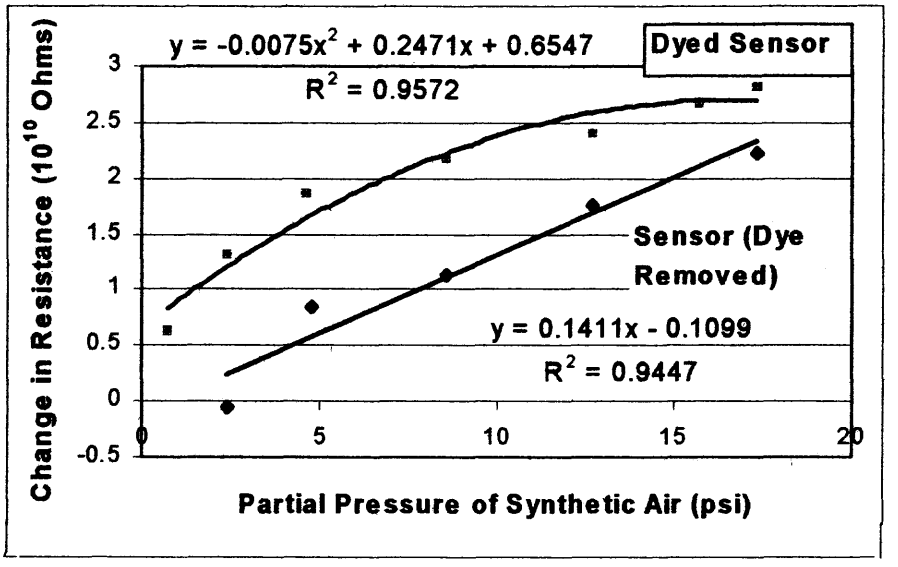

Figure 6.70 Change in resistance versus partial pressure of a 20% oxygen / 80% nitrogen gaseous mixture after 30 minutes of sensor exposure time (with and without the Rhodamine B dye).

This data agrees with Reference 1, which states that the dye makes the sensor more photosensitive.

The two plots shown in Figure 6.70 are graphs of photoresistance change versus the partial gas pressure of the synthetic air, after 30 minutes of sensor exposure for both the dyed and the undyed sensor chip, shown together for comparison purposes. This data shows that the change in resistance values due to oxygen exposure are increased when the Rhodamine B dye is present on the cadmium sulfide surface.

Figure 6.71 shows the graphed data obtained with the undyed sensor for the following runs containing nitrogen as the balance gas: nitrogen alone, nitrogen data containing 75% relative humidity, 25 and 50 ppm toluene/nitrogen.

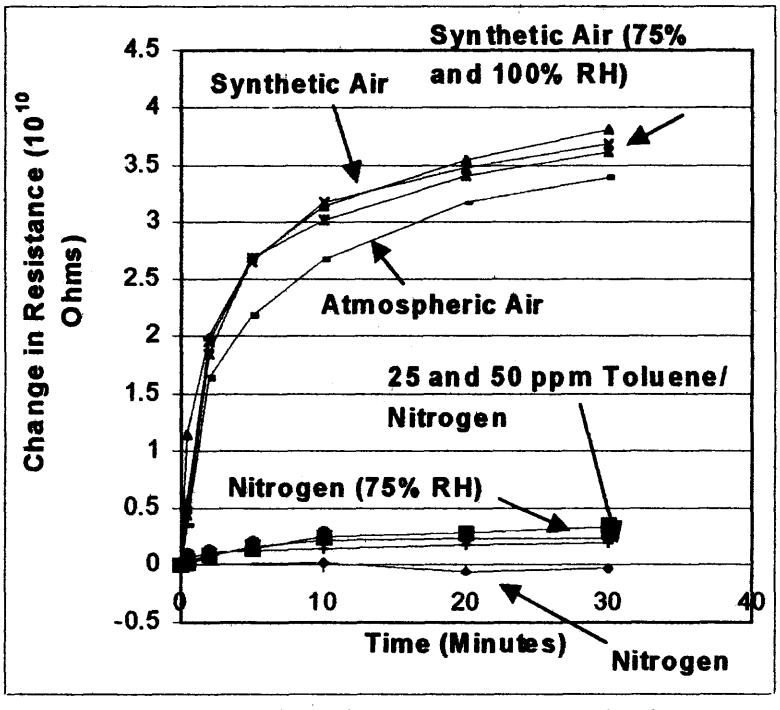

Figure 6.71 Change in resistance versus an undyed sensor's exposure Time to various types of air and nitrogen gaseous mixtures.

These four runs all gave similar curves, showing that the humidity, nitrogen and concentrations of toluene in the ppm range did not have much of an affect on the resistance of the sensor in comparison to oxygen exposure results.

The data obtained from the four runs containing oxygen, that are graphed in Figure 6.71, show a much greater increase in resistance due to exposure to the oxygen, than the nitrogen containing runs had. These four runs included: air taken from the laboratory environment (atmospheric air), synthetic air, and synthetic air that had been humidified to two different levels (75% and 100% relative humidity). The four oxygen

containing runs are very similar and show a much greater increase in resistance from their initial resistance than the nitrogen containing runs had.

The undyed sensor could not detect high humidity levels in either nitrogen or oxygen, and could not detect the difference between 25 and 50 ppm toluene concentrations in a nitrogen environment to any great extent.

6.10.1 Theory Explaining the Sensor's Response to a Rhodamine B Dye Molecule

The diagram contained in Figure 6.72 shows how the Rhodamine B dye molecule physically functions on the sensor surface. Figure 6.72 depicts the gaining of energy by the Rhodamine B dye molecule and the transfer of the energy and electron to the conduction band. [88]

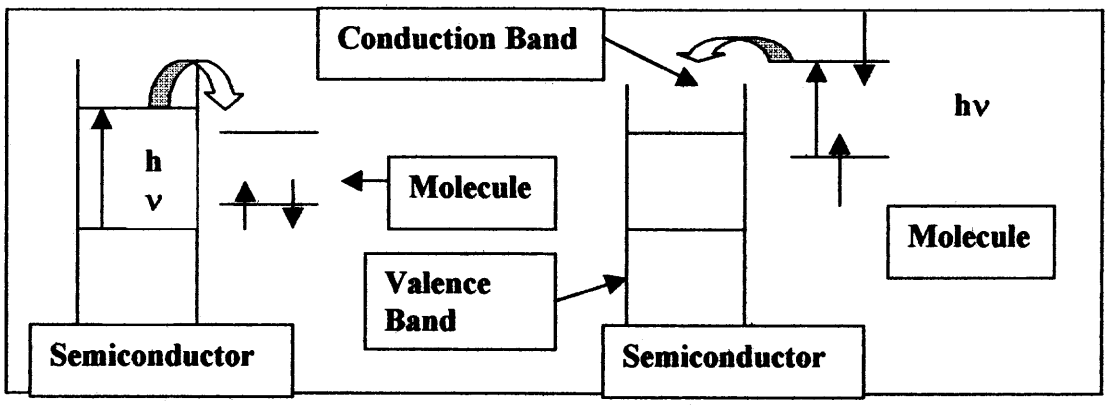

Figure 6.72 A diagram showing the absorption of a photon of energy by a surface molecule and the transfer of an electron by that molecule to the conduction band. [88]

6.11 The Effect of Helium on the Sensor

The sensor was tested for its response to helium gas. When helium gas, which has a thermal conductivity about six times greater than nitrogen and oxygen, was placed into

the chamber the resistance went down as shown in Figure 6.73. When the helium was taken out of the chamber through vacuum application the resistance went back up.

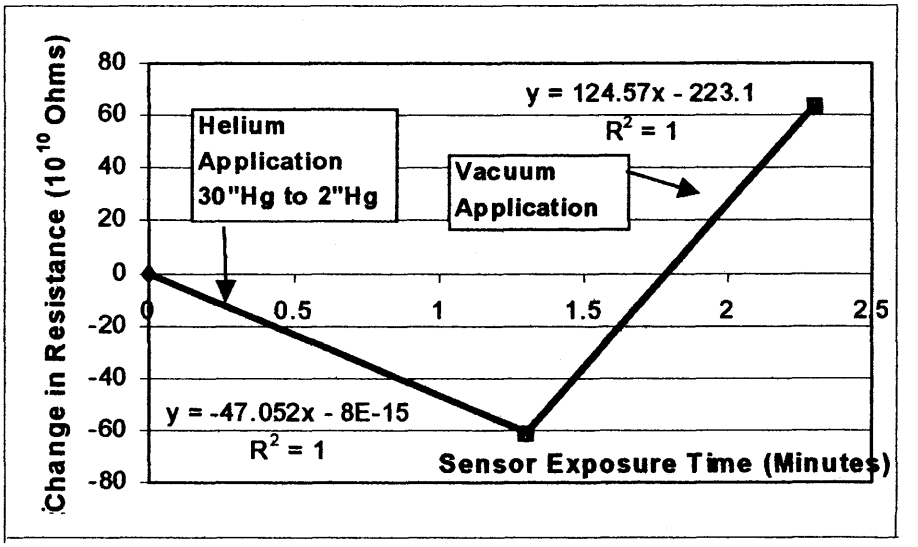

Figure 6.73 The change in resistance versus sensor exposure time for exposure to helium and subsequent vacuum application.

This is mostly due to a cooling effect. The sensor is at a temperature somewhat higher than the chamber walls, due to the energy of the light. The helium conducts this heat from the sensor to the walls. [89]

CHAPTER 7

CONCLUSIONS AND FUTURE WORK

1. The sensor used in this study, with the 0.5 micron thick cadmium sulfide layer and a Rhodamine B dye layer, detected toluene in the parts-per-million (ppm) concentration range when the balance gas was nitrogen, but not when the balance gas was oxygen. Without the surface dye, the sensor could not detect the difference between two gas mixtures with different toluene concentrations (25 and a 50 ppm toluene/nitrogen).
2. The sensor had a huge response to oxygen as compared to nitrogen or toluene, due to the quenching ability of the oxygen molecules.
3. Nitrogen was shown to have very little effect on the sensor's response.
4. The sensor with the thicker (4.5 micron) cadmium sulfide layer could detect toluene concentrations in the 0 – 20 ppm concentration range when air was the balance gas, as long as the oxygen concentration was kept constant.
5. The sensor was also found to be able to detect both the presence and the concentration of oxygen present in the sensor chamber, with both thicknesses (0.5 and 4.5 micron) of cadmium sulfide layer, due to the fact that the surface current on the sensor was reduced by the quenching by the oxygen molecules.
6. The dyed sensor with the 0.5 micron thick cadmium sulfide layer, was able to detect both the presence and concentration of humidity in both nitrogen and oxygen the environments, in many cases especially at very high humidity levels, whereas undyed sensor could not.

7. Water molecules were shown to interfere with the quenching of the sensor surface by oxygen, and at a relative humidity level of 90% all quenching by oxygen ceased.
8. Water molecules were shown to be weakly bonded to the sensor surface by the sudden increasing of the surface resistance (due to oxygen quenching), when a vacuum was pulled.
9. It has been shown by experimentation, that the resistance goes down when the surface contains a sufficient amount of sorbed polar molecules (such as water or toluene molecules), presumably due to the setting up of an alternative pathway for the electrons, to prevent their passage across the sulfide ions in the cadmium sulfide layer. (The amount of toluene in air needed to set up an alternative pathway on the surface is about a 25 ppm concentration).
10. Synthetic air (containing approximately 80% nitrogen and 20% oxygen) was shown to have a higher resistance, due to increased quenching by oxygen, than atmospheric air (a similar nitrogen/ oxygen mixture containing other impurities such as water vapor and carbon dioxide present in the ambient environment).
11. The reduction in resistance of the atmospheric air versus synthetic air was due to the hindrance of oxygen quenching by water vapor and other polar molecules, which become adsorbed to the ionic cadmium sulfide surface and block oxygen quenching.
12. Although atmospheric air produced much lower resistances in the sensor than synthetic air, both air types resulted in similar quenching, adsorption and desorption curves, when the air was flowing through the chamber.
13. The sensor had a large increase in resistance initially due to synthetic and atmospheric air exposure and oxygen quenching, but this response leveled out over

time (after about 30-60 minutes) as an equilibrium of the oxygen quenching, oxygen ion adsorption and oxygen ion desorption processes was achieved.

14. When the response of the sensor to atmospheric air or synthetic air was followed over time, after they were introduced into the sensor chamber at time zero, the sensor responded differently to the two different types of air, when the air was stationary in the sensor chamber.
15. Analysis of the sensor's change in resistance data versus percent oxygen, showed that the atmospheric air data was linear (as per the Stern-Volmer equation for quenching) whereas the synthetic air data was not, when the air was introduced into the chamber and allowed to equilibrate (without flowing). This difference was due to the fact that water molecules in the atmospheric air hindered quenching and did not allow adsorption of the oxygen ion to predominate. Therefore, quenching was the predominant process throughout the exposure period.
16. Experiments showed that approximately the same initial linear equations resulted for resistance versus percent oxygen data, whether the oxygen/nitrogen mixtures were made up in the sensor chamber or in a tank first, or whether there was an initial purge of the sensor chamber for the first 10 seconds of exposure time. However, when the oxygen/nitrogen mixture was allowed to flow through the tank for the first minute of sensor exposure time, there was a significant difference in the initial resistance versus percent oxygen data.
17. Heating of the sensor resulted in a desorption of oxygen ions off of the sensor surface, leading to a reduction in the sensor's resistance (an increase in surface current) and an increase in the percentage of oxygen in the sensor chamber.

18. Several cycles of nitrogen purge followed by evacuation were needed to desorb oxygen ions and toluene from the sensor surface.
19. Exposing the sensor to helium resulted in a reduction in resistance due to helium's high thermal conductivity, and it may also have surface desorbing abilities.
20. These experiments have proven that application of bandgap light to the sensor used in this study, resulted in a large increase of surface current for both 0.5 and 4.5 micron thick cadmium sulfide layers.
21. The Rhodamine B dye, used in this study, was shown to increase the photosensitivity of the sensor due to a new spectrum of photoconductivity consisting of the cadmium sulfide (CdS) photoconductivity band and a new additional peak due to the dye.

FUTURE WORK

The sensors studied in this research work, consisting of thin cadmium sulfide films coated with Rhodamine B dye, have the potential to be applied to the detection and measurement of volatile organic compounds (VOC), oxygen, or humidity. Additional research is needed to expand the realm of conclusions stated above, and the research studies outlined in this thesis have laid a base for these future studies.

The testing of the function of the fluorescent dye on the surface of the sensor is one of the areas in which additional work is needed. Fluorescent dyes, other than Rhodamine B, should also be tested for their possible use in a sensor array that could be used to distinguish among different VOC's.

More extensive testing can also be carried out on improving the sensor fabrication method and on determining the limitations of the sensor as a VOC detector especially with respect to higher humidities and temperatures.

Finally, analytical testing of the sensor surface should be made to determine surface morphology and to characterize the type and concentration of species adsorbed to the sensor surface due to exposures to gaseous mixtures containing various amounts of VOC's, oxygen and/or humidity.

APPENDIX

This Appendix contains the experimental data that was plotted in the figures contained in this report.

(The zero point for these data sets was taken at the start of the gas insertion into the chamber).

Table A.1 Figure 6.1 Data – Resistances with Nitrogen Alone

Time (minutes)	Change In Potential (millivolts)	Resistance (10^{10} ohms)	Change In Resistance (10^{10} ohms)
0	246.5	3.582	0
0.5	253.0	3.490	-0.092
1	247.5	3.568	-0.014
2	252.5	3.497	-0.085
3	249.5	3.539	-0.043
10	246.7	3.579	-0.003
20	250.0	3.532	-0.050
30	262.5	3.364	-0.218
40	296.5	2.978	-0.604
50	282.5	3.126	-0.456
60	302.5	2.919	-0.663

Table A.2 Figure 6.2 Data – Resistances with Air Alone

Time (minutes)	Change In Potential (millivolts)	Resistance (10^{10} ohms)	Change In Resistance (10^{10} ohms)
0	91.2	9.69	0
0.5	85.0	10.40	0.707
1	79.5	11.12	1.426
2	72.0	12.28	2.585
10	58.0	15.24	5.548
20	53.5	16.52	6.830
30	54.5	16.22	6.527
40	54.0	16.37	6.677
50	51.5	17.17	7.472
60	50.0	17.68	7.987

Table A.3 Figure 6.3 and Figure 6.72 Data – Results with Synthetic Air

Time (minutes)	Potentials (millivolts) Partial Pressures of Synthetic Air (psia) 0.7	2.4	4.6	8.6	12.7	15.7	17.3 psia
0	30.7	30.4	30.5	30.3	30.5	30.5	30.5
0.5	28.9	27.6	24.1	22.8	24.0	18.2	14.9
2	26.2	22.5	18.1	15.5	15.1	12.5	10.4
5	24.5	19.7	14.7	12.7	12.1	9.3	7.8
10	21.9	17.9	13.0	10.7	9.6	7.5	6.6
20	20.6	15.4	11.0	8.9	8.3	6.8	5.7
30	20.4	13.8	10.1	8.4	7.4	6.4	5.6

Time (minutes)	Change in Resistance (10^{10} ohms) Partial Pressures of Synthetic Air (psia) 0.7	2.4	4.6	8.6	12.7	15.7	17.3 psia
0	0.000	0.000	0.000	0.000	0.000	0.000	0.000
0.5	0.088	0.145	0.364	0.440	0.371	0.836	1.170
2	0.234	0.469	0.844	1.090	1.161	1.507	1.800
5	0.337	0.690	1.209	1.441	1.556	2.035	2.290
10	0.514	0.853	1.428	1.742	1.966	2.418	2.560
20	0.613	1.115	1.726	2.059	2.229	2.570	2.786
30	0.629	1.308	1.877	2.167	2.412	2.669	2.812

Table A.4 Figure 6.4 Data – the Initial Slopes for the First 2 Minutes of Sensor Exposure

Change in Resistance /Time (10^{10} ohms/min) Partial Pressures of Synthetic Air (psia) 0.7	2.4	4.6	8.6	12.7	15.7	17.3 psia
0.117	0.235	0.422	0.546	0.581	0.754	0.9

Table A.5 Figures 6.5 and 6.6 Data

Time (minutes)	Change in Resistance (10^{10} ohms)							
	18% O2	14.9% O2	9% O2	4.9% O2	3.2% O2	0% O2	1.3% O2	6.8% O2
0	0.00	0.00	0.00	0.00	0.00	0.00	0.00	0.00
1	0.861	0.725	0.655	0.405	0.259	0.230	0.245	
2	1.133	1.013	0.846	0.631	0.328	0.048	0.188	0.718
5	1.616	1.410	1.235	0.965	0.479	0.086	0.321	1.006
10	1.869	1.637	1.496	1.222	0.626	0.073	0.480	1.362
20	2.184	1.888	1.625	1.338	0.898	0.061	0.447	1.616
30	2.251	1.947	1.761	1.460	0.918	-0.024	0.447	1.840
40	2.320	2.008	1.818	1.563	0.937	-0.104	0.531	1.899
50	2.427	2.038	1.965	1.589	1.080	-0.036	0.583	2.022
60	2.464	2.070	2.026	1.537	1.167	-0.181	0.601	2.022

Time (minutes)	Change in Resistance (10^{10} ohms)						
	12.5% O2	15.5% O2	3.2% O2	19.5% O2	8.9% O2	10.8% O2	4.5% O2
0	0.00	0.00	0.00	0.00	0.00	0.00	0.00
1	0.592	0.713	0.259	0.736	0.499	0.648	0.355
2	0.898	0.977	0.34	1.133	0.773	0.886	0.491
5	1.234	1.422	0.523	1.485	1.133	1.314	0.853
10	1.549	1.794	0.725	1.725	1.460	1.616	1.051
20	1.911	2.065	0.949	1.929	1.753	1.929	1.362
30	2.002	2.263	1.009	2.053	1.899	2.118	1.509
40	2.130	2.368	1.071	2.184	1.990	2.184	1.613
50	2.229	2.476	1.092	2.391	1.990	2.356	1.613
60	2.297	2.513	1.201	2.356	2.118	2.391	1.640

Table A.6 Figures 6.5, 6.6, 6.8 and 6.10 Data

Experiment # 1 and 2 determinations of % O2 were made by weighing chart recorder peaks on a digital balance located in the physical chemistry laboratory at NJIT.

The data from Experiment #1 is as follows:

Experiment #1

Date (Run #)	% O2	Weight of O2 Peak	Weight of N2 Peak
1) 5/31/02 (Run#1)	18.0% O2	0.0156 g	0.0713 g
2) 5/31/02 (Run #2)	8.9% O2	0.0167 g	0.1711 g
3) 6/3/02 (Run #1)	14.9% O2	0.0144 g	0.0820 g
4) 6/3/02 (Run #2)	9.0 % O2	0.0104 g	0.1053 g
5) 6/5/02 (Run #1)	4.9% O2	0.0058 g	0.1128 g
6) 6/5/02 (Run #2)	0 % O2	0	
7) 6/6/02 (Run #1)	3.2 % O2	0.0033 g	0.1001 g
8) 6/7/02 (Run #1)	1.3% O2	0.0016 g	0.1257 g
9) 6/7/02 (Run #2)	3.2 % O2	0.0015 g	0.0456 g
10) 6/10/02 (Run # 1)	4.95 % O2	0.0045 g	0.0864 g
11) 6/10/02 (Run #2)	12.5 % O2	0.0170 g	0.1189 g
12) 6/11/02 (Run # 1)	15.5% O2	0.0129 g	0.0705 g
13) 6/12/02 (Run # 1)	19.5% O2	0.0194 g	0.0800 g
14) 6/18/02 (Run # 1)	4.5 % O2	0.0049 g	0.1031 g
15) 6/18/02 (Run # 2)	6.8 % O2	0.0057 g	0.0779 g
16) 6/20/02 (Run # 1)	10.8 % O2	0.0087 g	0.0722 g

Experiment #2 (Figure 6.8)

Date (Run #)	% O2	Weight of O2 Peak	Weight of N2 Peak
1) 6/26/02 (Run#1)	17.0% O2	0.0438 g	0.2141 g
2) 6/26/02 (Run #2)	8.0% O2	0.0198 g	0.2281 g
3) 7/1/02 (Run #1)	13.8% O2	0.0369 g	0.2299 g
4) 7/2/02 (Run #2)	1.4 % O2	0.0036 g	0.2592 g

Table A.7 Figures 6.8 and 6.10 Data

Time (minutes)	17.0% O2 Potential (millivolts)	17.0% O2 Change in Resistance (10^{10} ohms)	8% O2 Potential (millivolts)	8% O2 Change in Resistance (10^{10} ohms)
0	27.8	0.000	27.6	0.000
1	22.2	0.809	24.8	0.367
2	21.0	1.039	24.2	0.457
5	19.1	1.464	23.2	0.616
10	18.1	1.724	21.8	0.865
20	17.8	1.807	20.7	1.083
30	18.1	1.724	20.3	1.169
40	17.8	1.807	19.9	1.258
50	17.9	1.779	20.2	1.191
60	18.1	1.724	19.3	1.398
70	18.1	1.724	19.6	1.327

Time (minutes)	13.83% O2 Potential (millivolts)	13.83% O2 Change in Resistance (10^{10} ohms)	1.40% O2 Potential (millivolts)	1.40% O2 Change in Resistance (10^{10} ohms)
0	27.8	0.00	27.5	0.000
1	23.7	0.558	25.9	0.208
2	21.6	0.926	25.3	0.283
5	20.6	1.127	25.0	0.326
10	19.7	1.326	24.1	0.460
20	19.0	1.507	23.4	0.571
30	19.0	1.494	23.0	0.638
40	19.1	1.482	22.5	0.725
50	18.9	1.532	22.6	0.707
60	19.0	1.494	22.8	0.672
70	18.9	1.519	22.8	0.672

Table A.8 Figure 6.11 Data

Time (minutes)	19.3% O2 Potential (millivolts)	19.3% O2 Change in Resistance (10^{10} ohms)	3.26% O2 Potential (millivolts)	3.26% O2 Change in Resistance (10^{10} ohms)
0	27.3	0.00	27.3	0.000
1	21.7	0.847	23.9	0.467
2	19.7	1.266	22.6	0.683
5	17.9	1.724	21.6	0.866
10	16.7	2.083	20.1	1.176
20	15.8	2.389	19.4	1.337
30	15.5	2.499	19.0	1.434
40	15.7	2.425	19.1	1.409
50	15.7	2.425	18.6	1.535
60	15.4	2.536	18.7	1.509
70	15.4	2.536	18.6	1.535

Table A.8 Figure 6.11 Data (Continued)

Time (minutes)	0% O2 Potential (millivolts)	0% O2 Change in Resistance (10^{10} ohms)	0.93% O2 Potential (millivolts)	0.93% O2 Change in Resistance (10^{10} ohms)
0	27.6	0.000	27.4	0.000
1	27.2	0.048	25.0	0.314
2	27.4	0.024	24.2	0.432
5	28.1	-0.057	22.9	0.643
10	28.2	-0.063	21.9	0.821
20	28.9	-0.146	20.7	1.059
30	30.4	-0.299	20.0	1.210
40	30.6	-0.318	20.2	1.166
50	31.3	-0.383	20.3	1.144
60	32.1	-0.455	20.2	1.166
70	32.4	-0.481	20.4	1.122

Time (minutes)	12.82% O2 Potential (millivolts)	12.82% O2 Change in Resistance (10^{10} ohms)	7.55% O2 Potential (millivolts)	7.55% O2 Change in Resistance (10^{10} ohms)
0	28.0	0.000	27.3	0.000
1	23.1	0.679	23.6	0.515
2	21.4	0.987	22.5	0.700
5	19.4	1.419	20.4	1.110
10	18.2	1.723	19.2	1.385
20	17.0	2.071	17.8	1.752
30	16.8	2.133	17.2	1.927
40	16.6	2.198	16.7	2.083
50	16.3	2.314	16.2	2.249
60	16.4	2.263	16.2	2.249
70	16.2	2.331	16.1	2.283

Time (minutes)	14.69% O2 Potential (millivolts)	14.69% O2 Change in Resistance (10^{10} ohms)	9.21% O2 Potential (millivolts)	9.21% O2 Change in Resistance (10^{10} ohms)
0	27.5	0.000	27.8	0.000
1	21.5	0.909	22.8	0.707
2	19.9	1.245	21.3	0.984
5	18.5	1.585	19.4	1.396
10	17.5	1.862	18.3	1.687
20	16.9	2.044	17.3	1.956
30	16.4	2.205	16.6	2.175
40	16.1	2.307	16.3	2.274
50	15.6	2.486	16.1	2.342
60	15.8	2.413	16.1	2.342
70	15.6	2.486	15.9	2.412

Table A.9 Figure 6.15 Data

% Oxygen	0 Minute Potential (millivolts)	0 Minute Resistance (10^{10} Ohms)	1 Minute Potential (millivolts)	1 Minute Resistance (10^{10} ohms)	Change In Resistance (10^{10} ohms)
2.86	27.0	3.319	23.3	3.845	0.526
6.57	27.05	3.312	22.7	3.947	0.635
14.18	27.8	3.223	23.4	3.829	0.606
15.98	27.0	3.319	22.4	4.000	0.681
17.19	27.4	3.270	22.2	4.036	0.766
18.93	27.4	3.270	19.4	4.619	1.349

Table A.10 Figure 6.16 Data

Time (minutes)	(18.93% O2) Potential (millivolts)	Change in Resistance (10^{10} ohms)	Phase
0	27.4	0.000	Synthetic air flowing into sensor
1	19.4	1.349	chamber at 15 psig
2	18.3	1.626	
5	16.5	2.160	
10	15.4	2.548	
20	15.2	2.625	
25	15.0	2.703	
27	14.7	2.825	Vacuum #1
30	15.0	2.703	
33	15.1	2.664	Helium #2
38	15.6	2.474	
43	15.8	2.401	
48	16.7	2.095	Vacuum #3
53	17.3	1.909	
58	17.7	1.792	Nitrogen #4
63	18.1	1.680	
68	18.7	1.521	Vacuum #5
72	19.5	1.325	
78	20.1	1.188	Nitrogen #6
82	20.1	1.188	
88	20.4	1.122	Vacuum #7
92	21.6	0.878	
98	21.7	0.859	Nitrogen #8
102	21.7	0.859	
118	24.0	0.463	Vacuum #9
122	24.2	0.432	

Table A.10 Figure 6.16 Data (Continued)

Time (minutes)	Potential (millivolts)	Change in Resistance (10^{10} ohms)	Phase
128	24.7	0.358	Nitrogen #10
132	25.2	0.286	
138	25.5	0.244	Vacuum #11
142	25.7	0.216	
148	26.2	0.150	Nitrogen #12
152	26.5	0.111	
158	26.3	0.137	Vacuum #13
165	27.0	0.049	
173	27.5	-0.012	Nitrogen #14
179	27.9	-0.059	Vacuum #15
188	28.7	-0.148	
192	29.0	-0.180	Nitrogen #16
198	29.5	-0.233	
202	30.3	-0.313	Vacuum #17
208	29.6	-0.243	
211	30.6	-0.342	Nitrogen #18
218	30.7	-0.351	
222	31.2	-0.398	
229	32.9	-0.547	Vacuum #19
233	32.8	-0.538	
240	32.7	-0.530	Nitrogen #20
243	32.7	-0.530	
250	34.0	-0.635	Vacuum #21
252	33.6	-0.603	

Table A.11 Figure 6.19 and 6.43 Data (Synthetic Air)

Time(t) (minutes)	Potential ln(t/3+1)	Change in Current (10^{-10} amps)
1	3.045	0.80
1.5	3.434	0.86
2	3.714	0.91
3	4.110	0.99
4	4.394	1.03
5	4.615	1.09
7.5	5.017	1.15
10	5.303	1.20
12	5.485	1.22
14	5.638	1.22
16	5.771	1.23
20	5.994	1.23
25	6.217	1.23

Table A.12 Figure 6.29 Data

Time (minutes)	18.82% O2 Potential (millivolts)	18.82% O2 Change in Resistance (10^{10} ohms)	5.79% O2 Potential (millivolts)	5.79% O2 Change in Resistance (10^{10} ohms)
0	64.5	0.000	64.9	0.000
1	33.2	1.310	36.3	1.087
2	28.4	1.766	32.7	1.359
5	24.9	2.209	29.8	1.626
10	23.1	2.490	27.3	1.901
20	21.4	2.798	25.8	2.092
30	20.8	2.919	25.5	2.133
40	21.1	2.857	24.7	2.247
50	20.5	2.982	24.4	2.291
60	20.4	3.003	24.5	2.276

Time (minutes)	12.46% O2 Potential (millivolts)	12.46% O2 Change in Resistance (10^{10} ohms)	16.59% O2 Potential (millivolts)	16.59% O2 Change in Resistance (10^{10} ohms)
0	64.3	0.000	64.5	0.000
1	33.2	1.304	32.2	1.392
2	31.2	1.477	27.5	1.867
5	29.6	1.632	24.1	2.326
10	27.8	1.827	23.0	2.503
20	25.8	2.077	22.5	2.590
30	24.8	2.217	21.9	2.699
40	24.2	2.306	21.6	2.756
50	23.8	2.369	21.3	2.814
60	23.1	2.482	21.3	2.814

Time (minutes)	0.47% O2 Potential (millivolts)	0.47% O2 Change in Resistance (10^{10} ohms)	8.5% O2 Potential (millivolts)	8.5% O2 Change in Resistance (10^{10} ohms)
0	66.2	0.000	64.7	0.000
1	51.0	0.403	43.3	0.684
2	46.0	0.594	37.9	0.981
5	39.2	0.931	33.0	1.329
10	37.2	1.054	30.2	1.581
20	32.6	1.393	27.7	1.848
30	31.0	1.535	26.0	2.059
40	30.8	1.554	25.7	2.099
50	30.3	1.602	24.8	2.226
60	29.9	1.641	23.8	2.378

Table A.12 Figure 6.29 Data (Continued)

	7.27% O2	
Time (minutes)	Potential (millivolts)	Change in Resistance (10^{10} ohms)
0	64.9	0.000
1	41.6	0.772
2	35.8	1.121
5	31.2	1.490
10	28.7	1.739
20	26.4	2.011
30	26.2	2.037
40	25.1	2.187
50	23.3	2.462
60	23.7	2.397

Table A.13 The Ratio of the Initial Current to the Final Current for the Different Concentrations of Oxygen in Figure 6.29

	Ratio of Initial to Final Current Time (minutes)	
% Oxygen	1 minute	2 minutes
0.47	1.298	1.439
5.79	1.818	2.016
7.27	1.560	1.813
8.50	1.494	1.707
12.46	1.919	2.061
16.59	2.003	2.345
18.82	1.943	2.271

Table A.14 Figure 6.33 Data for Atmospheric Air Flowing at 15 Psig

Time (minutes)	Potential (millivolts)	Change Resistance (10^{10} ohms)
0	28.1	0.000
1	25.2	0.369
2	23.7	0.587
5	21.9	0.897
10	20.7	1.135
20	20.2	1.242
25	20.1	1.264
30	22.5	0.788
35	24.4	0.478
40	25.9	0.265
45	26.6	0.174
50	28.9	-0.094
55	32.3	-0.420
60	34.4	-0.589
65	35.7	-0.684
70	38.4	-0.861
75	40.5	-0.982
80	42.2	-1.071
85	43.5	-1.134
90	44.7	-1.190
95	49.1	-1.369
100	49.7	-1.391
105	51.0	-1.437
110	53.7	-1.525
115	55.4	-1.577
120	55.7	-1.585
125	55.5	-1.580
130	57.0	-1.622
135	57.2	-1.628
140	58.1	-1.652
145	60.2	-1.706
150	59.7	-1.693
155	62.2	-1.753

Table A.15 Figure 6.37 Data

Time (minutes)	2.9% O2 Potential (millivolts)	2.9% O2 Change in Resistance (10^{10} ohms)	7.8% O2 Potential (millivolts)	7.8% O2 Change in Resistance (10^{10} ohms)
0	27.1	0.000	27.8	0.000
1	24.6	0.336	25.4	0.299
2	23.9	0.443	24.5	0.428
5	21.8	0.804	23.4	0.600
10	20.8	1.002	22.8	0.701
20	20.3	1.108	22.6	0.736
30	20.3	1.108	22.4	0.771
40	20.6	1.044	22.3	0.789
50	20.1	1.152	22.3	0.789
60	19.7	1.242	22.1	0.825
70	19.2	1.361	22.1	0.825

Time (minutes)	10.9% O2 Potential (millivolts)	10.9% O2 Change in Resistance (10^{10} ohms)	14.95% O2 Potential (millivolts)	14.95% O2 Change in Resistance (10^{10} ohms)
0	27.5	0.000	27.2	0.000
1	25.3	0.284	21.3	0.913
2	24.5	0.399	20.3	1.120
5	23.3	0.587	21.0	0.973
10	23.0	0.638	20.3	1.131
20	22.9	0.655	20.1	1.164
30	22.2	0.778	19.8	1.231
40	21.9	0.833	19.8	1.231
50	21.8	0.852	19.8	1.231
60	21.7	0.871	19.9	1.209
70	21.7	0.871	20.3	1.131

Table A.16 Figure 6.39 Data for Atmospheric Air Flowing at 15 Psig (New Initial Resistance (Baseline) Value Used)

Time (minutes)	(17.99% O2) Potential (millivolts)	Change in Resistance (10^{10} ohms)
0	64.3	0.000
1	37.3	1.009
2	32.2	1.390
5	25.1	2.177
10	23.4	2.436
20	21.6	2.755
25	21.1	2.853
30	22.0	2.680
35	25.0	2.191
40	26.7	1.963
45	27.4	1.877
50	29.1	1.686
55	32.2	1.390
60	35.5	1.131
65	36.1	1.089
70	38.1	0.959
75	42.0	0.740
80	44.1	0.639
85	44.4	0.625
90	46.1	0.551
95	47.0	0.513
100	49.6	0.413
105	51.1	0.360
110	53.6	0.279
115	55.2	0.230
120	58.4	0.141
125	56.4	0.196
130	57.8	0.157
135	59.5	0.113

Table A.17 Figure 6.43 Data (Atmospheric Air)

Time(t) (minutes)	Potential ln(t/3+1)	Current (10^{-10} amps)	Change in Current (10^{-10} amps)
0		6.43	0.00
1	3.045	3.73	2.70
1.5	0.434	3.31	3.12
2	3.714	3.22	3.21
3	4.110	2.73	3.70
4	4.394	2.57	3.86
5	4.615	2.51	3.92
7.5	5.017	2.36	4.07
10	5.303	2.34	4.09
12	5.485	2.28	4.15
14	5.638	2.21	4.22
16	5.771	2.20	4.23
20	5.994	2.16	4.27
25	6.217	2.11	4.32

Table A.18 Figure 6.48 Data

	43.2% RH Nitrogen	
Time (minutes)	Potential (millivolts)	Change in Resistance (10^{10} ohms)
0	61.0	0.000
1	67.3	-0.137
2	66.3	-0.117
5	68.3	-0.157
10	70.5	-0.197
20	71.7	-0.219
30	75.5	-0.281
40	83.2	-0.391
50	84.7	-0.410
60	92.0	-0.493

With applied hot gun the mV reading increased from 92 to 99 mV

Table A.19 Figures 6.47 and 6.50 Data (Synthetic Air Data)

	Change in Resistance (10^{10} Ohms)					
Time (Minutes)	0% RH	9.5% RH	43.2% RH	60.4% RH	75.5% RH	85.2% RH
0	0.000	0.000	0.000	0.000	0.000	0.00
1	1.914	0.591	0.652	0.756	0.599	0.27
2	2.267	0.856	0.934	1.096	0.899	-0.83
5	2.985	1.303	1.453	1.409	0.280	-0.82
10	3.259	1.628	1.728	1.745	0.477	-0.75
20	3.488	2.045	2.139	2.132	0.757	-0.60
30	3.741	2.176	2.308	2.325	0.904	-0.52
40	3.683	2.176	2.350	2.452	1.015	-0.47
50	3.654	2.391	2.392	2.574	1.151	-0.45
60	3.683	2.407	2.526	2.703	1.240	-0.30

Table A.20 Nitrogen Data in Figures 6.47 and 6.50

	Change in Resistance (10^{10} Ohms)					
Time (Minutes)	0% RH Nitrogen	9.6% RH Nitrogen	43.2% RH Nitrogen	60.4% RH Nitrogen		85.4% RH Nitrogen
0	0.000	0.000	0.000	0.000	0.000	0.000
0.25					-0.152	
1	-0.017		-0.137	0.330	-0.049	
2	-0.027		-0.117	0.235	-0.092	-0.414
5	-0.054	0.081	-0.157	0.065	-0.255	-0.532
10	-0.087	0.085	-0.197	-0.149	-0.451	-0.722
20	-0.144	0.043	-0.219	-0.407	-0.645	-0.841
30	-0.165	0.020	-0.281	-0.564	-0.738	-0.903
40	-0.200	-0.037	-0.391	-0.626	-0.805	-0.944
50	-0.254	-0.070	-0.410	-0.689	-0.845	-0.968
	-0.292	-0.118	-0.493	-0.721	-0.892	-0.998

Table A.21 Figure 6.51 Data

Time (minutes)	59.6% RH Nitrogen Potential (millivolts)	59.6% RH Nitrogen Change in Resistance (10^{10} ohms)	75.4% RH Nitrogen Potential (millivolts)	75.4% RH Nitrogen Change in Resistance (10^{10} ohms)
0	66.8	0.000	64.0	0.000
0.25			71.8	-0.152
1	62.0	0.104	66.3	-0.049
2	64.2	0.055	68.5	-0.092
5	70.9	-0.077	78.3	-0.255
10	84.2	-0.276	94.5	-0.451
20	96.5	-0.412	118.9	-0.645
30	113.7	-0.552	135.7	-0.738
40	129.5	-0.648	151.0	-0.805
50	136.7	-0.684	162.0	-0.845
60	146.7	-0.729	177.0	-0.892

Table A.22 Figure 6.52 Data

Time (minutes)	59.4% RH Synthetic Air Potential (millivolts)	59.4% RH Synthetic Air Change in Resistance (10^{10} ohms)	75.5 % RH Synthetic Air Potential (millivolts)	75.5 % RH Synthetic Air Change in Resistance (10^{10} ohms)
0	66.0	0.000	65.6	0.000
0.25	40.9	0.831		
1	34.4	1.244	49.8	0.432
2	28.2	1.815	47.4	0.523
5	25.2	2.193	44.0	0.669
10	23.5	2.449	39.3	0.912
20	23.1	2.515	34.8	1.206
30	22.5	2.618	32.7	1.371
50	22.3	2.654	29.7	1.647
60	22.2	2.672	29.1	1.709

Table A.23 Figures 6.51 and 6.52 Data

	8.8% RH Air		9.1% RH Nitrogen	
Time (minutes)	Potential (millivolts)	Change in Resistance (10^{10} ohms)	Potential (millivolts)	Change in Resistance (10^{10} ohms)
0	72.0	0.000	66.0	0.000
1	54.0	0.414	62.2	0.083
2	44.4	0.772	61.6	-0.097
5	36.2	1.228	62.6	0.074
10	32.2	1.534	69.4	-0.066
20	30.0	1.738	74.7	-0.158
30	28.2	1.928	80.4	-0.242
40	28.0	1.951	86.4	-0.319
50	27.2	2.045	91.0	-0.372
60	26.8	2.094	95.5	-0.418
Vacuum then synthetic air up to 4.5 psig				
61			54.9	0.274
62			44.9	0.636
65			36.0	1.128
70			30.8	1.546
80			27.7	1.871
90			25.0	1.945
100			24.0	2.094
110			22.7	2.307
120			21.0	2.625

Table A.24 Figures 6.53 and 6.54 Data

Time (minutes)	84.9% RH Synthetic Air Potential (millivolts)	Change in Resistance (10^{10} ohms)	84.9% RH Nitrogen Potential (millivolts)	Change in Resistance (10^{10} ohms)
0	64.5	0.000	66.5	0.000
1	67.5	-0.061		
2	64.5	0.000	131.2	-0.662
5	58.0	0.156	146.3	-0.733
10	53.4	0.288	157.3	-0.775
20	50.3	0.391	163.3	-0.796
30	48.0	0.476	166.3	-0.806
40	47.1	0.512	163.7	-0.797
50	45.5	0.579	164.8	-0.801
60	46.0	0.557	157.3	-0.775

with vacuum potential jumped up to 22.7 mV

Time (minutes)	100% RH Nitrogen Potential (millivolts)	Change in Resistance (10^{10} ohms)	100% RH Synthetic Air Potential (millivolts)	Change in Resistance (10^{10} ohms)
0	65.4	0.000	64.5	0.000
1	125.9	-0.656		
2	134.9	-0.703		
3			83.4	-0.313
5	168.0	-0.833	83.0	-0.308
10	200.0	-0.918	76.9	-0.223
20	244.0	-0.999	72.5	-0.152
30	274.0	-1.039	71.0	-0.126
40	304.0	-1.071	68.4	-0.078
50	318.0	-1.084	68.2	-0.075
60	344.0	-1.105	67.8	-0.067

Time (minutes)	Synthetic Air Potential (millivolts)	Change in Resistance (10^{10} ohms)	Nitrogen Potential (millivolts)	Change in Resistance (10^{10} ohms)
0	64.4	0.000	73.0	0.000
1	54.4	0.255		
2	47.4	0.479	79.0	-0.093
5	40.5	0.818	81.3	-0.125
10	37.5	0.994	88.9	-0.219
20	35.0	1.164	95.5	-0.288
30	34.6	1.194	103.5	-0.360
40	33.2	1.303	107.0	-0.388
50	33.2	1.303	116.0	-0.453
60	32.7	1.344	117.5	-0.463

Table A.24 Figures 6.53 and 6.54 Data (Continued)

Time (minutes)	9.4% RH Nitrogen Potential (millivolts)	9.4% RH Nitrogen Change in Resistance (10^{10} ohms)	9.1% RH Synthetic Air Potential (millivolts)	9.1% RH Synthetic Air Change in Resistance (10^{10} ohms)
0	68.0	0.000	64.4	0.000
1	75.0	-0.122	60.6	0.087
2	77.0	-0.153	58.4	0.142
5	83.0	-0.237	52.6	0.311
10	89.0	-0.310	48.4	0.458
20	96.5	-0.388	45.1	0.593
30	101.5	-0.433	43.2	0.680
40	106.0	-0.471	42.5	0.714
50	111.0	-0.508	41.0	0.791
60	113.8	-0.528	40.7	0.807

With vacuum the mV reading dropped from 120 to 109

Table A.25 Figure 6.59 Data – Resistances with 35.4 ppm Toluene/Nitrogen

Time (minutes)	Potential (millivolts)	Columns A	B	C
0	71.1	1.277	0	0
0.5	68.9	1.318	0.041	0.133
1	67.9	1.337	0.060	0.074
2	67.4	1.347	0.070	0.155
3	66.4	1.367	0.091	0.134
10	63.4	1.432	0.155	0.158
20	55.4	1.639	0.362	0.412
30	54.2	1.675	0.390	0.616
40	53.6	1.694	0.417	1.021
50	54.1	1.678	0.401	0.857
60	53.9	1.685	0.408	1.071

Where:

Column A = Resistance (10^{10} ohms)

Column B = Change in Resistance (10^{10} ohms)

Column C = Change in Resistance of Nitrogen subtracted from Column B (10^{10} ohms)

Table A.25 Figure 6.59 Data (Continued)
Resistances with Air

Time (minutes)	Potential (millivolts)	Resistance (10^{10} ohms)	Change In Resistance (10^{10} ohms)
0	27.2	3.32	0
0.5	23.6	3.82	0.50
1	22.8	3.96	0.64
2	21.9	4.12	0.80
3	21.1	4.27	0.96
10	18.5	4.88	1.56
20	17.1	5.27	1.95
30	16.3	5.53	2.21
40	16.0	5.64	2.32
50	15.8	5.71	2.39
60	15.6	5.78	2.46

Table A.26 Figure 6.60 Data - Resistances with Air

Time (minutes)	Potential (millivolts)	Resistance (10^{10} ohms)	Change in Resistance (10^{10} ohms)
0	78.6	11.25	0
0.5	74	11.95	0.70
1	70	12.63	1.38
2	64.3	13.75	2.50
3	65	13.6	2.35
10	57.2	15.45	4.21
20	52.5	16.84	5.59
30	52	17.00	5.75
40	51.5	17.17	5.92
50	53.3	16.59	5.34
60	53.5	16.52	5.27

Table A.27 Figures 6.60 and 6.62 Data - Resistances with 29.3 ppm Toluene/Air

Time (minutes)	Potential (millivolts)	Resistance (10^{10} ohms)	Change in Resistance (10^{10} ohms)
0	79.7	11.09	0
0.5	73.3	12.06	0.97
1	71.0	12.45	1.36
2	69.0	12.81	1.72
3	68.3	12.94	1.85
10	65.4	13.52	2.43
20	55.3	15.99	4.90
30	54.3	16.28	5.19
40	53.0	16.68	5.59
50	48.8	18.11	7.03
60	50.5	17.5	6.42

Table A.28 Figure 6.61 Data - Resistances with 35.4 ppm Toluene/Air

Time (minutes)	Potential (millivolts)	Resistance (10^{10} ohms)	Change in Resistance (10^{10} ohms)
0	93	9.505	0
0.5	89	9.933	0.428
1	87.5	10.10	0.598
2	86	10.28	0.774
3	81.5	10.85	1.342
10	70.5	12.54	3.034
20	60.5	14.61	5.107
30	56.5	15.65	6.141
40	55	16.07	6.568
50	52.5	16.84	7.333
60	52	17.00	7.495

Table A.29 Figure 6.61 Data - Resistances with Air

Time (minutes)	Potential (millivolts)	Resistance (10^{10} ohms)	Change in Resistance (10^{10} ohms)
0	91.2	9.693	0
0.5	85	10.40	0.707
1	79.5	11.12	1.426
2	72	12.28	2.585
10	58	15.24	5.548
20	53.5	16.52	6.830
30	54.5	16.22	6.527
40	54	16.37	6.677
50	51.5	17.17	7.472
60	50	17.68	7.987

Table A.30 Figure 6.62 Data (Toluene/Air Gas Mixtures)

Time (minutes)	Change in Resistance (10^{10} ohms) 10 ppm	20 ppm	29.3 ppm	35.4 ppm
0	0	0	0	0
0.5	0.416	0.967	0.97	0.428
1	1.085	1.191	1.361	0.598
2	2.157	1.552	1.722	0.774
3	2.648	2.170	1.853	1.342
10	4.402	3.114	2.427	3.034
20	5.455	5.357	4.896	5.107
30	5.153	6.073	5.190	6.141
40	6.128	5.905	5.589	6.568
50	6.590	5.740	7.025	7.333
60	6.156	6.967	6.415	7.495

Table A.31 Figure 6.63 Data – NJIT Lab-made Dyed Sensor (1st Side of the Sensor)

29.8" Hg to 4.5 psi Synthetic Air

Time (minutes)	Potential (millivolts)	Resistance (10^{11} ohms)	Change in Resistance (10^{11} ohms)
0	110.3	0.802	0.000
5	47.0	1.883	1.081
10	40.6	2.180	1.380
20	38.9	2.280	1.470
30	38.0	2.339	1.527

50 ppm Toluene/Synthetic Air

Time (minutes)	Potential (millivolts)	Resistance (10^{11} ohms)	Change in Resistance (10^{11} ohms)
0	108.5	0.815	0.000
5	53.4	1.660	0.841
10	48.5	1.825	1.010
20	43.1	2.050	1.230
30	42.0	2.107	1.292

100 ppm Toluene/Synthetic Air

Time (minutes)	Potential (millivolts)	Resistance (10^{11} ohms)	Change in Resistance (10^{11} ohms)
0	102.0	0.868	0.000
5	45.1	1.960	1.092
10	40.1	2.210	1.342
20	38.3	2.310	1.442
30	37.4	2.370	1.499

Table A.32 Figure 6.64 Data – NJIT Lab-made Dyed Sensor (2nd Side of Sensor)

Data at room temperature

0 ppm Toluene/Synthetic Air

Time (minutes)	Potential (millivolts)	Resistance (10^{10} ohms)	Change in Resistance (10^{10} ohms)
0	379.0	2.330	0.000
2	104.0	8.490	6.160
5	75.5	11.700	9.370
10	65.0	13.580	11.250
20	55.5	15.910	13.580
30	53.5	16.500	14.170

5.6 ppm Toluene/Synthetic Air

Time (minutes)	Potential (millivolts)	Resistance (10^{10} ohms)	Change in Resistance (10^{10} ohms)
0	333	2.65	0.000
2	100	8.83	6.18
5	72	12.26	9.61
10	62	14.24	11.59
20	55	16.05	13.40
30	51	17.31	14.66

11.2 ppm Toluene/Synthetic Air

Time (minutes)	Potential (millivolts)	Resistance (10^{10} ohms)	Change in Resistance (10^{10} ohms)
0	331	2.67	0.00
2	94	9.39	6.72
5	67	13.18	10.51
10	57	15.49	12.82
20	49	18.02	15.35
30	47	18.79	16.12

22.4 ppm Toluene/Synthetic Air

Time (minutes)	Potential (millivolts)	Resistance (10^{10} ohms)	Change in Resistance (10^{10} ohms)
0	332	2.66	0.00
2	78	11.32	8.66
5	60	14.72	12.06
10	51	17.31	14.65
20	45	19.62	16.96
30	43	20.53	17.87

Table A.32 Figure 6.64 data – NJIT Lab-made Dyed Sensor (2nd Side of Sensor) (Continued)

28.5 ppm Toluene/Synthetic Air

Time (minutes)	Potential (millivolts)	Resistance (10^{10} ohms)	Change in Resistance (10^{10} ohms)
0	335	2.64	0.00
2	118	7.48	4.84
5	87	10.15	7.51
10	69	12.80	10.16
20	62	14.24	11.60
30	58	15.22	12.58

33.6 ppm Toluene/Synthetic Air

Time (minutes)	Potential (millivolts)	Resistance (10^{10} ohms)	Change in Resistance (10^{10} ohms)
0	334	2.64	0.00
2	105	8.41	5.77
5	77	11.47	8.83
10	65	13.58	10.94
20	59	14.97	12.33
30	55	16.05	13.41

56 ppm Toluene/Synthetic Air

Time (minutes)	Potential (millivolts)	Resistance (10^{10} ohms)	Change in Resistance (10^{10} ohms)
0	331	2.67	0.00
2	114	7.75	5.08
5	86	10.27	7.60
10	72	12.26	9.59
20	62	14.24	11.57
30	59	14.97	12.30

68 ppm Toluene/Synthetic Air

Time (minutes)	Potential (millivolts)	Resistance (10^{10} ohms)	Change in Resistance (10^{10} ohms)
0	363.2	2.430	0.000
2	215.2	4.103	1.673
5	125.2	7.050	4.620
10	91.2	9.680	7.250
20	76.2	11.590	9.160
30	71.2	12.400	9.970

Table A.32 Figure 6.64 data – NJIT Lab-made Dyed Sensor (2nd Side of Sensor) (Continued)

89.6 ppm Toluene/Synthetic Air

Time (minutes)	Potential (millivolts)	Resistance (10^{10} ohms)	Change in Resistance (10^{10} ohms)
0	323	2.73	0.00
2	144	6.13	3.40
5	105	8.41	5.68
10	83	10.64	7.91
20	68	12.99	10.26
30	65	13.58	10.85

112 ppm Toluene/Synthetic Air

Time (minutes)	Potential (millivolts)	Resistance (10^{10} ohms)	Change in Resistance (10^{10} ohms)
0	365	2.42	0.00
2	130	6.79	4.37
5	97	9.10	6.68
10	83	10.70	8.28
20	72	12.26	9.84
30	67	13.18	10.76

Data at a Higher Temperature (Around 47 °C)

0 ppm Toluene/Synthetic Air at 46 °C

Time (minutes)	Potential (millivolts)	Resistance (10^{10} ohms)	Change in Resistance (10^{10} ohms)
0	340	2.594	0.00
2	113	7.805	5.211
5	87	10.138	7.544
10	75	11.760	9.166
20	69	12.783	10.189
30	63	14.000	11.406

11.2 ppm Toluene/Synthetic Air at 46 °C

Time (minutes)	Potential (millivolts)	Resistance (10^{10} ohms)	Change in Resistance (10^{10} ohms)
0	331	2.665	0.00
2	119	7.412	4.747
5	88	10.023	7.358
10	75	11.760	9.095
20	69	12.783	10.118
30	68	12.971	11.306

Table A.32 Figure 6.64 Data – NJIT Lab-made Dyed Sensor (2nd Side of Sensor) (Continued)

22.4 ppm Toluene/Synthetic Air at 47 °C

Time (minutes)	Potential (millivolts)	Resistance (10^{10} ohms)	Change in Resistance (10^{10} ohms)
0	351	2.513	0.000
2	121	7.289	4.776
5	89	9.910	7.397
10	80	11.025	8.512
20	73	12.082	9.569
30	70	12.600	10.087

55.7 ppm Toluene/Synthetic Air at 47 °C

Time (minutes)	Potential (millivolts)	Resistance (10^{10} ohms)	Change in Resistance (10^{10} ohms)
0	369	2.390	0.000
2	142	6.211	3.821
5	102	8.647	6.257
10	88	10.023	7.633
20	74	11.919	9.529
30	71	12.423	10.033

85 ppm Toluene/Synthetic Air at 48 °C

Time (minutes)	Potential (millivolts)	Resistance (10^{10} ohms)	Change in Resistance (10^{10} ohms)
0	333	2.649	0.000
2	158	5.582	2.933
5	107	8.243	5.594
10	89	9.910	7.261
20	78	11.308	8.659
30	73	12.082	9.433

106 ppm Toluene/Synthetic Air at 47 °C

Time (minutes)	Potential (millivolts)	Resistance (10^{10} ohms)	Change in Resistance (10^{10} ohms)
0	334	2.641	0.000
2	140	6.300	3.659
5	98	9.000	6.359
10	86	10.256	7.615
20	79	11.165	8.524
30	75	11.760	9.119

Table A.32 Figure 6.64 Data – NJIT Lab-made Dyed Sensor (2st Side of Sensor) (Continued)

Room Temperature

0 ppm Toluene/Synthetic Air (First Time)

Time (minutes)	Potential (millivolts)	Resistance (10^{10} ohms)	Change in Resistance (10^{10} ohms)
0	202	43.713	0.000
2	99	89.192	45.479
5	80	111.069	67.356
10	71	124.366	80.653
20	67	131.791	88.078
30	64	137.969	94.256

0 ppm Toluene/Synthetic Air (Second Time)

Time (minutes)	Potential (millivolts)	Resistance (10^{10} ohms)	Change in Resistance (10^{10} ohms)
0	205.5	42.920	0.000
2	110.5	79.819	36.899
5	85.0	103.765	60.845
10	74.2	118.868	75.948
20	67.8	130.088	87.168
30	64.6	136.533	93.613

0 ppm Toluene/Synthetic Air (Third Time)

Time (minutes)	Potential (millivolts)	Resistance (10^{10} ohms)	Change in Resistance (10^{10} ohms)
0	205.5	42.920	0.000
2	110.5	79.819	36.899
5	85.0	103.765	60.845
10	74.2	118.868	75.948
20	67.8	130.088	87.168
30	64.6	136.533	93.613

5.6 ppm Toluene/Synthetic Air (First time)

Time (minutes)	Potential (millivolts)	Resistance (10^{10} ohms)	Change in Resistance (10^{10} ohms)
0	201.3	43.865	0.000
2	114.5	77.118	33.253
5	83.5	105.749	61.884
10	72.5	121.793	77.928
20	66.5	132.782	88.917
30	64.5	136.899	93.034

Table A.32 Figure 6.64 Data – NJIT Lab-made Dyed Sensor (2st Side of Sensor) (Continued)

5.6 ppm Toluene/Synthetic Air (Second Time)

Time (minutes)	Potential (millivolts)	Resistance (10^{10} ohms)	Change in Resistance (10^{10} ohms)
0	207.8	42.493	0.000
2	114	77.456	34.963
5	87	101.494	59.001
10	76.2	115.879	73.386
20	68.5	128.905	86.412
30	67.5	130.815	88.322

10 ppm Toluene/Synthetic Air

Time (minutes)	Potential (millivolts)	Resistance (10^{10} ohms)	Change in Resistance (10^{10} ohms)
0	224	39.420	0.000
2	117	75.470	36.050
5	95.5	92.461	53.041
10	77.5	113.935	74.515
20	69.2	127.601	88.181
30	67.5	130.815	91.395

13 ppm Toluene/Synthetic Air (First Time)

Time (minutes)	Potential (millivolts)	Resistance (10^{10} ohms)	Change in Resistance (10^{10} ohms)
0	201	43.881	0.000
2	118	74.746	30.865
5	88	100.227	56.346
10	79.5	110.943	67.062
20	71.5	123.357	79.476
30	68.5	128.759	84.878

13 ppm Toluene/Synthetic Air (Second Time)

Time (minutes)	Potential (millivolts)	Resistance (10^{10} ohms)	Change in Resistance (10^{10} ohms)
0	202	43.663	0.000
2	111	79.459	35.796
5	88.7	99.436	55.773
10	78	113.077	69.414
20	71	124.225	80.562
30	68	129.706	86.043

Table A.32 Figure 6.64 Data – NJIT Lab-made Dyed Sensor (2st Side of Sensor) (Continued)

17.8 ppm Toluene/Synthetic Air (Second Time)

Time (minutes)	Potential (millivolts)	Resistance (10^{10} ohms)	Change in Resistance (10^{10} ohms)
0	245.4	35.982	0.000
2	133	66.391	30.409
5	98.5	89.645	53.663
10	82.8	106.643	70.661
20	77.5	121.793	85.811
30	69.3	127.417	91.435

20 ppm Toluene/Synthetic Air (Second Time)

Time (minutes)	Potential (millivolts)	Resistance (10^{10} ohms)	Change in Resistance (10^{10} ohms)
0	203.8	43.327	0.000
2	114	77.456	34.129
5	89	99.213	55.886
10	77.3	114.230	70.903
20	68.6	128.717	85.390
30	67.4	131.009	87.682

26.7 ppm Toluene/Synthetic Air

Time (minutes)	Potential (millivolts)	Resistance (10^{10} ohms)	Change in Resistance (10^{10} ohms)
0	204.5	43.178	0.000
2	116.5	75.794	32.616
5	92.5	95.459	52.281
10	81.0	109.012	65.834
20	70.0	126.143	82.965
30	67.2	131.399	88.221

30 ppm Toluene/Synthetic Air

Time (minutes)	Potential (millivolts)	Resistance (10^{10} ohms)	Change in Resistance (10^{10} ohms)
0	213.5	41.358	0.000
2	125.5	70.359	29.001
5	96.0	91.979	50.621
10	83.0	106.386	65.028
20	72.0	122.639	81.281
30	71.5	123.497	82.139

Table A.32 Figure 6.64 Data – NJIT Lab-made Dyed Sensor (2st Side of Sensor) (Continued)

40 ppm Toluene/Synthetic Air

Time (minutes)	Potential (millivolts)	Resistance (10^{10} ohms)	Change in Resistance (10^{10} ohms)
0	194.8	45.329	0.000
2	124.3	71.038	25.709
5	93.6	94.338	49.009
10	82.6	106.901	61.572
20	73.6	119.973	74.644
30	69.1	127.786	82.457

48.9 ppm Toluene/Synthetic Air (First time)

Time (minutes)	Potential (millivolts)	Resistance (10^{10} ohms)	Change in Resistance (10^{10} ohms)
0	203.8	43.327	0.000
2	120.0	73.583	30.256
5	93.5	94.439	51.112
10	81.5	108.344	65.017
20	74.0	119.324	75.997
30	70.3	125.605	82.278

48.9 ppm Toluene/Synthetic Air (Second time)

Time (minutes)	Potential (millivolts)	Resistance (10^{10} ohms)	Change in Resistance (10^{10} ohms)
0	207.3	42.595	0.000
2	126.0	70.079	27.484
5	96.2	91.788	49.193
10	82.0	107.680	65.085
20	74.5	118.520	75.925
30	70.3	125.600	83.005

67 ppm Toluene/Synthetic Air

Time (minutes)	Potential (millivolts)	Resistance (10^{10} ohms)	Change in Resistance (10^{10} ohms)
0	226	39.071	0.000
2	150	58.867	19.796
5	113	78.142	39.071
10	92	95.978	56.907
20	78	113.205	74.134
30	75	117.733	78.162

Table A.32 Figure 6.64 Data – NJIT Lab-made Dyed Sensor (2st Side of Sensor) (Continued)

90.3 ppm Toluene/Synthetic Air

Time (minutes)	Potential (millivolts)	Resistance (10^{10} ohms)	Change in Resistance (10^{10} ohms)
0	203	43.498	0.000
2	120	73.583	30.085
5	95	92.947	49.449
10	82	107.683	64.185
20	74	119.324	75.826
30	70	126.143	82.648

Higher Temperature Data Runs

0 ppm Toluene/Synthetic Air at 46C

Time (minutes)	Potential (millivolts)	Resistance (10^{10} ohms)	Change in Resistance (10^{10} ohms)
0	203.8	43.278	0.000
2	146.5	60.205	16.927
5	131.5	67.072	23.794
10	124.9	71.129	27.851
20	121.5	72.593	29.315
30	117.4	75.128	31.850

8.9 ppm Toluene/Synthetic Air at 46 C

Time (minutes)	Potential (millivolts)	Resistance (10^{10} ohms)	Change in Resistance (10^{10} ohms)
0	205.2	42.982	0.000
2	157.0	56.178	13.196
5	132.5	66.566	23.584
10	123.5	71.417	28.435
20	118.5	74.430	31.448
30	117.5	75.064	32.082

30 ppm Toluene/Synthetic Air at 46 C

Time (minutes)	Potential (millivolts)	Resistance (10^{10} ohms)	Change in Resistance (10^{10} ohms)
0	234.8	37.564	0.000
2	176.0	50.114	12.550
5	153.5	57.459	19.895
10	141.5	62.332	24.768
20	133.0	66.316	28.752
30	125.5	70.279	32.715

Table A.32 Figure 6.64 Data – NJIT Lab-made Dyed Sensor (2st Side of Sensor) (Continued)

55.7 ppm Toluene/Synthetic Air at 46 C

Time (minutes)	Potential (millivolts)	Resistance (10^{10} ohms)	Change in Resistance (10^{10} ohms)
0	224.5	39.287	0.000
2	164.0	53.780	14.493
5	151.5	58.218	18.931
10	140.7	62.687	23.400
20	133.8	65.919	26.632
30	132.8	66.416	27.129

Table A.33 Figure 6.65 Data – NJIT Lab-made Dyed Sensor - Resistances with Synthetic Air

(2 psia)

Time (minutes)	Potential (millivolts)	Resistance (10^{11} ohms)	Change in Resistance (10^{11} ohms)
0	66.5	1.331	0.000
5	61.4	1.441	0.110
10	63.0	1.405	0.074
20	66.4	1.333	0.002
30	69.8	1.268	-0.063

8 psia

Time (minutes)	Potential (millivolts)	Resistance (10^{11} ohms)	Change in Resistance (10^{11} ohms)
0	59.5	1.487	0.000
5	42.2	2.097	0.610
10	39.6	2.235	0.748
20	38.8	2.281	0.794
30	38.0	2.329	0.842

14 psia

Time (minutes)	Potential (millivolts)	Resistance (10^{11} ohms)	Change in Resistance (10^{11} ohms)
0	60.8	1.456	0.000
5	35.5	2.493	1.037
10	33.9	2.611	1.155
20	32.6	2.715	1.259
30	32.4	2.731	1.275

Table A.33 Figure 6.65 Data – NJIT Lab-made Dyed Sensor - Resistances with Synthetic Air (Continued)

36 psia

Time (minutes)	Potential (millivolts)	Resistance (10^{11} ohms)	Change in Resistance (10^{11} ohms)
0	58.9	1.510	0.000
5	26.7	3.315	1.805
10	26.3	3.365	1.855
20	25.8	3.430	1.920
30	26.1	3.391	1.881

Table A.34 Figure 6.66 Data

	0% RH Synthetic Air		Desorption Curve/ Variac at 40	
Time (minutes)	Potential (millivolts)	Change in Resistance (10^{10} ohms)	Potential (millivolts)	Change in Resistance (10^{10} ohms)
0	65.0	0.000	45.7	0.000
1	48.7	0.460	51.3	-0.213
2	45.6	0.584	54.0	-0.300
5	40.0	0.859	61.8	-0.509
10	36.0	1.107	67.8	-0.636
20	33.5	1.292	76.7	-0.789
30	32.8	1.349	84.9	-0.901
40	32.0	1.417	91.5	-0.977
50	32.0	1.417	92.6	-0.989
60	31.0	1.507	94.0	-1.003

When applied hot gun the mV reading
Increased from 31 to 33.2 mV

	Desorption Curve (12/2/02) Variac at 50		Desorption Curve (12/2/02) Variac at 60	
Time (minutes)	Potential (millivolts)	Change in Resistance (10^{10} ohms)	Potential (millivolts)	Change in Resistance (10^{10} ohms)
0	47.0	0.000	50.0	0.000
1	51.3	-0.159	51.2	-0.042
2	55.0	-0.276	52.5	-0.085
5	61.5	-0.448	57.4	-0.230
10	67.5	-0.577	64.0	-0.390
20	76.1	-0.726	74.0	-0.579
30	83.1	-0.825	79.9	-0.668
40	87.7	-0.881	86.1	-0.748
50	88.7	-0.884	87.9	-0.769
60	88.8	-0.892	93.3	-0.828

Table A.35 Effect of Heat on Adsorption of Oxygen on the Sensor Surface (Figures 6.67 and 6.68 Data)

Variac on 90

Time (minutes)	Temperature (°C)	Application	Percent Oxygen	Resistance (10^{10} ohms)
0	25	Apply heat	11.50	2.977
3	40	Apply heat	11.74	2.967
10	47	Apply heat	11.77	2.843
20	53	Apply heat	11.87	2.781
30	53	Apply heat	11.78	2.781
40	55	Apply heat	11.85	2.730
41	39	Heat Off		2.781
51	39	Heat Off		2.928
61	39	Heat Off		2.977
66	29	Heat Off	11.73	
71	39	Heat Off		2.977
81	39	Heat Off		3.017
91	39	Heat Off		2.918

Table A.36 Figures 6.71 and 6.72 Data – Undyed Sensor - Resistances with Nitrogen and Synthetic Air (with and without Relative Humidity)

30"Hg to 4.5 psig with N2

Time (minutes)	Potential (millivolts)	Resistance (10^{10} ohms)	Change in Resistance (10^{10} ohms)
0	57.0	1.551	0.000
10	56.0	1.579	0.028
20	59.0	1.498	-0.053
30	58.2	1.519	-0.032

28"Hg to 4.5 psig with N2 thru NaCl saturated salt solution (75% RH)

Time (minutes)	Potential (millivolts)	Resistance (10^{10} ohms)	Change in Resistance (10^{10} ohms)
0	62.7	1.410	0.000
0.5	61.7	1.433	0.023
2	58.7	1.506	0.096
5	56.5	1.565	0.155
10	53.4	1.655	0.245
20	52.2	1.693	0.283
30	50.4	1.754	0.344

Table A.36 Figures 6.71 and 6.72 Data – Undyed Sensor - Resistances with Nitrogen and Synthetic Air (with and without Relative Humidity) (Continued)

Synthetic Air 29.5"Hg to 4.5 psig

Time (minutes)	Potential (millivolts)	Resistance (10^{10} ohms)	Change in Resistance (10^{10} ohms)
0	58.5	1.511	0.000
0.5	33.3	2.655	1.144
2	25.2	3.508	1.997
5	21.1	4.190	2.679
10	19.0	4.653	3.142
20	17.5	5.051	3.540
30	16.6	5.325	3.814

Synthetic Air through NaCl Saturated Solution (75% RH) to 4.7 psig

Time (minutes)	Potential (millivolts)	Resistance (10^{10} ohms)	Change in Resistance (10^{10} ohms)
0	57.0	1.511	0.000
0.5	42.2	2.095	0.544
2	25.2	3.508	1.957
5	21.0	4.210	2.659
10	18.7	4.727	3.176
20	17.6	5.023	3.472
30	16.9	5.231	3.680

Synthetic Air through Water (100% RH) 29"Hg to 4.8 psig

Time (minutes)	Potential (millivolts)	Resistance (10^{10} ohms)	Change in Resistance (10^{10} ohms)
0	56.8	1.556	0.000
0.5	44.2	2.000	0.444
2	26.0	3.400	1.844
5	20.8	4.250	2.694
10	19.3	4.580	3.024
20	17.8	4.966	3.410
30	17.1	5.170	3.614

Nitrogen through Water (100% RH) 29.5"Hg to 14.5 psig

Time (minutes)	Potential (millivolts)	Resistance (10^{10} ohms)	Change in Resistance (10^{10} ohms)
0	57.0	1.551	0.000
0.5	53.7	1.646	0.095
2	52.5	1.684	0.133
5	50.8	1.740	0.189
10	48.0	1.842	0.291
20	48.6	1.819	0.268
30	48.6	1.819	0.268

Table A.36 Figures 6.71 and 6.72 Data – Undyed Sensor - Resistances with Nitrogen and Synthetic Air (with and without Relative Humidity) (Continued)

50 ppm Toluene/N2 (30"Hg to 4.5 psig)

Time (minutes)	Potential (millivolts)	Resistance (10^{10} ohms)	Change in Resistance (10^{10} ohms)
0	56.3	1.570	0.000
0.5	55.9	1.581	0.011
2	53.8	1.643	0.073
5	50.8	1.740	0.170
10	49.3	1.793	0.223
20	48.8	1.811	0.241
30	49.0	1.804	0.234

Atmospheric Air

Time (minutes)	Potential (millivolts)	Resistance (10^{10} ohms)	Change in Resistance (10^{10} ohms)
0	56.2	1.573	0.000
0.5	46.0	1.922	0.349
2	27.5	3.215	1.642
5	23.5	3.762	2.189
10	20.8	4.250	2.677
20	18.6	4.753	3.180
30	17.8	4.966	3.393

25 ppm Toluene/N2

Time (minutes)	Potential (millivolts)	Resistance (10^{10} ohms)	Change in Resistance (10^{10} ohms)
0	53.7	1.646	0.000
0.5	52.1	1.697	0.051
2	50.4	1.754	0.108
5	49.8	1.775	0.129
10	49.3	1.793	0.147
20	48.5	1.823	0.177
30	47.8	1.849	0.203

Table A.36 Figures 6.71 and 6.72 Data – Undyed Sensor - Resistances with Nitrogen and Synthetic Air (with and without Relative Humidity) (Continued)

Undyed Sensor - Resistances with Synthetic Air (0% Relative Humidity)

2.4 psia

Time (minutes)	Potential (millivolts)	Resistance (10^{10} ohms)	Change in Resistance (10^{10} ohms)
0	28.2	3.131	0
0.5	28.0	3.154	0.023
2	22.6	3.199	0.068
5	27.5	3.211	0.080
10	27.5	3.211	0.080
20	28.6	3.087	-0.044
30	28.6	3.087	-0.044

4.8 psia

Time (minutes)	Potential (millivolts)	Resistance (10^{10} ohms)	Change in Resistance (10^{10} ohms)
0	27.5	3.211	0.000
0.5	26.5	3.332	0.121
2	25.4	3.476	0.265
5	23.7	3.726	0.515
10	23.2	3.806	0.595
20	22.0	4.014	0.803
30.	21.8	4.050	0.839

8.6 psia

Time (minutes)	Potential (millivolts)	Resistance (10^{10} ohms)	Change in Resistance (10^{10} ohms)
0	29.2	3.024	0.000
0.5	26.5	3.332	0.308
2	24.0	3.679	0.655
5	22.8	3.873	0.849
10	22.0	4.014	0.990
20	21.4	4.126	1.102
30	21.2	4.165	1.141

12.7 psia

Time (minutes)	Potential (millivolts)	Resistance (10^{10} ohms)	Change in Resistance (10^{10} ohms)
0	28.8	3.066	0.000
0.5	25.0	3.532	0.466
2	22.4	3.942	0.876
5	20.6	4.286	1.220
10	19.3	4.575	1.509
20	18.8	4.697	1.631
30	18.3	4.825	1.759

Table A.36 Figures 6.71 and 6.72 Data – Undyed Sensor - Resistances with Nitrogen and Synthetic Air (with and without Relative Humidity) (Continued)

17.3 psia

Time (minutes)	Potential (millivolts)	Resistance (10^{10} ohms)	Change in Resistance (10^{10} ohms)
0	28.5	3.098	0.000
0.5	21.5	4.107	1.010
2	19.1	4.623	1.530
5	17.6	5.017	1.920
10	16.8	5.256	2.160
20	16.6	5.319	2.220
30	16.6	5.319	2.220

REFERENCES

1. Kebbekus, B., V. Zaitsev, Development of Semiconductor-based Adsorption-Modified Photosensitization (SAMP) Sensors for a Sensor-array Device for the Monitoring of Organic Gases, http://web.mit.edu/airquality/www/AR99/7m1.htm, 6/3/03.

2. Woods, L. M., D. H. Levi, V. Kaydanov, G. Y. Robinson, R. K. Ahrenkiel, Electrical Characterization of CdTe Grain-boundary Properties from As Processed CdTe/CdS Solar Cells, *Proceedings of the 2nd World Conference and Exhibition on Photovoltaic Solar Energy Conversion*, Vienna, Austria, July 6-10, 1998.

3. Smyntyna, V., V. Golovanov, S. Kashulis, G. Mattogno and S. Viticoli, Dependence of Sensitivity and Reproducibility of CdS Oxygen Sensors, *Sensors and Actuators B*, vols. 18-19, pp. 460-463, 1994.

4. Golovan, N. and V. Smyntyna, The Sensitization of Semiconductor Gas Sensors, *Sensors and Actuators B*, vol. 6, pp. 289-292, 1992.

5. Smyntyna, V., V. Golovanov, S. Kaciulis, G. Mattogno, G. Righini, Influence of Chemical Composition on Sensitivity and Signal Reproducibility of CdS Sensors of Oxygen, *Sensors and Actuators B*, vols. 24-25, pp. 628-630, 1995.

6. Amalnerkar, D. P., S. Badrinarayanan, S.K. Date, and A.P.B. Sinha, X-Ray Photoelectron Spectroscopic Studies of Oxygen Chemisorption on Thick Films of Photoconducting Cadmium Sulphide, *Appl. Phys. Lett., vol.* 41, pp. 270-271, Aug. 1982.

7. Smyntyna, V.A., V. Gerasutenko, S. Kashulis, G. Mattogno and S. Reghini, The Causes of Thickness Dependence of CdSe and CdS Gas-Sensor Sensitivity to Oxygen, *Sensors and Actuators B*, vols.18-19, pp. 464-465, 1994.

8. Smyntyna, V., V. Gerasutenko, V. Golovanov, S. Kaciulis, G. Mattogno, S. Viticoli, Surface Spectroscopy Study of CdSe and CdS Thin-Film Oxygen Sensors, *Sensors and Actuators B*, vol. 22, pp. 189-194, 1994.

9. Gutman, E. E., V. F. Kiselev, G. S. Plotnikov, Vibronic Effects as a Clue to the Solution of the Selectivity Problem of Semiconductor Gas Sensors, *Sens. Actuators B, Chem*, vol. 44, p.468-473, 1997.

10. Meixner, H., H. Gerblinger, U. Lampe, M. Fleischer, Thin-film Gas Sensors Based on Semiconducting Metal Oxides, *Sens. Actuators B, Chem*, vol. 23, pp. 119-125, 1995.

11. Li, G. Q., P. T. Lai, S. H. Zeng, M. Q. Huang, and B. Li, A New Thin-film Humidity and Thermal Micro-Sensor With Al/$SrNb_xTi_{1-x}O_3$ /SiO_2/Si Structure, *Sensors and Actuators*, vol. 75, pp. 70-74, 1999.

12. Mark, P., *Phys. Rev.* 137, A203, 1965.

13. Lantto, V., V. Golovanov, A Comparison of Conductance Behavior between SnO2 and CdS Gas-sensitive Films, *Sens. Actuators, B, Chem*, vols. 24-25, pp. 614-618, 1995.

14. Ayers, M. R., A. J. Hunt, U.S. Patent 5,885,843, *Device and Method for Determining Oxygen Concentration and Pressure in Gases*, March 23, 1999.

15. Xu, W., K. A. Kneas, J. N. Demas and B. A. DeGraff, Oxygen Sensors Based on Luminescence Quenching of Metal Complexes: Osmium Complexes Suitable for Laser Diode Excitation, *Analytical Chemistry*, Vol. 68, pp. 2605-2609, Aug.1996.

16. Tata, M., S. Banerjee, V. John, Y. Waguespack, G. McPherson, Fluorescence Quenching of CdS Nanocrystallites in AOT Water-in-oil Microemulsions, *Colloids and Surfaces, A: Physicochemical and Engineering Aspects*, vol. 127, pp. 39-46, 1997.

17. Eaton, K., P. Douglas, Effect of Humidity on the Response Characteristics of Luminescent PtOEP Thin Film Optical Oxygen Sensors, *Sens. Actuators, B, Chem*, vol. 82, pp. 94-104, 2002.

18. Choi, M. and O. Tse, Humidity-sensitive Optode Membrane Based on a Fluorescent Dye Immobilized in Gelatin Film, *Analytica Chimica Acta*, vol. 378, pp. 127-134, 1999.

19. McNamara, K. P., X. Li, A. D. Stull, Z. Rosenzweig, Fiber-optic Oxygen Sensor Based on the Fluorescence Quenching of Tris(5-acrylamido, 1,10 phenanthroline) Ruthenium Chloride, *Analytica Chimica Acta*, vol. 361, pp. 73-83, 1998.

20. Mohr, G. J., O. S. Wolfbeis, Effects of the Polymer Matrix on an Optical Nitrate Sensor Based on a Polarity-Sensitive Dye, *Sens. Actuators, B, Chem*, vol. 37, pp. 103-109, 1996.

21. Preininger, C., G. J. Mohr, I. Klimant, O. S. Wolfbeis, Ammonia Fluorosensors Based on Reversible Lactonization of Polymer-entrapped Rhodamine Dyes, and the Effects of Plasticizers, *Analytica Chmica Acta*, vol. 334, pp. 113-123, 1996.

22. Razek, T., M. Miller, S. Hassan and M. Arnold, Optical Sensor for Sulfur Dioxide Based on Fluorescence Quenching, *Talanta*, vol. 50, pp. 491-498, 1999.

23. Khan, S. S., E. S. Jin, N. Sojic and P. Pantano, A Fluorescence-based Imaging-fiber Electrode Chemical Sensor for Hydrogen Peroxide, *Analytica Chimica Acta*, vol. 404, pp. 213-221, 2000.

24. Opitz, N., P. J. Rothwell, B. Oeke, P. Schwille, Single Molecule FCS-based Oxygen Sensor (O2-FCSensor): A New Intrinsically Calibrated Oxygen Sensor Utilizing Fluorescence Correlation Spectroscopy (FCS) with Single Fluorescent Molecule Detection Sensitivity, *Sens. Actuators, B, Chem*, in press, 2003.

25. Ohyama, T., Y. Y. Maruo, T. Tanaka and T. Hayashi, Fluorescence-intensity Changes in Organic Dyes Impregnated in Porous Glass on Exposure to NO2, *Sens. Actuators, B, Chem*, vol. 59, pp. 16-20, 1999.

26. Geddes, C. D., Optical Thin Film Polymeric Sensors for the Determination of Aqueous Chloride, Bromide, and Iodide Ions at High pH, Based on the Quenching of Fluorescence of Two Acridinium Dyes, *Dyes and Pigments*, vol. 45, pp. 243-251, 2000.

27. Agrawal, A., *Testing of Semiconductor-Based Adsorption Modified Photosensitive (SAMP) Sensor For Response To Toluene*, Chemical Engineering Master of Science Degree Thesis, New Jersey Institute of Technology, January 2001.

28. EPA Center on Airborne Organics Center, *2000 Annual Report*.

29. Jacob Fraden, *Handbook of Modern Sensors, Physics, Designs and Applications*, Second Edition, Springer-Verlag, New York, 1996.

30. Jasinski, P., T. Suzuki, H. Andersen, Nanocrystalline Undoped Ceria Oxygen Sensor, *Sensors and Actuators B*, vol. 95, pp. 73-77, 2003.

31. Izu, N., W. Shin and N. Murayama, Numerical Analysis of Response Time for Resistive Oxygen Gas Sensors, *Sensors and Actuators B: Chemical*, vol. 87, pp. 99-104, Nov. 2002.

32. Lee, J. and D. Lee, A SrF2-based Oxygen Sensor Operative at Low Temperature, *Sensors and Actuators B: Chemical*, pp. 169-173, May 1998.

33. Ogita, M., K. Higo, Y. Nikanishi and Y. Hatanaka, Ga2O3 Thin Film for Oxygen Sensor at High Temperature, Applied Surface Science, vols.175-176, pp. 721-725, 2001.

34. Izu, N., W. Shin and N. Murayama, Fast Response of Resistive-type Oxygen Gas Sensors Based on Nano-sized Ceria Powder, *Sensors and Actuators B: Chemical*, vol. 93, pp. 449-453, Aug. 2003.

35. Trinchi, A., Y. Li, W. Wlodarski, S. Kaciulis, L. Pandolfi, S. Russo, J. Duplessis, S. Viticoli, Investigation of Sol-gel Prepared Ga-Zn Oxide Thin Films for Oxygen Gas Sensing, *Sensors and Actuators A*, vol. 108, pp. 263-270, 2003.

36. Ogita, M., N. Saika, Y. Nakanishi, Y. Hatanaka, Ga2O3 Thin Films for High-Temperature Gas Sensors, *Applied Surface Science*, vol. 142, pp. 188-191, 1999.

37. Alderman, J., J. Hynes, S. M. Floyd, J. Kruger, R. O'Connor, D. B. Papkovsky, A Low-volume Platform for Cell-respirometric Screening Based on Quenched-Luminescence Oxygen Sensing, *Biosensors and Bioelectronics* (in press), 2004.

38. City Technology: Oxygen Sensors, www.citytech.com/technology/02-sensors.asp, March 2004.

39. Moos, R., F. Rettig, A. Hurland, and C. Plog, Temperature-independent Resistive Oxygen Exhaust Gas Sensor for Lean-burn Engines in Thick-film Technology, *Sensors and Actuators B*, vol. 93, pp. 43-50, 2003.

40. Golovanov, V., V. Smyntyna, Interaction Between Collective and Local Subsystems in Semiconductor Surface-active Structures, *Sensors and Actuators B*, vols. 24-25, pp. 647-652, 1995.

41. Mark, P., The Role of Chemisorption in Current Flow in Insulating CdS Crystals, *J. Phys. Chem. Solids*, vol. 26, pp. 959-972, 1965.

42. Bube, R. H., The Basic Significance of Oxygen Chemisorption on the Photoelectronic Properties of CdS and CdSe, *Journal of the Electrochemical Society*, vol. 113, pp. 793-798, Aug. 1966.

43. Yu, S., Q. Wu, M. Tabib-Azar and C. Liu, Development of a Silicon-based Yttria-stabilized-zirconia (YSZ) Amperometric Oxygen Sensor, *Sensors and Actuators, B: Chemical*, vol. 85, pp. 212-218, July 2002.

44. Artemyev, M.V., V. Sperling, U. Woggon, Electroluminescence in Thin Solid Films of Closely-Packed CdS Nanocrystals, *Journal of Crystal Growth*, vols.184-185, pp. 374-376, 1998.

45. Lee, D., Y. Kim, J. Huh and D. Lee, Fabrication and Characteristics of SnO2 Gas Sensor Array for Volatile Organic Compounds Recognition, *Thin Solid Films*, vol. 416, pp. 271 – 278, 2002.

46. Abbas, M. N., G. A. Moustafa, J. Mitrovics and W. Gopel, Multicomponent Gas Analysis of a Mixture of Chloroform, Octane and Toluene Using a Piezoelectric Quartz Crystal Sensor Array, *Analytica Chimica Acta,* vol. 393, pp. 67-76, 1999.

47. Zhu, B. L., C. S. Xie, W. Y. Wang, K. J. Huang, J. H. Hu, Improvement in Gas Sensitivity of ZnO Thick Film to Volatile Organic Compounds (VOCs) by Adding TiO_2, Materials Letters, vol. 58, pp. 624-629, 2004.

48. Wang, X., W. P. Carey, S. S. Yee, Monolithic Thin-film Metal-oxide Gas-sensor Arrays with Application to Monitoring of Organic Vapors, *Sensors and Actuators B,* vol. 28, pp. 63-70, 1995.

49. Szczurek, A., P. M. Szecowka, B. W. Licznerski, Application of Sensor Array and Neural Networks for Quantification of Organic Solvent Vapours in Air, *Sensors and Actuators B,* vol. 58, pp. 427-432, 1999.

50. Feng, J., A. G. MacDiarmid, Sensors Using Octaaniline for Volatile Organic Compounds, *Synthetic Metals,* vol. 102, pp. 1304-1305, 1999.

51. Barisci, J. N., G. G. Wallace, M. K. Andrews, A. C. Partridge and P. D. Harris, Conducting Polymer Sensors for Monitoring Aromatic Hydrocarbons Using an Electronic Nose, *Sensors and Actuators B,* vol. 84, pp. 252-257, 2002.

52. Van De Leur, R. H. M. and A. Van Der Waal, Gas and Vapour Detection Using Polypyrrole, *Synthetic Metals,* vol. 102, pp. 1330-1331, 1999.

53. Feller, J. and Y. Grohens, Evolution of Electrical Properties of Some Conductive Polymer Composite Textiles with Organic Solvent Vapours Diffusion, *Sensors And Actuators B,* vol. 97, pp. 231-242, 2004.

54. Joseph, Y., B. Guse, A. Yasuda and T. Vossmeyer, Chemiresistor Coatings from Pt- and Au-nanoparticle/nonanedithiol Films: Sensitivity to Gases and Solvent Vapors, *Sensors and Actuators B,* vol. 98, pp. 188-195, 2004.

55. Nanto, H., Y. Yokoi, T. Mukai, J. Fujioka, E. Kusano, A. Kinbara and Y. Douguchi, Novel Gas Sensor Using Polymer-film-coated Quartz Resonator for Environmental Monitoring, *Materials Science and Engineering: C,* vol.12, pp. 43-48, 2000.

56. Baratto, C., E. Comini, G. Faglia, G. Sberveglieri, G. DiFrancia, F. DeFilippo, V. LaFerrara, L. Quercia, L. Lancellotti, Gas Detection with a Porous Silicon Based Sensor, *Sensors and Actuators B,* vol. 65, pp. 257-259, 2000.

57. Ding, H., V. Erokhin, M. K. Ram, S. Paddeu, L. Valkova and C. Nicolini, A Physical Insight into the Gas-sensing Properties of Copper (II) Tetra-(tert-butyl)-5,10,15,20-Tetraazaporphyrin Langmuir-Blodgett Films, *Thin Solid Films,* vol. 379, pp. 279-286, 2000.

58. Casalini, R., J. N. Wilde, J. Nagel, U. Oertel and M. Petty, Organic Vapour Sensing Using Thin Films of a Co-ordination Polymer: Comparison of Electrical and Optical Techniques, *Sensors and Actuators B,* vol. 57, pp. 28-34, 1999.

59. Covington, J., J. Gardner, D. Briand and N. deRooij, A Polymer Gate FET Sensor Array for Detecting Organic Vapours, *Sensors and Actuators B,* vol. 77, pp. 155-162, 2001.

60. Abdelghani A., J. M. Chovelon, N. Jaffrezic-Renault, C. Veilla and H. Gagnaire, Chemical Vapour Sensing by Surface Plasmon Resonance Optical Fibre Sensor Coated with Fluoropolymer, *Analytica Chimica Acta,* vol. 337, pp. 225-232, 1997.

61. Althainz, P., A. Dahlke, M. Frietsch-Klarhof, J. Goschnick and H. Ache, Reception Tuning of Gas-sensor Microsystems by Selective Coatings, *Sensors and Actuators B,* vols. 24-25, pp. 366-369, 1995.

62. Dolbec, R., M. El Khakani, A. Serventi and R. Saint-Jacques, Influence of the Nanostructural Characteristics on the Gas Sensing Properties of Pulsed Laser Deposited Tin Oxide Thin Films, *Sensors and Actuators B,* vol. 93, pp. 566-571, 2003.

63. Althainz, P., L. Schuy, J. Goschnick and H.Ache, The Influence of Morphology on the Response of Iron-oxide Gas Sensors, *Sensors and Actuators, B,* vols. 24-25, pp. 448-450, 1995.

64. Zaitsev, V. B., The Use of Vibronic Phenomena in Adsorption Phase for Developing of Semiconductor Gas Sensors, M. V. Lomonosov Moscow State University, Physics Dept., *Materials Science*, vol. 20, 2002.

65. Keithley Instruments, Inc., *Instruction Manual, Model 427-Current Amplifier*, Document #29103, Cleveland, Ohio, USA, 1975.

66. Heupel, M., I. Gregor, St. Becker and E. Thiel, Photophysical and Photochemical Properties of Electronically Excited Fluorescent Dyes: A New Type of Time-resolved Laser-scanning Spectroscopy, Fachbereich Chemie-Biologie, der Universitat-GH Siegen, *International Journal of Photoenergy*, vol. 1, p. 165, 1999.

67. Enriquez, J. and X. Mathew, Influence of the Thickness on Structural, Optical and Electrical Properties of Chemical Bath Deposited CdS Thin Films, *Solar Energy Materials and Solar Cells*, vol. 76, pp. 313-322, 2003.

68. Rao, S., N. Srinivas and D. Rao, Nonlinear Absorption and Excited State Dynamics in Rhodamine B Studied Using Z-scan and Degenerate Four Wave Mixing Techniques, *Chemical Physics Letters*, vol. 361, pp. 439-445, 2002.

69. Keithley, *Low Level Measurements*, Fifth Edition, Keithley Instruments, Inc., Cleveland, Ohio 44139, 1998.

70. VALCO Instruments Co., Switching Valve Applications: Pamphlet and Attached VALCO Basic Sample Valve Designs, Figure 1, P.O. Box 19032, Houston, Texas 77024.

71. Cigoy, D., Configuring Your Data Acquisition or Test and Measurement System for Maximum Noise Immunity, Keithley White Paper, Keithley Instruments, Inc., Cleveland, Ohio, 1999.

72. Bowen, E. J.; Luminescence In Chemistry, D. Van Nostrand Co., Ltd. 1968.

73. Kebbekus, B., V. Zaitsev, *Development of Semiconductor-Based Adsorption-Modified Photosensitization (SAMP) Sensors For A Sensor-Array Device for the Monitoring of Organic Gases*, 2001 Annual Report Submitted to the Center on Airborne Organics, February, 2002.

74. Mark, P., *J. Phys. Chem. Sol.*, vol. 25, p. 911, 1964.

75. Website http://ece-www.colorado.edu/~bart/ecen3320/newbook, dated Aug. 2002.

76. Ruffolo, R., C. Evans, X. Liu, Y. Ni, Z. Pang, P. Park, A. McWilliams, X. Gu, X. Lu, A. Yekta, M. Winnik, and I. Manners, Phosphorescent Oxygen Sensors Utilizing Sulfur-Nitrogen-Phosphorus Polymer Matrixes: Synthesis, Characterization, and Evaluation of Poly(thionylphosphazene)-b-Poly(tetrahydrofuran) Block Copolymers, *Analytical Chemistry*, vol. 72, pp. 1894-1904, April, 2000.

77. Baron, A., J. Danielson, M. Gouterman, J. Wan, and J. Callis, Submillisecond Response Times of Oxygen-Quenched Luminescent Coatings, *Rev. Sci Instrum.*, vol. 64, pp. 3394-3402, Dec.1993.

78. Website, Fluorescence Sensor Technology, www.sentronic.de/sentronic02.nsf/ID/sens_tech_fluorescence_EN.html, Jan. 2002.

79. Ebbing, D., *General Chemistry*, Houghton Mifflin Co., Boston, Mass., 1996.

80. Sootha, G., G. Padam, and S. Gupta, *Phys. Status Solidi A*, vol. 58, pp. 615, 1980.

81. Somorjai, G. A., Charge Transfer Controlled Surface Interactions Between Oxygen and CdSe Films, *J. Phys. Chem. Solids*, Pergamon Press, Vol. 24, pp. 175-186, 1963.

82. Shear, H., E. Hilton, and R. Bube, Oxygen Chemisorption Effects on Photoconductivity in Sintered Layers, *Journal of the Electrochemical Society*, vol. 112, Oct. 1965.

83. Daniels, F. and R. Alberty, *Physical Chemistry*, Fourth Edition, John Wiley and Sons, Inc., 1975.

84. Roth, T., Luminescence-Based Oxygen Sensor, http://www.nogi.ch/chemistry, Jan. 2003.

85. Ernest Orlando Lawrence Berkeley National Laboratory, Optical Oxygen Sensor Based on Silica Aerogel, http://www.eande.lbl.gov/ecs/aerogels/sao2sens.ht

86. Ocean Optics, Inc., *Oxygen Sensor for Respiration Monitoring*, http://www.oceanoptics.com/products/respirati, website last modified Jan. 2002.

87. Zaitsev V., B. Kebbekus, *Development of Semiconductor-Based Adsorption-Modified Photosensitization (SAMP) Sensors For A Sensor-Array Device for the Monitoring of Organic Gases,* Research Proposal Submitted to the Center on Airborne Organics, June 1,1999 to May 31, 2001.

88. Rossetti, R. and L. Brus, Time-Resolved Raman Scattering Study of Adsorbed, Semioxidized Eosin Y Formed by Excited-State Electron Transfer into Colloidal TiO_2 Particles, *J. Am. Chem. Soc.*, vol. 106, pp. 4336-4340, 1984.

89. Reid, R., J. Prausnitz and B. Poling, *The Properties of Gases & Liquids*, McGraw-Hill, Inc., Fourth Edition, 1987.